

MCFM-10.3 manual

A Monte Carlo for FeMtobarn processes at Hadron Colliders

John M. Campbell (johnmc@fnal.gov)
R. Keith Ellis (ellis@fnal.gov)
Tobias Neumann (tneumann@fnal.gov)
Ciaran Williams (ciaranwi@buffalo.edu)

Updated January 2023

MCFM is a parton-level Monte Carlo program that gives predictions for a wide range of processes at hadron colliders. Almost all processes are available at NLO, but some processes are also available at NNLO or N³LO in QCD. The calculation of some processes can also account for NLO electroweak effects. Transverse momentum and jet veto resummation is available for the production of color singlet final states. Please look at the [list of available processes](#). This document is available as a [series of webpages](#) and as a [pdf file](#). Download and installation instructions are in Section 1.

Contents

1	Overview of MCFM	6
1.1	Download	6
1.2	Documentation	6
2	Installation and directories	6
2.1	Installation	6
2.1.1	Compiling at Fermilab	7
2.1.2	Compiling at CERN	8
2.1.3	LHAPDF	8
2.1.4	WW, WZ and ZZ with VVamp	8
2.1.5	OpenMP and MPI	9
2.2	Directory structure	9
2.3	References	10
3	New features in version 10.3	11
4	Process list	12
5	Configuration	21
5.1	Compile-time settings	21
5.2	Parton distributions	22
5.3	Electroweak corrections	22
6	Input file configuration	23
6.1	Run-time input file parameters	23
6.1.1	General	26
6.1.2	Resummation	26

6.1.3	NNLO	27
6.1.4	PDFs	28
6.1.5	LHAPDF	28
6.1.6	Scales	28
6.1.7	Masses	29
6.1.8	Basic jets	30
6.1.9	Mass cuts	30
6.1.10	Cuts	31
6.1.11	Cuts (continued)	32
6.1.12	Photon	33
6.1.13	Histograms	34
6.1.14	Integration	34
6.2	Process specific options	35
6.2.1	Single Top	35
6.2.2	Anomalous W/Z couplings	35
6.2.3	$W/Z+2$ jets	37
6.2.4	H jetmass	37
6.2.5	Anomalous H couplings	37
6.2.6	Extra	37
6.2.7	Dipoles	38
7	Histograms	38
7.1	Output	38
7.1.1	Traditional histograms	40
7.1.2	New style histograms	41
7.2	User modifications to cuts and reweighting	42
8	NNLO using non-local subtraction	42
8.1	Benchmark results at NNLO	42
9	CuTe-MCFM	42
9.1	N^3LL and N^4LL q_T^2 resummation for color-singlet processes in MCFM	44
9.2	Input file parameters	45
9.3	Plotting routine and transition function	46
9.4	Modifying the plotting routines and transition function.	46
10	Jet-vetoed cross sections	48
10.1	Benchmark results for jet-vetoed cross sections	48
11	Z production at N^3LO and N^4LL	51
11.1	N^4LL + matching at α_s^2 fixed-order (NLO Z+jet)	51
11.1.1	Purely resummed N^4LL	51
11.1.2	Fixed-order expansion of the resummed result	52
11.1.3	Fixed-order Z+jet at NLO	52
11.1.4	Combination and scale uncertainties	52
11.2	Adding α_s^3 matching corrections (Z+jet NNLO coefficient)	53
11.2.1	Fixed-order Z+jet NNLO coefficient	53
11.2.2	Fixed-order Z+jet NNLO coefficient	53

11.2.3	α_s^3 fixed-order expansion coefficient of the resummed result	53
11.2.4	Combination	53
11.3	Fixed order N ³ LO	54
12	C++ matrix element interface	55
12.1	Processes with C++ interface	55
12.2	Installation	56
12.3	Usage	56
12.4	Tests	58
13	Notes on specific processes	58
13.1	W -boson production, processes 1,6	58
13.2	EW corrections to W -boson production, processes 2,7	58
13.3	Photon-induced corrections to W -boson production, processes 3,8	58
13.4	W + jet production, processes 11,16	59
13.5	$W + b$ production, processes 12,17	59
13.6	$W + c$ production, processes 13,18	59
13.7	$W + c$ production ($m_c = 0$), processes 14,19	59
13.8	$W + b\bar{b}$ production, processes 20,25	60
13.9	$W + b\bar{b}$ production ($m_b = 0$), processes 21,26	60
13.10	$W + 2$ jets production, processes 22,27	60
13.11	$W + 3$ jets production, processes 23,28	61
13.12	$W + b\bar{b}$ + jet production ($m_b = 0$), processes 24,29	61
13.13	Z -boson production, processes 31–33	61
13.14	Z -boson production decaying to jets, processes 34–35	61
13.15	$t\bar{t}$ production mediated by Z/γ^* -boson exchange, process 36	62
13.16	Lepton pair production through photonic initial states, process 310	62
13.17	Z + jet production, processes 41–43	62
13.18	$Z + 2$ jets production, processes 44, 46	62
13.19	$Z + 3$ jets production, processes 45, 47	63
13.20	$Z + b\bar{b}$ production, $m_b \neq 0$, process 50	63
13.21	$Z + b\bar{b}$ production ($m_b = 0$), processes 51–53	63
13.22	$Z + b\bar{b}$ + jet production ($m_b = 0$), process 54	63
13.23	$Z + c\bar{c}$ production ($m_c = 0$), process 56	64
13.24	Di-boson production, processes 61–89	64
13.24.1	WW production, processes 61–65, 69	64
13.24.2	WZ production, processes 71–80	65
13.24.3	WZ with interference, processes 711 and 761	65
13.24.4	ZZ production, processes 81–84, 90	65
13.24.5	Anomalous WWZ	66
13.24.6	$WW+ZZ$ interfering, process 8211	66
13.25	WH production, processes 91–100, 900	67
13.26	ZH production, processes 101–110	67
13.27	Higgs production, ($m_t = \infty$), processes 111–121	68
13.28	$H \rightarrow W^+W^-$ production, ($m_t = \text{finite}$), processes 123–127	68
13.29	$H \rightarrow ZZ \rightarrow e^-e^+\mu^-\mu^+$ production, ($m_t = \text{finite}$), processes 128–133	69

13.30 $e^-e^+\nu_e\bar{\nu}_e$ production, processes 1281, 1311, 1321	70
13.31 $e^-e^+\nu\bar{\nu}$ production, processes 1282, 1312, 1322	70
13.32 $H + b$ production, processes 136–138	70
13.33 $t\bar{t}$ production with 2 semi-leptonic decays, processes 141–145	71
13.34 $t\bar{t}$ production with decay and a gluon, process 143	71
13.35 $t\bar{t}$ production with one hadronic decay, processes 146–151	72
13.36 $Q\bar{Q}$ production, processes 157–159	72
13.37 $t\bar{t}$ + jet production, process 160	72
13.38 Single-top-quark production and decay at NNLO, process 1610	72
13.39 Single-top-quark production and decay at NNLO, process 1650	75
13.40 Off-shell single top production in SM and SMEFT, processes 164,169	75
13.41 Wt production, processes 180–187	76
13.42 Di-jet production, processes 190–191	77
13.43 H + jet production, $m_t = \text{finite}$, process 200	77
13.44 H + jet production, processes 201–210	78
13.44.1 $m_t = \text{finite}$, 201,202,206,207	78
13.44.2 $m_t = \infty$, 203,204,208,209,210	78
13.45 Higgs production via WBF, processes 211–217	78
13.46 $e^-e^+\nu_\mu\bar{\nu}_\mu$ -pair production via WBF, processes 220,2201,222,2221	79
13.47 $\tau^+\tau^-$ production, process 221	79
13.48 $\nu_e e^+ \mu^- \mu^+$ -pair production via WBF, processes 223,2231	79
13.49 $e^- \bar{\nu}_e \nu_\mu \mu^+$ -pair production via WBF, processes 224,2241	79
13.50 $e^- \bar{\nu}_e \mu^- \mu^+$ -pair production via WBF, processes 225,2251	79
13.51 $e^- e^+ \bar{\nu}_e \nu_e$ -pair production via WBF, processes 226	80
13.52 $\nu_e e^+ \nu_\mu \mu^+$ -pair production via WBF, processes 228,2281	80
13.53 $e^- \bar{\nu}_e \mu^- \bar{\nu}_\mu$ -pair production via WBF, processes 229,2291	80
13.54 t -channel single top with an explicit b -quark, processes 231–240	80
13.55 W^+W^+ +jets production, processes 251,252	81
13.56 $WZ + 2$ jet production, process 253-254	81
13.57 $WZ + b +$ jet production, process 255-256	81
13.58 $WZ + 2b$ production, process 259-260	81
13.59 $Z + Q$ production, processes 261–267	81
13.60 Higgs+2 jet, processes 269	82
13.61 $H + 2$ jet production, ($m_t = \infty$), processes 270–274	82
13.62 $H + 3$ jet production, ($m_t = \infty$), processes 275-279	82
13.63 Direct γ production, processes 280–282	82
13.64 Direct $\gamma +$ heavy flavour production, processes 283–284	83
13.65 $g(-p_1) + g(-p_2) \rightarrow \gamma(p_3) + \gamma(p_4)$	83
13.66 $g(-p_1) + g(-p_2) \rightarrow \gamma(p_3) + \gamma(p_4)$, (top loops at LO)	83
13.67 Diphoton production	83
13.68 Transverse momentum resummation	84
13.69 $g(-p_1) + g(-p_2) \rightarrow \gamma(p_3) + \gamma(p_4) + f(p_5)$	84
13.70 $\gamma\gamma$ +jet production, process 286	84
13.71 $\gamma\gamma\gamma$ production, process 287	85
13.72 $\gamma\gamma\gamma\gamma$ production, process 289	85
13.73 $W\gamma$ production, processes 290-299, 2941, 2991	86
13.73.1 Anomalous $WW\gamma$ couplings	86

13.74	$Z\gamma$, production, processes 300, 305	87
13.74.1	Anomalous $ZZ\gamma$ and $Z\gamma\gamma$ couplings	87
13.75	$Z\gamma\gamma$ production processes, 301, 306	88
13.76	$Z\gamma j$, production, processes 302, 307	88
13.77	$Z\gamma\gamma j$ and $Z\gamma jj$, 303, 304, 308 and 309	88
13.78	$W + Q$ + jet production processes 311–326	89
13.79	$W + c$ + jet production, processes 331, 336	89
13.80	$Z + Q$ +jet production, processes 341–357	89
13.81	$c\bar{s} \rightarrow W^+$, processes 361–363	90
13.82	$W\gamma\gamma$ production, processes 370–371	90
13.83	$W + Q$ production in the 4FNS, processes 401–408	90
13.84	$W + Q$ production in the 5FNS, processes 411, 416	91
13.85	$W + Q$ production in combined 4FNS/5FNS, processes 421, 426	91
13.86	$W + b\bar{b}$ + jet production, processes 431,436	91
13.87	Diboson+jet production, processes 461–487	91
13.88	$W + t\bar{t}$ processes 500–516	92
13.89	$Zt\bar{t}$ production, processes 529–533	92
13.90	Ht and $H\bar{t}$ production, processes 540–557	92
13.91	Zt and $Z\bar{t}$ production, processes 560–569	93
13.92	HH production, processes 601–602	93
13.93	WH production, process 609	93
13.94	Associated production of WH and a jet, processes 610–618	94
13.95	Associated production of ZH and a jet, processes 620–623	94
13.96	$Ht\bar{t}$ production, processes 640–667	94
14	New features in MCFM-10	94
14.1	Downloads of earlier versions, MCFM-10	94
14.2	New features in MCFM-10.2	95
14.3	New features in MCFM-10.0	95
15	New features in MCFM-9	96
15.1	Download of MCFM-9	96
15.2	Description of MCFM-9	96
16	Versions prior to MCFM-9	102
16.1	MCFM-8	102
16.2	MCFM-7	102
16.3	MCFM-6	103
16.4	MCFM-5 and before	104

Contents

1 Overview of MCFM

MCFM is a parton-level Monte Carlo program that gives predictions for a wide range of processes at hadron colliders. Almost all processes are available at NLO, but some processes are also available at NNLO or N³LO in QCD. The calculation of some processes can also account for NLO electroweak effects. Transverse momentum and jet veto resummation is available for the production of color singlet final states. Please look at the [list of available processes](#). Thanks to [htlatex](#) this document is available as a [series of webpages](#) and as a [pdf file](#).

1.1 Download

[MCFM-10.3.tar.gz](#) (January 2023)

Download and changelog for earlier versions of MCFM-10 and MCFM-9 are in sections [14.1](#) and [15.1](#) respectively. Versions prior to MCFM9 are available in section [16](#).

1.2 Documentation

Also relevant is the full [list of processes](#) (with links to web-pages for every process), where examples of input files can be found.

2 Installation and directories

2.1 Installation

The external requirements for (CuTe-)MCFM are `cmake` (≥ 3.13) and `gcc/g++/gfortran` (≥ 7).

Optional external dependencies are LHAPDF (6.2.X or 6.5.X) and an MPI implementation (we recommend OpenMPI) or Coarrays implementation

By default MCFM is bundled with LHAPDF 6.5.1. It can optionally be compiled with an external LHAPDF installation. Note that LHAPDF 6.3.X has a multithreading bug and therefore we do not recommend to use it. Either use LHAPDF 6.2.X or 6.5.X. Version 5 of LHAPDF is not supported.

The MCFM package may be downloaded from the MCFM homepage at <https://mcfm.fnal.gov>. After extracting, in the simplest case, the source can be compiled by running `cmake ..` in the Bin directory:

```
tar -xzf MCFM-X.Y.tar.gz
cd MCFM-X.Y/Bin
```

To compile with default options just run `cmake ..` in the Bin directory or a new “build” directory, then run `make` to compile the MCFM program. If you compile in a directory different than “Bin”, please run `make install` to copy some required files over from the Bin directory. The Bin directory contains several example input files that can be used as an argument to `mcfm`.

By default all necessary dependencies, including LHAPDF, are compiled with the default compiler that `cmake` detects. The following parameters can be added to choose a custom compiler. For example with MPI the wrapper `mpifort` will have to be chosen as the Fortran compiler:

```
-DCMAKE_C_COMPILER=gcc-8
-DCMAKE_CXX_COMPILER=g++-8
-DCMAKE_Fortran_COMPILER=gfortran-8
```

Please ensure that your compiler is working and can produce executable program files. Please also ensure that it is at least version 7 (e.g. `gfortran -version`). For example when your compiler has been installed into a non-standard location you probably need to append the compiler library path to `LD_LIBRARY_PATH` (`DYLD_FALLBACK_LIBRARY_PATH` on OS X). This can be achieved, for example, as follows:

```
export LD_LIBRARY_PATH=${LD_LIBRARY_PATH}:/home/user/local/lib/gcc7
```

Additional complications may arise especially on OS X systems, where by default `gcc/g++` is linked to the clang compiler. Please make sure to set the compiler names/paths to the correct GNU versions.

If CMake does not report any problems you can start the compilation of MCFM with `make -j4`, where 4 (or more) is the number of compilation threads.

Upon successful compilation, the executable `mcfm` is produced and can be called with an input file (+path) as argument, for example:

```
./mcfm input_Z.ini
```

It can happen that the CMake cache gets corrupted with wrong configuration options. If you change options and errors occur, please try to delete the file `CMakeCache.txt` and directory `CMakeFiles` and restart `cmake ..` with the appropriate arguments.

2.1.1 Compiling at Fermilab

To compile at Fermilab on the Wilson cluster (`wc.fnal.gov`):

```
cd MCFM-10.3/Bin/
cmake -DCMAKE_Fortran_COMPILER=gfortran -DCMAKE_C_COMPILER=gcc -DCMAKE_CXX_COMPILER=g++ ..
make -j
```

2.1.2 Compiling at CERN

On the lxplus machine at CERN (lxplus.cern.ch):

```
cd MCFM-10.3/Bin/  
cmake3 -DCMAKE_Fortran_COMPILER=gfortran -DCMAKE_C_COMPILER=gcc -DCMAKE_CXX_COMPILER=g++  
make -j
```

2.1.3 LHAPDF

The following parameter specifies the use of LHAPDF (internal, external):

```
-Duse_internal_lhapdf=ON (default)
```

and can be set to OFF to link against an external LHAPDF library.

When an external LHAPDF is used, cmake might not find the library. A library search path can be added with `-DCMAKE_PREFIX_PATH=/usr/local`, for example. Additionally, the LHAPDF include path can be set with `-Dlhpdf_include_path=/usr/local/include` if it deviates from a standard location.

For the bundled LHAPDF, PDF sets go into the directory `Bin/PDFs`. This installation includes the central PDF members of CT18NNLO and NNPDF31_nnlo_as_0118 with their resummation grids, as well as the PDF sets for LUXqed17_plus_PDF4LHC15_nnlo_30. Additional PDFs can be downloaded from <https://lhpdf.hepforge.org/pdfsets.html> and untar'ed in the PDFs directory.

Additional PDF directories can be added to the LHAPDF search path by using, for example:

```
export LHAPDF_DATA_PATH=/usr/local/share/LHAPDF
```

2.1.4 WW, WZ and ZZ with VVamp

The processes WW,WZ and ZZ at NNLO require compilation of the VVamp amplitudes, which are about 100MB of additional sourcecode and add significant additional compilation time. The following flag disables these amplitudes:

```
-Dwith_vvamp=OFF
```


2.1.5 OpenMP and MPI

MCFM uses OMP (Open Multi-Processing) to implement multi-threading and automatically adjusts to the number of available CPU threads. The multi-threading is implemented with respect to the integration routine Vegas, which distributes the event evaluations over the threads and combines all events at the end of every iteration.

Two environment variables are useful. On some systems, depending on the OMP implementation, the program will crash when calculating some of the more complicated processes, for example $W + 2$ jet production at NLO. Then, adjusting `OMP_STACKSIZE` may be needed for the program to run correctly. Setting this variable to 16000, for instance in the Bash shell by using the command `export OMP_STACKSIZE=16000`, has been found to be sufficient for all processes. The second useful variable `OMP_NUM_THREADS` may be used to directly control the number of threads used during OMP execution (the default is the maximum number of threads available on the system).

To prepare MCFM with MPI support add the argument `-Duse_mpi=ON` to the cmake call before running `make`. At the same time custom compiler command names must be specified with:

```
-DCMAKE_C_COMPILER=mpicc
-DCMAKE_CXX_COMPILER=mpic++
-DCMAKE_Fortran_COMPILER=mpifort
```

Such commands must be used when compiling with MPI support and their names can depend on the MPI implementation. Please consult the manual of your MPI installation or cluster system. Please ensure again that `mpifort -version` and `mpic++ -version` report the GNU compiler and a version greater than 7.

Alternatively also a Fortran Coarray implementation can be used with:

```
-Duse_coarray=ON
```

This option is experimental and cannot be used together with MPI.

2.2 Directory structure

The directory structure of MCFM is as follows:

- **Doc.** The source for this document.
- **Bin.** The directory containing the executable `mcfm`, and various essential files – notably the options file `input.ini`.
- **Bin/Pdfdata.** The directory containing the internal PDF data-files.
- **Bin/PDFs.** Directory for LHAPDF grid files used by bundled LHAPDF.
- **src.** The Fortran source files in various subdirectories.

- `lib/TensorReduction` General tensor reduction code based on the work of Passarino and Veltman [1] and Oldenborgh and Vermaseren [2].
- `lib/qcdloop-2.0.5`. The source files to the library QCDLoop [3, 4].
- `lib/oneloop`. The source files to the library OneLOop [5].
- `lib/qd-2.3.22`. Library to support double-double and quad-double precision data types [6].
- `lib/AMOS`. Library for AMOS, “A Portable Package for Bessel Functions of a Complex Argument and Nonnegative Order”, taken from <http://www.netlib.org/amos/>.
- `lib/SpecialFns`. Library containing the implementation of special functions from a variety of sources.
- `lib/VVamp`. Library containing the implementation of two-loop helicity amplitudes for $q\bar{q} \rightarrow V_1 V_2$, from the results of Ref. [7].
- The `lib/handyG` Library for the evaluation of generalized polylogarithms [8].

2.3 References

The program has been developed over a number of years and results have been presented in a number of published papers. The papers describing the original code and the most significant developments in the NLO implementation are:

- J. M. Campbell and R. K. Ellis,
“An update on vector boson pair production at hadron colliders,”
Phys. Rev. D **60**, 113006 (1999) [arXiv:hep-ph/9905386](#).
- J. M. Campbell, R. K. Ellis and C. Williams,
“Vector boson pair production at the LHC,”
JHEP **1107**, 018 (2011) [arXiv:1105.0020](#) [hep-ph].
- J. M. Campbell, R. K. Ellis and W. Giele,
“A Multi-Threaded Version of MCFM”,
EPJ **C75**, 246 (2015) [arXiv:1503.06182](#) [hep-ph].

As of **v8.0** MCFM can also compute selected color-singlet processes through NNLO in QCD perturbation theory. The processes available at this precision, as well as benchmark numbers, are detailed in Section 8. When using MCFM 8.0 or newer for NNLO calculations please refer to:

- R. Boughezal, J. M. Campbell, R. K. Ellis,
C. Focke, W. Giele, X. Liu, F. Petriello and C. Williams,
“Color singlet production at NNLO in MCFM”, [arXiv:1605.08011](#).

A significant overhaul of MCFM was undertaken in **v9.0** of MCFM. If you use this version or newer please cite

- John M. Campbell and Tobias Neumann,
“Precision Phenomenology with MCFM”, [arXiv:1909.09117](#)

Version **10.0** includes SCET-based q_T resummation and is called CuTe-MCFM when this feature is used. When you use the q_T resummation please cite

- Thomas Becher and Tobias Neumann,
“Fiducial q_T^2 resummation of color-singlet processes at $N^3LL+NNLO$ ”, [arXiv:2009.11437](#)

The manual for the resummation functionality can be found in `cute-mcfm.pdf`.

Version **10.1** includes a C++ interface to many of the 1-loop matrix elements included in the code. When you use this functionality please cite

- John M. Campbell, Stefan Höche and Christian T. Preuss,
Accelerating LHC phenomenology with analytic one-loop amplitudes: A C++ interface to MCFM, [arXiv:2107.04472](#)

A guide to the structure of the interface is included in this paper.

Version **10.2** includes a more complete treatment of color singlet production processes at NNLO, especially colour singlet processes involving pairs of bosons.

- John M. Campbell, R. Keith Ellis and Satyajit Seth,
“Non-local slicing approaches for NNLO QCD in MCFM”, [arXiv:2202.07738](#) [hep-ph]

3 New features in version 10.3

- Calculation of Z production at N^3LO fixed-order through q_T subtractions and resummation at the level of N^4LL . These calculations include the Z+jet process at NNLO using jettness subtractions. Based on Ref.[9]. Detailed documentation can be found in Section 11.
- Jet veto resummation added for color singlet final states, achieving partial N^3LL accuracy, as described in Ref. [10]. Vetoing energetic jet activity is a crucial tool for suppressing backgrounds and enabling new physics searches at the LHC, but the introduction of a veto scale can introduce large logarithms that may need to be resummed. We present an implementation of jet-veto resummation for color-singlet processes at the level of N^3LL_p matched to fixed-order NNLO predictions. Resummation is implemented for vetos of jet activity in productions of a single boson, such as Z/γ^* , W^\pm or H , or of a pair of vector bosons, such as W^+W^- , $W^\pm Z$ or ZZ . The implementation relies on recent calculations of the soft and beam functions in the presence of a jet veto over all rapidities, with jets defined using a sequential recombination algorithm with jet radius R . However one of the ingredients that is required to reach full N^3LL accuracy is only known approximately, hence N^3LL_p .

Benchmark results, taken from Ref. [10], are detailed in Section 10.

4 Process list

nproc	$f(-p_1) + f(-p_2) \rightarrow \dots$	Order	Cite
1	$W^+(\rightarrow \nu(p_3) + e^+(p_4))$	NNLO	[11]
2	$W^+(\rightarrow \nu(p_3) + e^+(p_4))$ [EW+ $\gamma(p_5)$]	NLO	[12]
3	$W^+(\rightarrow \nu(p_3) + e^+(p_4))$ [EW γ -induced + $q(p_5)$]	NLO	[12]
6	$W^-(\rightarrow e^-(p_3) + \bar{\nu}(p_4))$	NNLO	[11]
7	$W^-(\rightarrow e^-(p_3) + \bar{\nu}(p_4))$ [EW+ $\gamma(p_5)$]	NLO	
8	$W^-(\rightarrow e^-(p_3) + \bar{\nu}(p_4))$ [EW γ -induced + $q(p_5)$]	NLO	
11	$W^+(\rightarrow \nu(p_3) + e^+(p_4)) + f(p_5)$	NLO	
12	$W^+(\rightarrow \nu(p_3) + e^+(p_4)) + b(p_5)$	NLO	
13	$W^+(\rightarrow \nu(p_3) + e^+(p_4)) + \bar{c}(p_5)$	NLO	
14	$W^+(\rightarrow \nu(p_3) + e^+(p_4)) + \bar{c}(p_5)$ [massless]	LO	
16	$W^-(\rightarrow e^-(p_3) + \bar{\nu}(p_4)) + f(p_5)$	NLO	
17	$W^-(\rightarrow e^-(p_3) + \bar{\nu}(p_4)) + \bar{b}(p_5)$	NLO	
18	$W^-(\rightarrow e^-(p_3) + \bar{\nu}(p_4)) + c(p_5)$	NLO	
19	$W^-(\rightarrow e^-(p_3) + \bar{\nu}(p_4)) + c(p_5)$ [massless]	LO	
20	$W^+(\rightarrow \nu(p_3) + e^+(p_4)) + b(p_5) + \bar{b}(p_6)$ [massive b-quarks]	NLO	[13]
21	$W^+(\rightarrow \nu(p_3) + e^+(p_4)) + b(p_5) + \bar{b}(p_6)$	NLO	[14]
22	$W^+(\rightarrow \nu(p_3) + e^+(p_4)) + f(p_5) + f(p_6)$	NLO	[15–17]
23	$W^+(\rightarrow \nu(p_3) + e^+(p_4)) + f(p_5) + f(p_6) + f(p_7)$	LO	[15, 16]
24	$W^+(\rightarrow \nu(p_3) + e^+(p_4)) + b(p_5) + \bar{b}(p_6) + f(p_7)$ [massless b-quarks]	LO	
25	$W^-(\rightarrow e^-(p_3) + \bar{\nu}(p_4)) + b(p_5) + \bar{b}(p_6)$ [massive b-quarks]	NLO	[13]
26	$W^-(\rightarrow e^-(p_3) + \bar{\nu}(p_4)) + b(p_5) + \bar{b}(p_6)$	NLO	[14]
27	$W^-(\rightarrow e^-(p_3) + \bar{\nu}(p_4)) + f(p_5) + f(p_6)$	NLO	[15–17]
28	$W^-(\rightarrow e^-(p_3) + \bar{\nu}(p_4)) + f(p_5) + f(p_6) + f(p_7)$	LO	[15, 16]
29	$W^-(\rightarrow e^-(p_3) + \bar{\nu}(p_4)) + b(p_5) + \bar{b}(p_6) + f(p_7)$ [massive b-quarks]	LO	
31	$Z(\rightarrow e^-(p_3) + e^+(p_4))$	NNLO	[11]
310	$\gamma(-p_1) + \gamma(-p_2) \rightarrow e^-(p_3) + e^+(p_4)$ [photon induced]	LO	
32	$Z(\rightarrow 3 \times (\nu(p_3) + \bar{\nu}(p_4)))$	NNLO	[11]
33	$Z(\rightarrow b(p_3) + \bar{b}(p_4))$	NLO	
34	$Z(\rightarrow 3 \times (d(p_5) + \bar{d}(p_6)))$	NLO	
35	$Z(\rightarrow 2 \times (u(p_5) + \bar{u}(p_6)))$	NLO	
36	$Z \rightarrow t(\rightarrow \nu(p_3) + e^+(p_4) + b(p_5)) + \bar{t}(\rightarrow \bar{b}(p_6) + e^-(p_7) + \bar{\nu}(p_8))$	LO	
41	$Z(\rightarrow e^-(p_3) + e^+(p_4)) + f(p_5)$	NLO	
42	$Z_0(\rightarrow 3 \times (\nu(p_3) + \bar{\nu}(p_4))) + f(p_5)$	NLO	
43	$Z(\rightarrow b(p_3) + \bar{b}(p_4)) + f(p_5)$	NLO	
44	$Z(\rightarrow e^-(p_3) + e^+(p_4)) + f(p_5) + f(p_6)$	NLO	[15–17]
45	$Z(\rightarrow e^-(p_3) + e^+(p_4)) + f(p_5) + f(p_6) + f(p_7)$	LO	
46	$Z(\rightarrow 3 \times (\nu(p_3) + \bar{\nu}(p_4)) + f(p_5) + f(p_6)$	NLO	[15–17]
47	$Z(\rightarrow 3 \times (\nu(p_3) + \bar{\nu}(p_4)) + f(p_5) + f(p_6) + f(p_7)$	LO	

50	$Z(\rightarrow e^-(p_3) + e^+(p_4)) + \bar{b}(p_5) + b(p_6)$ [massive b-quark]	LO	[18]
51	$Z(\rightarrow e^-(p_3) + e^+(p_4)) + b(p_5) + \bar{b}(p_6)$ [massless b-quark]	NLO	[18]
52	$Z_0(\rightarrow 3 \times (\nu(p_3) + \bar{\nu}(p_4))) + b(p_5) + \bar{b}(p_6)$ [massless b-quark]	NLO	[18]
53	$Z(\rightarrow b(p_3) + \bar{b}(p_4)) + b(p_5) + \bar{b}(p_6)$ [massless b-quark]	NLO	[18]
54	$Z(\rightarrow e^-(p_3) + e^+(p_4)) + b(p_5) + \bar{b}(p_6) + f(p_7)$	LO	
56	$Z(\rightarrow e^-(p_3) + e^+(p_4)) + c(p_5) + \bar{c}(p_6)$	NLO	
61	$W^+(\rightarrow \nu(p_3) + \mu^+(p_4)) + W^-(\rightarrow e^-(p_5) + \bar{\nu}(p_6))$	NNLO	[11, 19, 20]
62	$W^+(\rightarrow \nu(p_3) + \mu^+(p_4)) + W^-(\rightarrow q(p_5) + \bar{q}(p_6))$	NLO	
63	$W^+(\rightarrow \nu(p_3) + \mu^+(p_4)) + W^-(\rightarrow q(p_5) + \bar{q}(p_6))$ [rad.in.dk]	NLO	
64	$W^-(\rightarrow e^-(p_3) + \bar{\nu}(p_4))W^+(\rightarrow q(p_5) + \bar{q}(p_6))$	NLO	
65	$W^-(\rightarrow e^-(p_3) + \bar{\nu}(p_4))W^+(\rightarrow q(p_5) + \bar{q}(p_6))$ [rad.in.dk]	NLO	
69	$W^+(\rightarrow \nu(p_3) + \mu^+(p_4)) + W^-(\rightarrow e^-(p_5) + \bar{\nu}(p_6))$ [no pol]	LO	
71	$W^+(\rightarrow \nu(p_3) + e^+(p_4)) + Z(\rightarrow \mu^-(p_5) + \mu^+(p_6))$	NNLO	[11, 19, 20]
711	$W^+(\rightarrow \nu(p_3) + e^+(p_4)) + Z(\rightarrow e^-(p_5) + e^+(p_6))$	NNLO	[11, 19, 20]
72	$W^+(\rightarrow \nu(p_3) + e^+(p_4)) + Z(\rightarrow 3 \times (\nu_\mu(p_5) + \bar{\nu}_\mu(p_6)))$	NLO	
73	$W^+(\rightarrow \nu(p_3) + e^+(p_4)) + Z(\rightarrow b(p_5) + \bar{b}(p_6))$	NLO	
74	$W^+(\rightarrow \nu(p_3) + e^+(p_4)) + Z(\rightarrow 3 \times (d(p_5) + \bar{d}(p_6)))$	NLO	
75	$W^+(\rightarrow \nu(p_3) + e^+(p_4)) + Z(\rightarrow 2 \times (u(p_5) + \bar{u}(p_6)))$	NLO	
76	$W^-(\rightarrow e^-(p_3) + \bar{\nu}(p_4)) + Z(\rightarrow \mu^-(p_5) + \mu^+(p_6))$	NNLO	[11, 19, 20]
761	$W^-(\rightarrow e^-(p_3) + \bar{\nu}(p_4)) + Z(\rightarrow e^-(p_5) + e^+(p_6))$	NNLO	[11, 19, 20]
77	$W^-(\rightarrow e^-(p_3) + \bar{\nu}(p_4)) + Z(\rightarrow 3 \times (\nu_e(p_5) + \bar{\nu}_e(p_6)))$	NLO	[19, 20]
78	$W^-(\rightarrow e^-(p_3) + \bar{\nu}(p_4)) + Z(\rightarrow b(p_5) + \bar{b}(p_6))$	NLO	[19, 20]
79	$W^-(\rightarrow e^-(p_3) + \bar{\nu}(p_4)) + Z(\rightarrow 3 \times (d(p_5) + \bar{d}(p_6)))$	NLO	[19, 20]
80	$W^-(\rightarrow e^-(p_3) + \bar{\nu}(p_4)) + Z(\rightarrow 2 \times (u(p_5) + \bar{u}(p_6)))$	NLO	[19, 20]
81	$Z(\rightarrow e^-(p_3) + e^+(p_4)) + Z(\rightarrow \mu^-(p_5) + \mu^+(p_6))$	NNLO	[11, 19, 20]
82	$Z(\rightarrow e^-(p_3) + e^+(p_4)) + Z(\rightarrow \nu_\mu(p_5) + \bar{\nu}_\mu(p_6))$	NNLO	[11, 19, 20]
8211	$Z(\rightarrow e^-(p_3) + e^+(p_4)) + Z(\rightarrow \nu_e(p_5) + \bar{\nu}_e(p_6))$ [both $WW + ZZ$]	NNLO	[11, 19, 20]
83	$Z(\rightarrow e^-(p_3) + e^+(p_4)) + Z(\rightarrow b(p_5) + \bar{b}(p_6))$	NLO	[19, 20]
84	$Z(\rightarrow b(p_3) + \bar{b}(p_4)) + Z(\rightarrow 3 \times (\nu(p_5) + \bar{\nu}(p_6)))$	NLO	[19, 20]
90	$Z(\rightarrow e^-(p_3) + e^+(p_4)) + Z(\rightarrow e^-(p_5) + e^+(p_6))$	NLO	[11, 19–21]
900	$(W^+ + W^-) + H(\rightarrow \tau(p_5) + \bar{\tau}(p_6))$	NNLO	[11, 22]
91	$W^+(\rightarrow \nu(p_3) + e^+(p_4)) + H(\rightarrow \tau(p_5) + \bar{\tau}(p_6))$	NNLO	[11, 22]
92	$W^+(\rightarrow \nu(p_3) + e^+(p_4)) + H(\rightarrow b(p_5) + \bar{b}(p_6))$	NNLO	[11, 22]
920	$W^+(\rightarrow \nu(p_3) + e^+(p_4)) + H(\rightarrow b(p_5) + \bar{b}(p_6))$ [rad.in.dk]	NLO	
93	$W^+(\rightarrow \nu(p_3) + e^+(p_4)) + H(\rightarrow \gamma(p_5) + \gamma(p_6))$	NNLO	[11, 22]
94	$W^+(\rightarrow \nu(p_3) + e^+(p_4)) + H(\rightarrow W^+(\nu(p_5), e^+(p_6))W^-(e^-(p_7), \bar{\nu}(p_8)))$	NNLO	[11, 22]
95	$W^+(\rightarrow \nu(p_3) + e^+(p_4)) + H(\rightarrow Z(e^-(p_5), e^+(p_6)) + Z(\mu^-(p_7), \mu(p_8)))$	NNLO	[11, 22]
96	$W^-(\rightarrow e^-(p_3) + \bar{\nu}(p_4)) + H(\rightarrow \tau(p_5) + \bar{\tau}(p_6))$	NNLO	[11, 22]
97	$W^-(\rightarrow e^-(p_3) + \bar{\nu}(p_4)) + H(\rightarrow b(p_5) + \bar{b}(p_6))$	NNLO	[11, 22]
970	$W^-(\rightarrow e^-(p_3) + \bar{\nu}(p_4)) + H(\rightarrow b(p_5) + \bar{b}(p_6))$ [rad.in.dk]	NLO	
98	$W^-(\rightarrow e^-(p_3) + \bar{\nu}(p_4)) + H(\rightarrow \gamma(p_5) + \gamma(p_6))$	NNLO	
99	$W^-(\rightarrow e^-(p_3) + \bar{\nu}(p_4)) + H(\rightarrow W^+(\nu(p_5), e^+(p_6))W^-(e^-(p_7), \bar{\nu}(p_8)))$	NNLO	[11, 22]
100	$W^-(\rightarrow e^-(p_3) + \bar{\nu}(p_4)) + H(\rightarrow Z(e^-(p_5), e^+(p_6)) + Z(\mu^-(p_7), \mu^+(p_8)))$	NNLO	[11, 22]

101	$Z(\rightarrow e^-(p_3) + e^+(p_4)) + H(\rightarrow b(p_5) + \bar{b}(p_6))$	NNLO	[11, 2]
1010	$Z(\rightarrow e^-(p_3) + e^+(p_4)) + H(\rightarrow b(p_5) + \bar{b}(p_6))[\text{rad.in.dk}]$	NLO	[22]
102	$Z(\rightarrow 3 \times (\nu(p_3) + \bar{\nu}(p_4))) + H(\rightarrow b(p_5) + \bar{b}(p_6))$	NLO	[22]
103	$Z(\rightarrow b(p_3) + \bar{b}(p_4)) + H(\rightarrow b(p_5) + \bar{b}(p_6))$	NLO	[22]
104	$Z(\rightarrow e^-(p_3) + e^+(p_4)) + H(\rightarrow \gamma(p_5) + \gamma(p_6))$	NNLO	[11, 2]
105	$Z(\rightarrow 3 \times (\nu(p_3) + \bar{\nu}(p_4))) + H(\rightarrow \gamma(p_5) + \gamma(p_6))$	NLO	[11, 2]
106	$Z(\rightarrow e^-(p_3) + e^+(p_4)) + H(\rightarrow W^+(\nu(p_5), e^+(p_6))W^-(e^-(p_7), \bar{\nu}(p_8)))$	NNLO	[11, 2]
107	$Z(\rightarrow 3 \times (\nu(p_3) + \bar{\nu}(p_4))) + H(\rightarrow W^+(\nu(p_5), e^+(p_6))W^-(e^-(p_7), \bar{\nu}(p_8)))$	NLO	[22]
108	$Z(\rightarrow b(p_3) + \bar{b}(p_4)) + H(\rightarrow W^+(\nu(p_5), e^+(p_6))W^-(e^-(p_7), \bar{\nu}(p_8)))$	NLO	[22]
109	$Z(\rightarrow e^-(p_3) + e^+(p_4)) + H(\rightarrow Z(e^-(p_5), e^+(p_6)) + Z(\rightarrow \mu^-(p_7), \mu^+(p_8)))$	NLO	[22]
110	$Z(\rightarrow e^-(p_3) + e^+(p_4)) + H(\rightarrow \tau^-(p_5)\tau^+(p_6))$	NNLO	[11, 2]
111	$H(\rightarrow b(p_3) + \bar{b}(p_4))$	NNLO	[11, 2]
112	$H(\rightarrow \tau^-(p_3) + \tau^+(p_4))$	NNLO	[11, 2]
113	$H(\rightarrow W^+(\nu(p_3) + e^+(p_4)) + W^-(e^-(p_5) + \bar{\nu}(p_6)))$	NLO	
114	$H(\rightarrow W^+(\nu(p_3) + e^+(p_4)) + W^-(q(p_5) + \bar{q}(p_6)))$	NLO	
115	$H(\rightarrow W^+(\nu(p_3) + e^+(p_4)) + W^-(q(p_5) + \bar{q}(p_6)))[\text{rad.in.dk}]$	NLO	
116	$H(\rightarrow Z(\rightarrow e^-(p_3) + e^+(p_4)) + Z(\rightarrow \mu^-(p_5) + \mu^+(p_6)))$	NLO	
117	$H(\rightarrow Z(\rightarrow 3 \times (\nu(p_3) + \bar{\nu}(p_4))) + Z(\rightarrow \mu^-(p_5) + \mu^+(p_6)))$	NLO	
118	$H(\rightarrow Z(\rightarrow \mu^-(p_3) + \mu^+(p_4)) + Z(\rightarrow b(p_5) + \bar{b}(p_6)))$	NLO	
119	$H(\rightarrow \gamma(p_3) + \gamma(p_4))$	NNLO	[11, 2]
120	$H(\rightarrow Z(\rightarrow \mu^-(p_3) + \mu^+(p_4)) + \gamma(p_5))$	NLO	
121	$H(\rightarrow Z(\rightarrow 3 \times (\nu(p_3) + \bar{\nu}(p_4)))) + \gamma(p_5))$	NLO	
123	$H(\rightarrow W^+(\nu(p_3) + e^+(p_4)) + W^-(e^-(p_5) + \bar{\nu}(p_6)))$ [t, b loops, exact]	LO	[23, 2]
124	$H(\rightarrow W^+(\nu(p_3) + e^+(p_4)) + W^-(e^-(p_5) + \bar{\nu}(p_6)))$ [only H, gg→WW int]	LO	[23, 2]
125	$H(\rightarrow W^+(\nu(p_3) + e^+(p_4)) + W^-(e^-(p_5) + \bar{\nu}(p_6)))$ [$ H ^2$ and H,gg→WW int]	LO	[23, 2]
126	$W^+(\nu(p_3) + e^+(p_4)) + W^-(e^-(p_5) + \bar{\nu}(p_6))$ [gg only, (H + gg→WW) squared]	LO	[23, 2]
127	$W^+(\nu(p_3) + e^+(p_4)) + W^-(e^-(p_5) + \bar{\nu}(p_6))$ [(gg→WW squared)]	LO	[23, 2]
128	$H(\rightarrow Z(\rightarrow e^-(p_3) + e^+(p_4)) + Z(\rightarrow \mu^-(p_5) + \mu^+(p_6)))$ [t, b loops, exact]	LO	[25]
129	$H(\rightarrow Z(\rightarrow e^-(p_3) + e^+(p_4)) + Z(\rightarrow \mu^-(p_5) + \mu^+(p_6)))$ [only H, gg→ZZ int]	LO	[25]
130	$H(\rightarrow Z(\rightarrow e^-(p_3) + e^+(p_4)) + Z(\rightarrow \mu^-(p_5) + \mu^+(p_6)))$ [$ H ^2$ and H,gg→ZZ int]	LO	[25]
131	$Z(\rightarrow e^-(p_3) + e^+(p_4)) + Z(\rightarrow \mu^-(p_5) + \mu^+(p_6))$ [gg only, $ H + gg \rightarrow ZZ ^2$]	LO	[25]
132	$Z(\rightarrow e^-(p_3) + e^+(p_4)) + Z(\rightarrow \mu^-(p_5) + \mu^+(p_6))$ [(gg→ZZ) squared]	LO	[25]
133	$Z(\rightarrow e^-(p_3) + e^+(p_4)) + Z(\rightarrow \mu^-(p_5) + \mu^+(p_6) + f(p_7))$ [intf with SM, no cut on p7]	LO	[25]
1281	$H(\rightarrow e^-(p_3) + e^+(p_4)\nu_e(p_5) + \bar{\nu}_e(p_6))$ [top, bottom loops, exact]	LO	
1311	$e^-(p_3) + e^+(p_4) + \nu_e(p_5) + \bar{\nu}_e(p_6)$ [gg only, (H + gg→ZZ) squared]	LO	
1321	$e^-(p_3) + e^+(p_4) + \nu_e(p_5) + \bar{\nu}_e(p_6)$ [(gg→ZZ) squared]	LO	
1282	$H(\rightarrow e^-(p_3) + e^+(p_4) + \nu(p_5) + \bar{\nu}(p_6))$ [top, bottom loops, exact]	LO	
1312	$e^-(p_3) + e^+(p_4) + \nu(p_5) + \bar{\nu}(p_6)$ [gg only, (H + gg→ZZ) squared]	LO	
1322	$e^-(p_3) + e^+(p_4) + \nu(p_5) + \bar{\nu}(p_6)$ [(gg→ZZ) squared]	LO	
133	$H(\rightarrow Z(\rightarrow e^-(p_3) + e^+(p_4)) + Z(\rightarrow \mu^-(p_5) + \mu^+(p_6) + f(p_7)))$ [intf,no p7 cut]	LO	[26]

136	$H(\rightarrow b(p_3) + \bar{b}(p_4)) + b(p_5)(+g(p_6))$	NLO	[27]
137	$H(\rightarrow b(p_3) + \bar{b}(p_4)) + \bar{b}(p_5)(+b(p_6))$	(REAL)	
138	$H(\rightarrow b(p_3) + \bar{b}(p_4)) + b(p_5) + \bar{b}(p_6)$ [both observed]	(REAL)	
141	$t(\rightarrow \nu(p_3) + e^+(p_4) + b(p_5)) + \bar{t}(\rightarrow \bar{b}(p_6) + e^-(p_7) + \bar{\nu}(p_8))$	NLO	[28, 29]
142	$t(\rightarrow \nu(p_3) + e^+(p_4) + b(p_5)) + \bar{t}(\rightarrow \bar{b}(p_6) + e^-(p_7) + \bar{\nu}(p_8))$ [rad.in.dk]	NLO	[28]
143	$t(\rightarrow \nu(p_3) + e^+(p_4) + b(p_5)) + \bar{t}(\rightarrow \bar{b}(p_6) + e^-(p_7) + \bar{\nu}(p_8)) + f(p_9)$	LO	[28]
144	$t(\rightarrow \nu(p_3) + e^+(p_4) + b(p_5)) + \bar{t}(\rightarrow \bar{b}(p_6) + e^-(p_7) + \bar{\nu}(p_8))$ (uncorr)	NLO	
145	$t(\rightarrow \nu(p_3) + e^+(p_4) + b(p_5)) + \bar{t}(\rightarrow \bar{b}(p_6) + e^-(p_7) + \bar{\nu}(p_8))$ [rad.in.dk],uncorr	NLO	
146	$t(\rightarrow \nu(p_3) + e^+(p_4) + b(p_5)) + \bar{t}(\rightarrow \bar{b}(p_6) + q(p_7) + \bar{q}(p_8))$	NLO	[28]
147	$t(\rightarrow \nu(p_3) + e^+(p_4) + b(p_5)) + \bar{t}(\rightarrow \bar{b}(p_6) + q(p_7) + \bar{q}(p_8))$ [rad.in.top.dk]	NLO	[28]
148	$t(\rightarrow \nu(p_3) + e^+(p_4) + b(p_5)) + \bar{t}(\rightarrow \bar{b}(p_6) + q(p_7) + \bar{q}(p_8))$ [rad.in.W.dk]	NLO	[28]
149	$t(\rightarrow q(p_3) + \bar{q}(p_4) + b(p_5)) + \bar{t}(\rightarrow \bar{b}(p_6) + e^-(p_7) + \bar{\nu}(p_8))$	NLO	[28]
150	$t(\rightarrow q(p_3) + \bar{q}(p_4) + b(p_5)) + \bar{t}(\rightarrow \bar{b}(p_6) + e^-(p_7) + \bar{\nu}(p_8))$ [rad.in.top.dk]	NLO	[28]
151	$t(\rightarrow q(p_3) + \bar{q}(p_4) + b(p_5)) + \bar{t}(\rightarrow \bar{b}(p_6) + e^-(p_7) + \bar{\nu}(p_8))$ [rad.in.W.dk]	NLO	[28]
157	$t\bar{t}$ [for total Xsect]	NLO	[30]
158	$b\bar{b}$ [for total Xsect]	NLO	[30]
159	$c\bar{c}$ [for total Xsect]	NLO	[30]
160	$t\bar{t} + g$ [for total Xsect]	LO	[30]
161	$t(\rightarrow \nu(p_3) + e^+(p_4) + b(p_5)) + q(p_6)$ [t-channel]	NLO	[31, 32]
1610	$t(\rightarrow \nu(p_3) + e^+(p_4) + b(p_5)) + q(p_6)$ [t-channel]	NNLO	[33]
162	$t(\rightarrow \nu(p_3) + e^+(p_4) + b(p_5)) + q(p_6)$ [decay]	NLO	[31]
163	$t(\rightarrow \nu(p_3) + e^+(p_4) + b(p_5)) + q(p_6)$ [t-channel] $mb > 0$	NLO	[31]
164	$t(\rightarrow \nu(p_3) + e^+(p_4) + b(p_5)) + q(p_6)$ [full off-shell t-channel] $mb = 0$	NLO	[31]
1650	$t(\rightarrow \nu(p_3) + e^+(p_4) + b(p_5)) + q(p_6) + g(p_7)$ [t-channel]	NLO	[31]
166	$\bar{t}(\rightarrow e^-(p_3) + \bar{\nu}(p_4) + \bar{b}(p_5)) + q(p_6)$ [t-channel]	NLO	[31]
167	$\bar{t}(\rightarrow e^-(p_3) + \bar{\nu}(p_4) + \bar{b}(p_5)) + q(p_6)$ [rad.in.dk]	NLO	[31]
168	$\bar{t}(\rightarrow e^-(p_3) + \bar{\nu}(p_4) + \bar{b}(p_5)) + q(p_6)$ [t-channel] $mb > 0$	NLO	[31]
169	$\bar{t}(\rightarrow e^-(p_3) + \bar{\nu}(p_4) + \bar{b}(p_5)) + q(p_6)$ [full off-shell t-channel] $mb = 0$	NLO	[31]
171	$t(\rightarrow \nu(p_3) + e^+(p_4) + b(p_5)) + \bar{b}(p_6)$ [s-channel]	NLO	[31]
172	$t(\rightarrow \nu(p_3) + e^+(p_4) + b(p_5)) + \bar{b}(p_6)$ [rad.in.dk]	NLO	[31]
176	$\bar{t}(\rightarrow e^-(p_3) + \bar{\nu}(p_4) + \bar{b}(p_5)) + b(p_6)$ [s-channel]	NLO	[31]
177	$\bar{t}(\rightarrow e^-(p_3) + \bar{\nu}(p_4) + \bar{b}(p_5)) + b(p_6)$ [rad.in.dk]	NLO	[31]
180	$W^-(\rightarrow e^-(p_3) + \bar{\nu}(p_4)) + t(p_5)$	NLO	[34]
181	$W^-(\rightarrow e^-(p_3) + \bar{\nu}(p_4)) + t(\nu(p_5) + e^+(p_6) + b(p_7))$	NLO	[34]
182	$W^-(\rightarrow e^-(p_3) + \bar{\nu}(p_4)) + t(\nu(p_5) + e^+(p_6) + b(p_7))$ [rad.in.dk]	NLO	[34]
183	$W^-(\rightarrow e^-(p_3) + \bar{\nu}(p_4)) + t(\nu(p_5) + e^+(p_6) + b(p_7)) + b(p_8)$	LO	[34]
184	$W^-(\rightarrow e^-(p_3) + \bar{\nu}(p_4)) + t(p_5) + b(p_6)$ [massive b]	LO	[34]
185	$W^+(\rightarrow \nu(p_3) + e^+(p_4)) + \bar{t}(p_5)$	NLO	[34]
186	$W^+(\rightarrow \nu(p_3) + e^+(p_4)) + \bar{t}(e^-(p_5) + \bar{\nu}(p_6) + \bar{b}(p_7))$	NLO	[34]
187	$W^+(\rightarrow \nu(p_3) + e^+(p_4)) + \bar{t}(e^-(p_5) + \bar{\nu}(p_6) + \bar{b}(p_7))$ [rad.in.dk]	NLO	[34]

190	$f(p_3) + f(p_4)$	LO	
191	$f(p_3) + f(p_4)$ [mixed QCD/EW]	NLO	[35]
200	$H + f(p_5)$	NLO	
201	$H(\rightarrow b(p_3) + \bar{b}(p_4)) + f(p_5)$ [full mt dep.]	LO	
2011	$f(p_1) + f(p_2) - - > H(- - > b(p_3) + \bar{b}(p_4)) + f(p_5)$ [scalar loop]	LO	
202	$H(\rightarrow \tau^-(p_3) + \tau^+(p_4)) + f(p_5)$ [full mt dep.]	LO	
203	$H(\rightarrow b(p_3) + \bar{b}(p_4)) + f(p_5), (m_t = \infty)$	NLO	
204	$H(\rightarrow \tau^-(p_3) + \tau^+(p_4)) + f(p_5), (m_t = \infty)$	NLO	
205	$H(\rightarrow Z(\mu^-(p_3) + \mu^+(p_4)) + \gamma(p_5)) + f(p_5), (m_t = \infty)$	NLO	
206	$A(\rightarrow b(p_3) + \bar{b}(p_4)) + f(p_5)$ [full mt dep.]	LO	
207	$A(\rightarrow \tau^-(p_3) + \tau^+(p_4)) + f(p_5)$ [full mt dep.]	LO	
208	$H(\rightarrow W^+(\nu(p_3), e^+(p_4))W^-(e^-(p_5), \bar{\nu}(p_6))) + f(p_7), (m_t = \infty)$	NLO	
209	$H(\rightarrow Z(\rightarrow e^-(p_3), e^+(p_4))Z(\rightarrow \mu^-(p_5), \mu^+(p_6))) + f(p_7), (m_t = \infty)$	NLO	
210	$H(\rightarrow \gamma(p_3) + \gamma(p_4)) + f(p_5), (m_t = \infty)$	NLO	
211	$H(\rightarrow b(p_3) + \bar{b}(p_4)) + f(p_5) + f(p_6)$ [WBF]	NLO	[36]
212	$H(\rightarrow \tau^-(p_3) + \tau^+(p_4)) + f(p_5) + f(p_6)$ [WBF]	NLO	[36]
213	$H(\rightarrow W^+(\nu(p_3), e^+(p_4))W^-(e^-(p_5), \bar{\nu}(p_6))) + f(p_7) + f(p_8)$ [WBF]	NLO	[36]
214	$H(\rightarrow Z(\rightarrow e^-(p_3), e^+(p_4)) + Z(\rightarrow \mu^-(p_5), \mu^+(p_6))) + f(p_7) + f(p_8)$ [WBF]	NLO	[36]
215	$H(\rightarrow \gamma(p_3) + \gamma(p_4)) + f(p_5) + f(p_6)$ [WBF]	NLO	[36]
216	$H(\rightarrow b(p_3) + \bar{b}(p_4)) + f(p_5) + f(p_6) + f(p_7)$ [WBF+jet]	LO	[36]
217	$H(\rightarrow \tau^-(p_3) + \tau^+(p_4)) + f(p_5) + f(p_6) + f(p_7)$ [WBF+jet]	LO	[36]
221	$\tau^-(\rightarrow e^-(p_3) + \bar{\nu}_e(p_4) + \nu_\tau(p_5)) + \tau^+(\rightarrow \bar{\nu}_\tau(p_6) + \nu_e(p_7) + e^+(p_8))$	LO	
220	$Z(\rightarrow e^-(p_3), e^+(p_4))Z(\rightarrow \mu^-(p_5), \mu^+(p_6))) + f(p_7) + f(p_8)$ [weak]	LO	[37]
2201	$Z(\rightarrow e^-(p_3), e^+(p_4))Z(\rightarrow \mu^-(p_5), \mu^+(p_6))) + f(p_7) + f(p_8)$ [strong]	LO	[37]
222	$Z(\rightarrow e^-(p_3), e^+(p_4))Z(\rightarrow \nu_\mu(p_5), \bar{\nu}_\mu(p_6))) + f(p_7) + f(p_8)$ [weak]	LO	[37]
2221	$Z(\rightarrow e^-(p_3), e^+(p_4))Z(\rightarrow \nu_\mu(p_5), \bar{\nu}_\mu(p_6))) + f(p_7) + f(p_8)$ [strong]	LO	[37]
224	$W^-(e^-(p_3), \bar{\nu}_e(p_6)))W^+(\nu_\mu(p_5), \mu^+(p_4)) + f(p_7) + f(p_8)$ [weak]	LO	[37]
2241	$W^-(e^-(p_3), \bar{\nu}_e(p_6)))W^+(\nu_\mu(p_5), \mu^+(p_4)) + f(p_7) + f(p_8)$ [strong]	LO	[37]
226	$e^-(p_3) + e^+(p_4) + \nu_e(p_5) + \bar{\nu}_e(p_6) + f(p_7) + f(p_8)$ [weak]	LO	[37]
228	$W^+(\nu_e(p_3), e^+(p_4))W^+(\nu_\mu(p_5), \mu^+(p_6)) + f(p_7) + f(p_8)$ [weak]	LO	[37]
2281	$W^+(\nu_e(p_3), e^+(p_4))W^+(\nu_\mu(p_5), \mu^+(p_6)) + f(p_7) + f(p_8)$ [strong]	LO	[37]
229	$W^-(e^-(p_3), \bar{\nu}_e(p_4))W^-(\mu^-(p_5), \bar{\nu}_\mu(p_6)) + f(p_7) + f(p_8)$ [weak]	LO	[37]
2291	$W^-(e^-(p_3), \bar{\nu}_e(p_4))W^-(\mu^-(p_5), \bar{\nu}_\mu(p_6)) + f(p_7) + f(p_8)$ [strong]	LO	[37]
223	$W^+(\nu_e(p_3), e^+(p_4))Z(\rightarrow \mu^-(p_5), \mu^+(p_6))) + f(p_7) + f(p_8)$ [weak]	LO	[37]
2231	$W^+(\nu_e(p_3), e^+(p_4))Z(\rightarrow \mu^-(p_5), \mu^+(p_6))) + f(p_7) + f(p_8)$ [strong]	LO	[37]
225	$W^-(e^-(p_3), \bar{\nu}_e(p_4))Z(\rightarrow \mu^-(p_5), \mu^+(p_6))) + f(p_7) + f(p_8)$ [weak]	LO	[37]
2251	$W^-(e^-(p_3), \bar{\nu}_e(p_4))Z(\rightarrow \mu^-(p_5), \mu^+(p_6))) + f(p_7) + f(p_8)$ [strong]	LO	[37]

231	$t(p_3) + \bar{b}(p_4) + q(p_5)$ [t-channel]	NLO	[38]
232	$t(p_3) + \bar{b}(p_4) + q(p_5) + q(p_6)$ [t-channel]	LO	[38]
233	$t(\rightarrow \nu(p_3) + e^+(p_4) + b(p_5)) + \bar{b}(p_6) + q(p_7)$ [t-channel]	NLO	[38]
234	$t(\rightarrow \nu(p_3) + e^+(p_4) + b(p_5)) + \bar{b}(p_6) + q(p_7)$ [t-channel, rad.in.dk]	NLO	[38]
235	$t(\rightarrow \nu(p_3) + e^+(p_4) + b(p_5)) + \bar{b}(p_6) + q(p_7) + f(p_8)$ [t-channel]	LO	[38]
236	$\bar{t}(p_3) + b(p_4) + q(p_5)$ [t-channel]	NLO	[38]
237	$\bar{t}(p_3) + b(p_4) + q(p_5) + q(p_6)$ [t-channel]	LO	[38]
238	$\bar{t}(\rightarrow e^-(p_3) + \bar{\nu}(p_4) + \bar{b}(p_5)) + b(p_6) + q(p_7)$ [t-channel]	NLO	[38]
239	$\bar{t}(\rightarrow e^-(p_3) + \bar{\nu}(p_4) + \bar{b}(p_5)) + b(p_6) + q(p_7)$ [t-channel, rad.in.dk]	NLO	[38]
240	$\bar{t}(\rightarrow e^-(p_3) + \bar{\nu}(p_4) + \bar{b}(p_5)) + b(p_6) + q(p_7) + f(p_8)$ [t-channel]	LO	[38]
251	$W^+(\rightarrow \nu(p_3) + e^+(p_4)) + W^+(\rightarrow \nu(p_5) + e^+(p_6)) + f(p_7) + f(p_8)$	LO	[39]
252	$W^+(\rightarrow \nu(p_3) + e^+(p_4)) + W^+(\rightarrow \nu(p_5) + e^+(p_6)) + f(p_7) + f(p_8) + f(p_9)$	LO	[39]
253	$W^+(\rightarrow \nu(p_3) + e^+(p_4)) + Z(\rightarrow e^-(p_5) + e^+(p_6)) + f(p_7) + f(p_8)$	LO	[39]
254	$W^-(\rightarrow e^-(p_3) + \bar{\nu}(p_4)) + Z(\rightarrow e^-(p_5) + e^+(p_6)) + f(p_7) + f(p_8)$	LO	[39]
255	$W^+(\rightarrow \nu(p_3) + e^+(p_4)) + Z(\rightarrow e^-(p_5) + e^+(p_6)) + b(p_7) + f(p_8)$	LO	[39]
256	$W^-(\rightarrow e^-(p_3) + \bar{\nu}(p_4)) + Z(\rightarrow e^-(p_5) + e^+(p_6)) + b(p_7) + f(p_8)$	LO	[39]
259	$W^+(\rightarrow \nu(p_3) + e^+(p_4)) + Z(\rightarrow e^-(p_5) + e^+(p_6)) + b(p_7) + \bar{b}(p_8)$	LO	[39]
260	$W^-(\rightarrow e^-(p_3) + \bar{\nu}(p_4)) + Z(\rightarrow e^-(p_5) + e^+(p_6)) + b(p_7) + \bar{b}(p_8)$	LO	[39]
261	$Z(\rightarrow e^-(p_3) + e^+(p_4)) + b(p_5)$	NLO	
262	$Z(\rightarrow e^-(p_3) + e^+(p_4)) + c(p_5)$	NLO	
263	$Z(\rightarrow e^-(p_3) + e^+(p_4)) + \bar{b}(p_5) + b(p_6)$ [1 b-tag]	LO	
264	$Z(\rightarrow e^-(p_3) + e^+(p_4)) + \bar{c}(p_5) + c(p_6)$ [1 c-tag]	LO	
266	$Z(\rightarrow e^-(p_3) + e^+(p_4)) + b(p_5)(+\bar{b}(p_6))$	NLO	
267	$Z(\rightarrow e^-(p_3) + e^+(p_4)) + c(p_5)(+\bar{c}(p_6))$	NLO	
269	$H(\gamma(p_3) + \gamma(p_4)) + f(p_5) + f(p_6)$ [full mt dep.]	NLO	[40, 41]

270	$H(\gamma(p_3) + \gamma(p_4)) + f(p_5) + f(p_6)$ [in heavy top limit]	NLO	[42]
271	$H(b(p_3) + \bar{b}(p_4)) + f(p_5) + f(p_6)$ [in heavy top limit]	NLO	[42]
272	$H(\tau^-(p_3) + \tau^+(p_4)) + f(p_5) + f(p_6)$ [in heavy top limit]	NLO	[42]
273	$H(\rightarrow W^+(\nu(p_3), e^+(p_4))W^-(e^-(p_5), \bar{\nu}(p_6))) + f(p_7) + f(p_8)$	NLO	[42]
274	$H(\rightarrow Z(e^-(p_3), e^+(p_4))Z(\mu^-(p_5), \mu^+(p_6))) + f(p_7) + f(p_8)$	NLO	[42]
275	$H(b(p_3) + \bar{b}(p_4)) + f(p_5) + f(p_6) + f(p_7)$ [in heavy top limit]	LO	[42]
276	$H(\tau^-(p_3) + \tau^+(p_4)) + f(p_5) + f(p_6) + f(p_7)$ [in heavy top limit]	LO	[42]
278	$H(\rightarrow W^+(\nu(p_3), e^+(p_4))W^-(e^-(p_5), \bar{\nu}(p_6))) + f(p_7) + f(p_8) + f(p_9)$	LO	[42]
279	$H(\rightarrow Z(e^-(p_3), e^+(p_4))Z(\mu^-(p_5), \mu^+(p_6))) + f(p_7) + f(p_8) + f(p_9)$	LO	[42]
280	$\gamma(p_3) + f(p_4)$	NLO+F	
282	$f(p_1) + f(p_2) \rightarrow \gamma(p_3) + f(p_4) + f(p_5)$	LO	
283	$f(p_1) + f(p_2) \rightarrow \gamma(p_3) + b(p_4)$	LO	
284	$f(p_1) + f(p_2) \rightarrow \gamma(p_3) + c(p_4)$	LO	
285	$f(p_1) + f(p_2) \rightarrow \gamma(p_3) + \gamma(p_4)$	NLO+F, NNLO	[43]
2851	$g(p_1) + g(p_2) \rightarrow \gamma(p_3) + \gamma(p_4)$	NLO	[43]
286	$f(p_1) + f(p_2) \rightarrow \gamma(p_3) + \gamma(p_4) + f(p_5)$	LO	[43]
2861	$g(p_1) + g(p_2) \rightarrow \gamma(p_3) + \gamma(p_4) + f(p_5)$	LO	[43]
287	$f(p_1) + f(p_2) \rightarrow \gamma(p_3) + \gamma(p_4) + \gamma(p_5)$	NLO+F	[43]
289	$f(p_1) + f(p_2) \rightarrow \gamma(p_3) + \gamma(p_4) + \gamma(p_5) + \gamma(p_6)$	NLO+F	[43]
290	$f(p_1) + f(p_2) \rightarrow W^+(\rightarrow \nu(p_3) + e^+(p_4)) + \gamma(p_5)$	NNLO	[12, 20]
292	$f(p_1) + f(p_2) \rightarrow W^+(\rightarrow \nu(p_3) + e^+(p_4)) + \gamma(p_5) + f(p_6)$	NLO	[12, 20]
293	$f(p_1) + f(p_2) \rightarrow W^+(\rightarrow \nu(p_3) + e^+(p_4)) + \gamma(p_5) + f(p_6) + f(p_7)$	LO	
294	$f(p_1) + \gamma(p_2) \rightarrow W^+(\rightarrow \nu(p_3) + e^+(p_4)) + \gamma(p_5) + f(p_6)$	NLO	
2941	$f(p_1) + \gamma(p_2) \rightarrow W^+(\rightarrow \nu(p_3) + e^+(p_4)) + \gamma(p_5) + f(p_6) + f(p_7)$	NLO	
295	$f(p_1) + f(p_2) \rightarrow W^-(\rightarrow e^-(p_3) + \bar{\nu}(p_4)) + \gamma(p_5)$	NNLO	
297	$f(p_1) + f(p_2) \rightarrow W^-(\rightarrow e^-(p_3) + \bar{\nu}(p_4)) + \gamma(p_5) + f(p_6)$	NLO	
298	$f(p_1) + f(p_2) \rightarrow W^-(\rightarrow e^-(p_3) + \bar{\nu}(p_4)) + \gamma(p_5) + f(p_6) + f(p_7)$	LO	
299	$f(p_1) + \gamma(p_2) \rightarrow W^-(\rightarrow e^-(p_3) + \bar{\nu}(p_4)) + \gamma(p_5) + f(p_6)$	NLO	
2991	$f(p_1) + \gamma(p_2) \rightarrow W^-(\rightarrow e^-(p_3) + \bar{\nu}(p_4)) + \gamma(p_5) + f(p_6) + f(p_7)$	NLO	
300	$Z(\rightarrow e^-(p_3) + e^+(p_4)) + \gamma(p_5)$	NNLO	
301	$Z(\rightarrow e^-(p_3) + e^+(p_4)) + \gamma(p_5) + \gamma(p_6)$	NLO + F	
302	$Z(\rightarrow e^-(p_3) + e^+(p_4)) + \gamma(p_5) + f(p_6)$	NLO	
303	$Z(\rightarrow e^-(p_3) + e^+(p_4)) + \gamma(p_5) + \gamma(p_6) + f(p_7)$	LO	
304	$Z(\rightarrow e^-(p_3) + e^+(p_4)) + \gamma(p_5) + f(p_6) + f(p_7)$	LO	
305	$Z(\rightarrow 3(\nu(p_3) + \bar{\nu}(p_4))) + \gamma(p_5)$	NNLO	
306	$Z(\rightarrow 3(\nu(p_3) + \bar{\nu}(p_4))) + \gamma(p_5) + \gamma(p_6)$	NLO + F	
307	$Z(\rightarrow 3(\nu(p_3) + \bar{\nu}(p_4))) + \gamma(p_5) + f(p_6)$	NLO	
308	$Z(\rightarrow 3(\nu(p_3) + \bar{\nu}(p_4))) + \gamma(p_5) + \gamma(p_6) + f(p_7)$	LO	
309	$Z(\rightarrow 3(\nu(p_3) + \bar{\nu}(p_4))) + \gamma(p_5) + f(p_6) + f(p_7)$	LO	
311	$f(p_1) + b(p_2) \rightarrow W^+(\rightarrow \nu(p_3) + e^+(p_4)) + b(p_5) + f(p_6)$	LO	
316	$f(p_1) + b(p_2) \rightarrow W^-(\rightarrow e^-(p_3) + \bar{\nu}(p_4)) + b(p_5) + f(p_6)$	LO	
321	$f(p_1) + c(p_2) \rightarrow W^+(\rightarrow \nu(p_3) + e^+(p_4)) + c(p_5) + f(p_6)$	LO	
326	$f(p_1) + c(p_2) \rightarrow W^-(\rightarrow e^-(p_3) + \bar{\nu}(p_4)) + c(p_5) + f(p_6)$	LO	

331	$W^+(\rightarrow \nu(p_3) + e^+(p_4)) + c(p_5) + f(p_6)$ [c-s interaction]	LO	
336	$W^-(\rightarrow e^-(p_3) + \bar{\nu}(p_4)) + c(p_5) + f(p_6)$ [c-s interaction]	LO	
341	$f(p_1) + b(p_2) \rightarrow Z(\rightarrow e^-(p_3) + e^+(p_4)) + b(p_5) + f(p_6)[+f(p_7)]$	NLO	
342	$f(p_1) + b(p_2) \rightarrow Z(\rightarrow e^-(p_3) + e^+(p_4)) + b(p_5) + f(p_6)[+\bar{b}(p_7)]$	(REAL)	
346	$f(p_1) + b(p_2) \rightarrow Z(\rightarrow e^-(p_3) + e^+(p_4)) + b(p_5) + f(p_6) + f(p_7)$	LO	
347	$f(p_1) + b(p_2) \rightarrow Z(\rightarrow e^-(p_3) + e^+(p_4)) + b(p_5) + f(p_6) + \bar{b}(p_7)$	LO	
351	$f(p_1) + c(p_2) \rightarrow Z(\rightarrow e^-(p_3) + e^+(p_4)) + c(p_5) + f(p_6)[+f(p_7)]$	NLO	
352	$f(p_1) + c(p_2) \rightarrow Z(\rightarrow e^-(p_3) + e^+(p_4)) + c(p_5) + f(p_6)[+\bar{c}(p_7)]$	(REAL)	
356	$f(p_1) + c(p_2) \rightarrow Z(\rightarrow e^-(p_3) + e^+(p_4)) + c(p_5) + f(p_6) + f(p_7)$	LO	
357	$f(p_1) + c(p_2) \rightarrow Z(\rightarrow e^-(p_3) + e^+(p_4)) + c(p_5) + f(p_6) + \bar{c}(p_7)$	LO	
361	$c(p_1) + \bar{s}(p_2) \rightarrow W^+(\rightarrow \nu(p_3) + e^+(p_4))$ [mc=0 in NLO]	NLO	
362	$c(p_1) + \bar{s}(p_2) \rightarrow W^+(\rightarrow \nu(p_3) + e^+(p_4))$ [massless corrections only]	NLO	
363	$c(p_1) + \bar{s}(p_2) \rightarrow W^+(\rightarrow \nu(p_3) + e^+(p_4))$ [massive charm in real]	NLO	
370	$W^+(\rightarrow \nu(p_3) + e^+(p_4)) + \gamma(p_5) + \gamma(p_6)$	LO	
371	$W^-(\rightarrow e^-(p_3) + \bar{\nu}(p_4)) + \gamma(p_5) + \gamma(p_6)$	LO	
401	$W^+(\rightarrow \nu(p_3) + e^+(p_4)) + b(p_5)$, [1,2 or 3 jets, 4FNS]	NLO	
402	$W^+(\rightarrow \nu(p_3) + e^+(p_4)) + (b + \bar{b})(p_5)$, [1 or 2 jets, 4FNS]	NLO	
403	$W^+(\rightarrow \nu(p_3) + e^+(p_4)) + b(p_5) + \bar{b}(p_6)$, [2 or 3 jets, 4FNS]	NLO	
406	$W^-(\rightarrow e^-(p_3) + \bar{\nu}(p_4)) + b(p_5)$, [1,2 or 3 jets, 4FNS]	NLO	
407	$W^-(\rightarrow e^-(p_3) + \bar{\nu}(p_4)) + (b + \bar{b})(p_5)$, [1 or 2 jets, 4FNS]	NLO	
408	$W^-(\rightarrow e^-(p_3) + \bar{\nu}(p_4)) + b(p_5) + \bar{b}(p_6)$, [2 or 3 jets, 4FNS]	NLO	
411	$f(p_1) + b(p_2) \rightarrow W^+(\rightarrow \nu(p_3) + e^+(p_4)) + b(p_5) + f(p_6)$ [5FNS]	NLO	
416	$f(p_1) + b(p_2) \rightarrow W^-(\rightarrow e^-(p_3) + \bar{\nu}(p_4)) + b(p_5) + f(p_6)$ [5FNS]	NLO	
421	$W^+(\rightarrow \nu(p_3) + e^+(p_4)) + b(p_5)$, [1,2 or 3 jets, 4FNS+5FNS]	NLO	
426	$W^-(\rightarrow e^-(p_3) + \bar{\nu}(p_4)) + b(p_5)$, [1,2 or 3 jets, 4FNS+5FNS]	NLO	
431	$W^+(\rightarrow \nu(p_3) + e^+(p_4)) + b(p_5) + \bar{b}(p_6) + f(p_7)$, [massive]	LO	
436	$W^-(\rightarrow e^-(p_3) + \bar{\nu}(p_4)) + b(p_5) + \bar{b}(p_6) + f(p_7)$, [massive]	LO	
461	$W^+(\rightarrow \nu(p_3) + \mu^+(p_4)) + W^-(\rightarrow e^-(p_5) + \bar{\nu}(p_6)) + f(p_7)$	NLO	[44–46]
462	$W^+(\rightarrow \nu(p_3) + \mu^+(p_4)) + W^-(\rightarrow e^-(p_5) + \bar{\nu}(p_6)) + f(p_7) + f(p_8)$	LO	
471	$W^+(\rightarrow \nu(p_3) + e^+(p_4)) + Z(\rightarrow \mu^-(p_5) + \mu^+(p_6)) + f(p_7)$	NLO	
476	$W^-(\rightarrow e^-(p_3) + \bar{\nu}(p_4)) + Z(\rightarrow \mu^-(p_5) + \mu^+(p_6)) + f(p_7)$	NLO	
481	$Z(\rightarrow e^-(p_3) + e^+(p_4)) + Z(\rightarrow \mu^-(p_5) + \mu^+(p_6)) + f(p_7)$	NLO	[19, 20]
482	$Z(\rightarrow e^-(p_3) + e^+(p_4)) + Z(\rightarrow \nu_\mu(p_5) + \bar{\nu}_\mu(p_6)) + f(p_7)$	NLO	[19, 20]
486	$Z(\rightarrow \mu^-(p_3) + \mu^+(p_4)) + Z(\rightarrow e^-(p_5) + e^+(p_6)) + f(p_7)$ [no γ^*]	NLO	[19, 20]
487	$Z(\rightarrow e^-(p_3) + e^+(p_4)) + Z(\rightarrow \nu_\mu(p_5) + \bar{\nu}_\mu(p_6)) + f(p_7)$ [no γ^*]	NLO	[19, 20]
500	$W^+(\rightarrow \nu(p_3) + e^+(p_4)) + t(p_5) + \bar{t}(p_6)$ [massive]	NLO	
501	$t(\rightarrow \nu(p_3) + e^+(p_4) + b(p_5)) + \bar{t}(\rightarrow \bar{b}(p_6) + e^-(p_7) + \bar{\nu}(p_8)) + W^+(\nu(p_9), \mu^+(p_{10}))$	NLO	
502	(same as process 501 but with radiation in decay)	NLO	
503	$t(\rightarrow \nu(p_3) + e^+(p_4) + b(p_5)) + \bar{t}(\rightarrow \bar{b}(p_6) + q(p_7) + \bar{q}(p_8)) + W^+(\nu(p_9), \mu^+(p_{10}))$	NLO	
506	$t(\rightarrow q(p_3) + \bar{q}(p_4) + b(p_5)) + \bar{t}(\rightarrow \bar{b}(p_6) + e^-(p_7) + \bar{\nu}(p_8)) + W^+(\nu(p_9), \mu^+(p_{10}))$	NLO	

510	$W^-(\rightarrow e^-(p_3) + \bar{\nu}(p_4)) + t(p_5) + \bar{t}(p_6)[\text{massive}]$	NLO	[47]
511	$t(\rightarrow \nu(p_3) + e^+(p_4) + b(p_5)) + \bar{t}(\rightarrow \bar{b}(p_6) + e^-(p_7) + \bar{\nu}(p_8)) + W^-(\mu^-(p_9), \bar{\nu}(p_{10}))$	NLO	[47]
512	(same as process 511 but with radiation in decay)	NLO	[47]
513	$t(\rightarrow \nu(p_3) + e^+(p_4) + b(p_5)) + \bar{t}(\rightarrow \bar{b}(p_6) + q(p_7) + \bar{q}(p_8)) + W^-(\mu^-(p_9), \bar{\nu}(p_{10}))$	NLO	
516	$t(\rightarrow q(p_3) + \bar{q}(p_4) + b(p_5)) + \bar{t}(\rightarrow \bar{b}(p_6) + e^-(p_7) + \bar{\nu}(p_8)) + W^-(\mu^-(p_9), \bar{\nu}(p_{10}))$	NLO	
529	$Z(\rightarrow e^-(p_3) + e^+(p_4)) + t(p_5) + \bar{t}(p_6)$	LO	
530	$t(\rightarrow \nu(p_3) + e^+(p_4) + b(p_5)) + \bar{t}(\rightarrow e^-(p_7) + \bar{\nu}(p_8) + \bar{b}(p_6)) + Z(e^-(p_9), e^+(p_{10}))$	LO	
531	$t(\rightarrow \nu(p_3) + e^+(p_4) + b(p_5)) + \bar{t}(\rightarrow e^-(p_7) + \bar{\nu}(p_8) + \bar{b}(p_6)) + Z(b(p_9), \bar{b}(p_{10}))$	LO	
532	$t(\rightarrow \nu(p_3) + e^+(p_4) + b(p_5)) + \bar{t}(\rightarrow q(p_7) + \bar{q}(p_8) + \bar{b}(p_6)) + Z(e^-(p_9), e^+(p_{10}))$	LO	
533	$t(\rightarrow q(p_3) + \bar{q}(p_4) + b(p_5)) + \bar{t}(\rightarrow e^-(p_7) + \bar{\nu}(p_8) + \bar{b}(p_6)) + Z(e^-(p_9), e^+(p_{10}))$	LO	
540	$H(b(p_3) + \bar{b}(p_4)) + t(p_5) + q(p_6)$	NLO	[48]
541	$H(b(p_3) + \bar{b}(p_4)) + \bar{t}(p_5) + q(p_6)$	NLO	[48]
544	$H(b(p_3) + \bar{b}(p_4)) + t(\nu(p_5) + e^+(p_6) + b(p_7)) + q(p_8)$	NLO	[48]
547	$H(b(p_3) + \bar{b}(p_4)) + \bar{t}(e^-(p_5) + \bar{\nu}(p_6) + b(p_7)) + q(p_8)$	NLO	[48]
550	$H(\gamma(p_3) + \gamma(p_4)) + t(p_5) + q(p_6)$	NLO	[48]
551	$H(\gamma(p_3) + \gamma(p_4)) + \bar{t}(p_5) + q(p_6)$	NLO	[48]
554	$H(\gamma(p_3) + \gamma(p_4)) + t(\nu(p_5) + e^+(p_6) + b(p_7)) + q(p_8)$	NLO	[48]
557	$H(\gamma(p_3) + \gamma(p_4)) + \bar{t}(e^-(p_5) + \bar{\nu}(p_6) + b(p_7)) + q(p_8)$	NLO	[48]
560	$Z(e^-(p_3) + e^+(p_4)) + t(p_5) + q(p_6)$	NLO	[48]
561	$Z(e^-(p_3) + e^+(p_4)) + \bar{t}(p_5) + q(p_6)$	NLO	[48]
562	$Z(e^-(p_3) + e^+(p_4)) + t(p_5) + q(p_6) + f(p_7)$	LO	[48]
563	$Z(e^-(p_3) + e^+(p_4)) + \bar{t}(p_5) + q(p_6) + f(p_7)$	LO	[48]
564	$Z(e^-(p_3) + e^+(p_4)) + t(\rightarrow \nu(p_5) + e^+(p_6) + b(p_7)) + q(p_8)$	NLO	[48]
566	$Z(e^-(p_3) + e^+(p_4)) + t(\rightarrow \nu(p_5) + e^+(p_6) + b(p_7)) + q(p_8) + f(p_9)$	LO	[48]
567	$Z(e^-(p_3) + e^+(p_4)) + \bar{t}(\rightarrow e^-(p_5) + \bar{\nu}(p_6) + \bar{b}(p_7)) + q(p_8)$	NLO	[48]
569	$Z(e^-(p_3) + e^+(p_4)) + \bar{t}(\rightarrow e^-(p_5) + \bar{\nu}(p_6) + \bar{b}(p_7)) + q(p_8) + f(p_9)$	LO	[48]
601	$H(b(p_3) + \bar{b}(p_4)) + H(\tau^-(p_5) + \tau^+(p_6))$	LO	[49]
602	$H(b(p_3) + \bar{b}(p_4)) + H(\gamma(p_5) + \gamma(p_6))$	LO	[49]
609	$(W^+ + W^-) + H(\rightarrow \tau(p_5) + \bar{\tau}(p_6)) + g(p_7)$	NLO	
610	$W^+(\rightarrow \nu(p_3) + e^+(p_4)) + H(\rightarrow \tau(p_5) + \bar{\tau}(p_6)) + g(p_7)$	NLO	
611	$W^+(\rightarrow \nu(p_3) + e^+(p_4)) + H(\rightarrow b(p_5) + \bar{b}(p_6)) + g(p_7)$	NLO	
612	$W^+(\rightarrow \nu(p_3) + e^+(p_4)) + H(\rightarrow \gamma(p_5) + \gamma(p_6)) + g(p_7)$	NLO	
613	$W^+(\rightarrow \nu(p_3) + e^+(p_4)) + H(\rightarrow W^+(\nu(p_5), e^+(p_6))W^-(e^-(p_7), \bar{\nu}(p_8))) + g(p_9)$	NLO	
615	$W^-(\rightarrow e^-(p_3) + \bar{\nu}(p_4)) + H(\rightarrow \tau(p_5) + \bar{\tau}(p_6)) + g(p_7)$	NLO	
616	$W^-(\rightarrow e^-(p_3) + \bar{\nu}(p_4)) + H(\rightarrow b(p_5) + \bar{b}(p_6)) + g(p_7)$	NLO	
617	$W^-(\rightarrow e^-(p_3) + \bar{\nu}(p_4)) + H(\rightarrow \gamma(p_5) + \gamma(p_6)) + g(p_7)$	NLO	
618	$W^-(\rightarrow e^-(p_3) + \bar{\nu}(p_4)) + H(\rightarrow W^+(\nu(p_5), e^+(p_6))W^-(e^-(p_7), \bar{\nu}(p_8))) + g(p_9)$	NLO	
620	$Z(\rightarrow e^-(p_3) + e^+(p_4)) + H(\rightarrow \tau^-(p_5) + \tau^+(p_6)) + g(p_7)$	NLO	
621	$Z(\rightarrow e^-(p_3) + e^+(p_4)) + H(\rightarrow b(p_5) + \bar{b}(p_6)) + g(p_7)$	NLO	
622	$Z(\rightarrow e^-(p_3) + e^+(p_4)) + H(\rightarrow \gamma(p_5) + \gamma(p_6)) + g(p_7)$	NLO	
623	$Z(\rightarrow e^-(p_3) + e^+(p_4)) + H(\rightarrow W^+(\nu(p_5), e^+(p_6))W^-(e^-(p_7), \bar{\nu}(p_8))) + g(p_9)$	NLO	

Table 1: Different options for the scheme used to fix the electroweak parameters of the Standard Model and the corresponding default input values. M_W and M_Z are taken from ref. [50].

Parameter	Name (_inp)	Input Value	Output Value determined by <code>ewscheme</code>			
			-1	0	1	2
G_F	<code>Gf</code>	1.16639×10^{-5}	input	calculated	input	input
$\alpha(M_Z)$	<code>aemmz</code>	1/128.89	input	input	calculated	input
$\sin^2 \theta_w$	<code>xw</code>	0.2223	calculated	input	calculated	input
M_W	<code>wmass</code>	80.385 GeV	input	calculated	input	calculated
M_Z	<code>zmass</code>	91.1876 GeV	input	input	input	calculated
m_t	<code>mt</code>	<code>input.ini</code>	calculated	input	input	input

640	$t(p_3) + \bar{t}(p_4) + H(p_5)$	LO
641	$t(\rightarrow \nu(p_3) + e^+(p_4) + b(p_5)) + \bar{t}(\rightarrow \bar{\nu}(p_7) + e^-(p_8) + \bar{b}(p_6)) + H(b(p_9) + \bar{b}(p_{10}))$	LO
644	$t(\rightarrow \nu(p_3) + e^+(p_4) + b(p_5)) + \bar{t}(\rightarrow \bar{q}(p_7) + q(p_8) + \bar{b}(p_6)) + H(b(p_9) + \bar{b}(p_{10}))$	LO
647	$t(\rightarrow q(p_3) + \bar{q}(p_4) + b(p_5)) + \bar{t}(\rightarrow \bar{\nu}(p_7) + e^-(p_8) + \bar{b}(p_6)) + H(b(p_9) + \bar{b}(p_{10}))$	LO
651	$t(\rightarrow \nu(p_3) + e^+(p_4) + b(p_5)) + \bar{t}(\rightarrow \bar{\nu}(p_7) + e^-(p_8) + \bar{b}(p_6)) + H(\gamma(p_9) + \gamma(p_{10}))$	LO
654	$t(\rightarrow \nu(p_3) + e^+(p_4) + b(p_5)) + \bar{t}(\rightarrow \bar{q}(p_7) + q(p_8) + \bar{b}(p_6)) + H(\gamma(p_9) + \gamma(p_{10}))$	LO
657	$t(\rightarrow q(p_3) + \bar{q}(p_4) + b(p_5)) + \bar{t}(\rightarrow \bar{\nu}(p_7) + e^-(p_8) + \bar{b}(p_6)) + H(\gamma(p_9) + \gamma(p_{10}))$	LO
661	$t(\rightarrow \nu(p_3)e^+(p_4)b(p_5)) + \bar{t}(\rightarrow \bar{\nu}(p_7)e^-(p_8)\bar{b}(p_6)) + H(W^+(p_9, p_{10})W^-(p_{11}, p_{12}))$	LO
664	$t(\rightarrow \nu(p_3)e^+(p_4)b(p_5)) + \bar{t}(\rightarrow \bar{q}(p_7)q(p_8)\bar{b}(p_6)) + H(W^+(p_9, p_{10})W^-(p_{11}, p_{12}))$	LO
667	$t(\rightarrow q(p_3)\bar{q}(p_4)b(p_5)) + \bar{t}(\rightarrow \bar{\nu}(p_7)e^-(p_8)\bar{b}(p_6)) + H(W^+(p_9, p_{10})W^-(p_{11}, p_{12}))$	LO
902	Check of Volume of 2 particle phase space	
903	Check of Volume of 3 particle phase space	
904	Check of Volume of 4 particle phase space	
905	Check of Volume of 5 particle phase space	
906	Check of Volume of 6 particle phase space	
908	Check of Volume of 8 particle phase space	
909	Check of Volume of 4 particle massive phase space	
910	Check of Volume of 3 particle (2 massive) phase space	
911	Check of Volume of 5 particle W+t (with decay) massive phase space	
912	Check of Volume of 5 particle W+t (no decay) massive phase space	
913	Check of Volume of 5 particle W+t+g (in decay) massive phase space	
914	Check of Volume of 5 particle W+t+g (in production) massive phase space	

5 Configuration

5.1 Compile-time settings

MCFM allows the user to choose between a number of schemes for defining the electroweak couplings. These choices are summarized in Table 1. The scheme is selected by modifying the value of `ewscheme` in `src/User/mdata.f` prior to compilation, which also contains the values of all input parameters (see also Table 2).

Table 2: Default values for the remaining parameters in MCFM. Γ_W and Γ_Z from ref. [50].

Parameter	Fortran name	Default value
m_τ	mtau	1.777 GeV
m_τ^2	mtausq	3.1577 GeV ²
Γ_τ	tauwidth	2.269×10^{-12} GeV
Γ_W	wwidth	2.093 GeV
Γ_Z	zwidth	2.4952 GeV
V_{ud}	Vud	0.975
V_{us}	Vus	0.222
V_{ub}	Vub	0.
V_{cd}	Vcd	0.222
V_{cs}	Vcs	0.975
V_{cb}	Vcb	0.

The default scheme corresponds to `ewscheme=+1`. As described below, this corresponds to a scheme in which the top quark mass is an input parameter so that it is more suitable for many processes now included in the program.

The choice of (`ewscheme=-1`) enforces the use of an effective field theory approach, which is valid for scales below the top mass. In this approach there are 4 independent parameters (which we choose to be G_F , $\alpha(M_Z)$, M_W and M_Z). For further details, see Georgi [51].

For all the other schemes (`ewscheme=0,1,2`) the top mass is simply an additional input parameter and there are 3 other independent parameters from the remaining 5. The variable `ewscheme` then performs exactly the same role as `idef` in MadEvent [52]. `ewscheme=0` is the old MadEvent default and `ewscheme=1` is the new MadEvent default, which is also the same as that used in Alpgen [53] and LUSIFER [54]. For processes in which the top quark is directly produced it is preferable to use the schemes (`ewscheme=0,1,2`), since in these schemes one can adjust the top mass to its physical value (in the input file `input.ini`). Schemes where the W and Z masses are fixed to their measured values are the most appropriate for W and Z production processes.

5.2 Parton distributions

The value of $\alpha_s(M_Z)$ is not adjustable; it is hardwired with the parton distribution. In addition, the parton distribution also specifies the number of loops that should be used in the running of α_s . As default the code uses the LHAPDF library for PDF evaluation; a native implementation of some (mostly older) PDF sets is also retained.

5.3 Electroweak corrections

As of version 8.1, MCFM allows the calculation of weak corrections to a selection of processes: 31 (neutral-current DY), 157 (top-pair production) and 190 (di-jet production). This is controlled by the flag `ewcorr` in the input file. A complete description of the calculations is provided in Ref. [35].

By setting `ewcorr` to `sudakov`, the program performs a calculation of the leading weak corrections to these processes using a Sudakov approximation that is appropriate at high energies. The calculation of the weak corrections using the exact form of the one-loop amplitudes is obtained by using the flag `exact`. A comparison between the two approaches, together with discussions of the validity of the Sudakov approximation, may be found in Ref. [35].

For the case of top-pair and di-jet production, the weak one-loop corrections contain infrared divergences that must be cancelled against corresponding real radiation contributions (in much the same manner as a regular NLO QCD calculation). For this reason the screen output will contain two sets of iterations corresponding to the virtual and real contributions.

For all processes, performing the calculation of weak corrections enables a special mode of phase-space integration that is designed to better-sample events produced at high-energies. For this reason the VEGAS output that appears on the screen does not correspond to a physical cross-section – and a corresponding warning message to this effect will be displayed. In many cases the quantity of most interest is the relative correction to the leading order result (δ_{wk}) given by,

$$\delta_{\text{wk}} = \frac{d\sigma_{\text{wk}}^{\text{NLO}} - d\sigma^{\text{LO}}}{d\sigma^{\text{LO}}} . \quad (1)$$

It is straightforward to compute this quantity for a distribution by editing the appropriate `nplotter` routine. This is achieved by filling a histogram with the weight corresponding to the LO result, another with the weight for the NLO weak result and then an additional placeholder histogram that contains the special string `'+RELEW+'`. Examples of the syntax and correct calling sequence can be seen in the code. (The appropriate `nplotter` routine is displayed on the process web-page, reachable from the tables in Section 4.)

6 Input file configuration

6.1 Run-time input file parameters

MCFM execution is performed in the `Bin/` directory, with syntax:

`mcfm input.ini`

If no command line options are given, then MCFM will default to using the file `input.ini` in the current directory for choosing options. The `input.ini` file can be in any directory and then the first argument to `mcfm` should be the location of the file. Furthermore, one can overwrite or append single configuration options with additional parameters like:

`./mcfm benchmark/input.ini -general%part=nlo -lhpdf%dopdferrors=.true.`

Here specifying a parameter uses a single dash, then the section name as in the input file (see below), followed by a percent sign, followed by the option name, followed by an equal sign and the actual value of the setting.

All default settings in the input file are explained below, as well as further optional parameters. The top level setting `mcfm_version` specifies the input file version number and it must match the version of the code being used.

The general structure of a fixed-order calculation up to NNLO is as follows:

$$\sigma = \sigma_0 + \Delta\sigma_1 + \Delta\sigma_2, \quad (2)$$

where $\Delta\sigma_k$ is of order α_s^k with respect to the leading order cross section σ_0 , thus representing the $N^k\text{LO}$ contribution to the cross section. When performing the NLO calculation using dipole subtraction its contribution to the cross section can be decomposed as,

$$\Delta\sigma_1 = \Delta\sigma_1^v + \Delta\sigma_1^r. \quad (3)$$

$\Delta\sigma_1^v$ includes virtual (loop) contributions, as well as counterterms that render them finite. $\Delta\sigma_1^r$ includes contributions from diagrams involving real parton emission, again with counterterms to make them finite. Only the sum of $\Delta\sigma_1^v$ and $\Delta\sigma_1^r$ is physical.

This contribution can also be computed using a slicing method with the corresponding decomposition,

$$\Delta\sigma_1^a = \Delta\sigma_1^{a,<} + \Delta\sigma_1^{a,>}. \quad (4)$$

a labels the slicing resolution variable, which in MCFM can be either 0-jettiness, q_T (of a color-singlet system) or p_T^{j1} (lead jet p_T) (thus corresponding to a jet veto). $\Delta\sigma_1^{a,<}$ is termed the below-cut slicing contribution which is computed by the means of a factorization theorem and includes loop contributions. $\Delta\sigma_1^{a,>}$ is the above-cut contribution containing radiation of an additional parton. Only the sum $\Delta\sigma_1^a$ is physical and contains a dependence on the slicing resolution variable a_{cut} that tends to zero as $a_{\text{cut}} \rightarrow 0$.

At NNLO only slicing calculations are available. The decomposition is,

$$\Delta\sigma_2^a = \Delta\sigma_2^{a,<} + \Delta\sigma_2^{a,v>} + \Delta\sigma_2^{a,r>}. \quad (5)$$

$\Delta\sigma_2^{a,<}$ is the below-cut slicing contribution containing 2-loop contributions. $\Delta\sigma_1^{a,v>}$ is the above-cut contribution containing loop corrections to radiation of an additional parton. $\Delta\sigma_1^{a,r>}$ is the above-cut contribution representing radiation of up to two additional partons. Only the sum $\Delta\sigma_2^a$ is physical and contains a dependence on the slicing resolution variable a_{cut} that tends to zero as $a_{\text{cut}} \rightarrow 0$.

The type of computation that is performed depends on the parameter `part` in the `general` section. The list of possible values, and the associated meaning, is shown in Tables 3 and 4. They can also be listed by setting `part` equal to `help` in the input file.

Table 3: Possible values for the parameter `part` that correspond to performing a fixed-order calculation.

<code>part</code>	description
<code>lo/lord</code>	σ_0
<code>virt</code>	$\Delta\sigma_1^v$
<code>real</code>	$\Delta\sigma_1^r$
<code>nlocoeff/totacoeff</code>	$\Delta\sigma_1$

nlo/tota	$\sigma_0 + \Delta\sigma_1$. For photon processes that include fragmentation, nlo also includes the calculation of the fragmentation (frag) contributions.
frag	Processes 280, 285, 290, 295, 300-302, 305-307, 820-823 only, see sections 13.67, 13.73 and 13.74 below.
nlo dk/todk	Processes 114, 161, 166, 171, 176, 181, 186, 141, 146, 149, 233, 238, 501, 511 only, see sections 13.39 and 13.41 below.
snloR	$\Delta\sigma_1^{a,>}$
snloV	$\Delta\sigma_1^{a,<}$
snlocoeff/scetnlocoeff	$\Delta\sigma_1^a$
snlo/scetnlo	$\sigma_0 + \Delta\sigma_1^a$
nnloVVcoeff	$\Delta\sigma_2^{a,<}$
nnloRVcoeff	$\Delta\sigma_2^{a,v>}$
nnloRRcoeff	$\Delta\sigma_2^{a,r>}$
nnloVV	$\Delta\sigma_1^{a,<} + \Delta\sigma_2^{a,<}$
nnloRV	$\Delta\sigma_1^{a,>} + \Delta\sigma_2^{a,v>}$
nnloRR	$\Delta\sigma_2^{a,r>}$
nnlocoeff	$\Delta\sigma_2^a$
nnlo	$\sigma_0 + \Delta\sigma_1 + \Delta\sigma_2^a$

Table 4: Possible values for the parameter **part** that correspond to performing a calculation including large-log resummation.

part	description
resL0	NLL resummed and matched
resonlyL0	NLL resummed only
resonlyL0p	NLLp resummed only
resexpNLO	NNLL resummed expanded to NLO
resonlyNLO	NNLL resummed
resaboveNLO	fixed-order matching to NLO
resmatchcorrNLO	matching corrections at NLO
resonlyNLOp	NNLLp resummed
resexpNNLO	N ³ LL resummed expanded to NNLO
resonlyNNLO	N ³ LL resummed
resaboveNNLO	fixed-order matching to NLO
resmatchcorrNNLO	matching corrections at NLO
resL0p	NLLp resummed and matched
resNLO	NNLL resummed, matched to NLO
resNLOp	N ³ LL resummed, matched to NLO
resNNLO	N ³ LL resummed, matched to NNLO
resNNLOp	N ³ LLp resummed, matched to NNLO
resonlyNNLOp	N ³ LLp resummed

6.1.1 General

Section general	Description
<code>nproc</code>	The process to be studied is given by choosing a process number, according to Tables in Section 4. $f(p_i)$ denotes a generic partonic jet. Processes denoted as “LO” may only be calculated in the Born approximation. For photon processes, “NLO+F” signifies that the calculation may be performed both at NLO and also including the effects of photon fragmentation and experimental isolation. In contrast, “NLO” for a process involving photons means that no fragmentation contributions are included and isolation is performed according to the procedure of Frixione [55].
<code>part</code>	The type of calculation to be performed. Possible values are given in Tables 3 and 4.
<code>runstring</code>	When MCFM is run, it will write output to several files. The label <code>runstring</code> will be included in the names of these files.
<code>rundir</code>	Directory for output and snapshot files
<code>sqrts</code>	Center of mass energy in GeV.
<code>ih1, ih2</code>	The identities of the incoming hadrons may be set with these parameters, allowing simulations for both $p\bar{p}$ (such as the Tevatron) and pp (such as the LHC). Setting <code>ih1</code> equal to <code>+1</code> corresponds to a proton, whilst <code>-1</code> corresponds to an anti-proton.
<code>zerowidth</code>	When set to <code>.true.</code> then all bosons are produced on-shell. This is appropriate for calculations of <i>total</i> cross-sections (such as when using <code>removebr</code> equal to <code>.true.</code> , below). When interested in decay products of the bosons this should be set to <code>.false.</code>
<code>removebr</code>	When set to <code>.true.</code> the branching ratios are removed for unstable particles such as vector bosons or top quarks. See the process notes in Section 13, or the process web-pages accessed via the list of processes for further details.
<code>ewcorr</code>	Specifies whether or not to compute EW corrections for the process. Default is <code>none</code> . May be set to <code>exact</code> or <code>sudakov</code> for processes 31 (neutral-current DY), 157 (top-pair production) and 190 (di-jet production). For more details see section 5.3.

6.1.2 Resummation

Section resummation	Description
<code>makegrid</code>	If <code>.true.</code> , then MCFM performs the convolution required to produce beam functions from PDFs and saves the result as an LHAPDF grid file. The generated grid files are placed in the directory <code>gridoutpath</code> from LHAPDF grids in the directory <code>gridinpath</code> . After the grid generation MCFM stops and should be run subsequently with <code>makegrid = .false.</code> and <code>usegrid = .true.</code> . When <code>lhpdf%dopdferrors=.true.</code> then also grids for the error sets are generated.

<code>usegrid</code>	<code>.true.</code> or <code>.false.</code> determines whether pregenerated LHAPDF interpolation grids should be used for the resummation beam functions. Setting <code>usegrid = .true.</code> is much more efficient, after a suitable run with <code>makegrid = .true.</code> (see above).
<code>gridoutpath</code>	Output directory for LHAPDF grid files, for example <code>/home/tobias/local/share/LHAPDF/</code>
<code>gridinpath</code>	Input directory for LHAPDF grid files, for example <code>/home/tobias/local/share/LHAPDF/</code>
<code>res_range</code>	Integration range of purely resummed part, for example <code>0.0 80.0</code> for q_T integration between 0 and 80 GeV.
<code>resexp_range</code>	Integration range of fixed-order expanded resummed part, for example <code>1.0 80.0</code> for q_T integration between 1 and 80 GeV.
<code>fo_cutoff</code>	Lower q_T cutoff q_0 for the fixed-order part. Typically the value should agree with the lower range of <code>resexp_range</code> .
<code>transitionswitch</code>	Parameter passed to the plotting routine to modify the transition function, see text.

6.1.3 NNLO

Section mnlo	Description
<code>taucut</code>	Optional. This sets the value of the jettiness variable τ_{cut} , as a multiple of the invariant mass of the Born system, i.e.
	$\tau_{\text{cut}} = \text{taucut} \times Q \quad (6)$
<code>tcutarray</code>	This variable separates the resolved and unresolved regions in NNLO calculations that use zero-jettiness. The default value results in total inclusive cross sections with less than 1% residual cutoff effects. Optional. Array that specifies multiple <code>taucut</code> values that should be sampled on the fly in addition to the nominal <code>taucut</code> value. Both larger and smaller values than the nominal one can be specified, although uncertainties for smaller values will be large. We generally do not recommend smaller values than the nominal one chosen with <code>taucut</code> . Default values are chosen to be 2, 4, 8, 20, 40 times the nominal choice of <code>taucut</code> .
<code>dynamictau</code>	Optional. If <code>.false.</code> , the <code>taucut</code> value specified is not multiplied by the invariant mass of the Born system. Default is <code>.true.</code> .
<code>useqt</code>	Flag to use q_T slicing, rather than 0-jettiness, in the calculation of NNLO contributions. Default is <code>.false.</code>
<code>useGLY</code>	If <code>.true.</code> , implement non-local q_T subtraction using formulas from Gehrmann et al.(GLY) [56]. Default is <code>.true.</code> when <code>useqt</code> is enabled. If <code>.false.</code> , implement non-local q_T subtraction using formulas from Billis et al.(BEMT) [57].
<code>qtcut</code>	If <code>useqt</code> is enabled, the value of the slicing parameter, defined in the same way as <code>taucut</code> described above.
<code>tauboot</code>	When using 0-jettiness, perform the slicing cut in the centre-of-mass of the color singlet system. Default is <code>.true.</code>
<code>incpowcorr</code>	When using 0-jettiness, include leading power corrections in the below-cut calculation. Default is <code>.false.</code>

<code>onlypowcorr</code>	When using 0-jettiness, only compute the power corrections to the below-cut calculation. Default is <code>.false</code> .
<code>usept</code>	This flag has two separate uses. In a fixed-order slicing calculation, e.g. <code>part</code> is equal to <code>snlo</code> or <code>nnlo</code> , the code uses p_T^{veto} slicing, rather than 0-jettiness, in the calculation of higher-order contributions. In a resummed calculation, e.g. <code>part</code> is equal to <code>resNLO</code> or <code>resNNLO</code> , it enables the use of p_T^{veto} resummation rather than q_T resummation. In this case the value of the jet veto (<code>ptveto</code>) is set separately in the <code>resummation</code> block. Default is <code>.false</code> .
<code>useBNR</code>	Implements p_T^{veto} formalism using the refactorized approach of Ref. [58]. Otherwise uses original ' $B \times B \times S$ ' factorization of below-cut cross-section into beam and soft functions (that gives identical results). Default is <code>.true</code> .

6.1.4 PDFs

Section pdf	Description
<code>pdlabel</code>	This specifies the parton distributions used in the case when the code has been built with <code>PDFROUTINES = NATIVE</code> . The choice of parton distribution is made by inserting the appropriate 7-character code from Table ?? or in Tables ?? and ?? for historical PDF sets. As mentioned above, this also sets the value of $\alpha_S(M_Z)$.

6.1.5 LHAPDF

Section lhpdf	Description
<code>lhpdfset</code>	Specifies the parton distributions used in the case when the code has been built with <code>PDFROUTINES = LHAPDF</code> . For a default global installation the PDFs reside in <code>/usr/share/LHAPDF/</code> or <code>/usr/local/share/LHAPDF/</code> , and the name equals the set name from https://lhpdf.hepforge.org/pdfsets.html , which is also the directory name of the sets. Multiple PDF sets separated by a space can be specified.
<code>lhpdfmember</code>	Specifies the individual members of the parton distribution sets. A value of zero corresponds to the central value for Hessian sets. In the case when multiple sets have been specified above, each one needs a member number separated by space.
<code>dopdferrors</code>	When this is set to <code>.true.</code> , PDF uncertainties are calculated for every specified PDF set according to the routines provided by LHAPDF. The <code>lhpdfmember</code> numbers are ignored but must still be set for each member.

6.1.6 Scales

Section scales	Description
<code>renscale</code>	This parameter may be used to adjust the value of the <i>renormalization</i> scale. This is the scale at which α_S is evaluated and will typically be set to a mass scale appropriate to the process (M_W , M_Z , m_t for instance).

<code>facscale</code>	This parameter may be used to adjust the value of the <i>factorization</i> scale and will typically be set to a mass scale appropriate to the process (M_W , M_Z , m_t for instance).
<code>dynamicscale</code>	This character string is used to specify whether the renormalization, factorization and fragmentation scales are dynamic, i.e. recalculated on an event-by-event basis. If this string is set to ‘ none ’ then the scales are fixed for all events at the values specified by <code>renscale</code> , <code>facscale</code> as well as <code>fragmentation_scale</code> as defined further below. The type of dynamic scale to be used is selected by using a particular string for the variable <code>dynamicscale</code> , as indicated in Table 12. Not all scales are defined for each process, with program execution halted if an invalid selection is made in the input file. The selection chooses a reference scale, μ_0 . The actual scales used in the code are then,

$$\mu_{\text{ren}} = \text{renscale} \times \mu_0, \quad \mu_{\text{fac}} = \text{facscale} \times \mu_0 \quad (7)$$

<code>doscalevar</code>	Note that, for simplicity, the fragmentation scale (relevant only for processes involving photons) is set equal to the renormalization scale. In some cases it is possible for the dynamic scale to become very large. This can cause problems with the interpolation of data tables for the PDFs and fragmentation functions. As a result if a dynamic scale exceeds a maximum of 60 TeV (PDF) or 990 GeV (fragmentation) this value is set by default to the maximum. This additional option can be set to <code>.true.</code> to enable scale variation. It performs a variation of the scales used in 7 by a factor of two so that it surveys the additional possibilities,
-------------------------	--

$$(2\mu_{\text{ren}}, 2\mu_{\text{fac}}), (\mu_{\text{ren}}/2, \mu_{\text{fac}}/2)$$

$$(2\mu_{\text{ren}}, \mu_{\text{fac}}), (\mu_{\text{ren}}/2, \mu_{\text{fac}}),$$

$$(\mu_{\text{ren}}, 2\mu_{\text{fac}}), (\mu_{\text{ren}}, \mu_{\text{fac}}/2).$$
(8)

<code>maxscalevar</code>	The histograms corresponding to these different choices are included in the output file, from which an envelope of theoretical uncertainty may be constructed by the user. Number of additional scale variation points to choose, can be set to two or six. For two it just samples the first two variations as in Eq. 8.
--------------------------	--

6.1.7 Masses

Section masses	Description
<code>hmass</code>	Higgs pole mass
<code>mt</code>	Top-quark pole mass
<code>mb</code>	Bottom-quark pole mass
<code>mc</code>	Charm-quark pole mass
<code>wmass</code>	W-boson pole mass
<code>zmass</code>	Z-boson pole mass

dynamic scale	μ_0^2	comments
m(34)	$(p_3 + p_4)^2$	M = mass of particle 3+4 M = mass of particle 3+4+5 M = mass of particle 3+4 M = mass(3+4), j_1 = leading p_T jet
m(345)	$(p_3 + p_4 + p_5)^2$	
m(3456)	$(p_3 + p_4 + p_5 + p_6)^2$	
sqrt(M^2+pt34^2)	$M^2 + (\vec{p}_{T3} + \vec{p}_{T4})^2$	
sqrt(M^2+pt345^2)	$M^2 + (\vec{p}_{T3} + \vec{p}_{T4} + \vec{p}_{T5})^2$	
sqrt(M^2+pt5^2)	$M^2 + \vec{p}_{T5}^2$	
sqrt(M^2+ptj1^2)	$M^2 + \vec{p}_{Tj_1}^2$	
pt(photon)	$\vec{p}_{T\gamma}^2$	
pt(j1)	$\vec{p}_{Tj_1}^2$	
HT	$\sum_{i=1}^n p_{Ti}$	
		n particles (partons, not jets)

Table 12: Choices of the input parameter `dynamic scale` that result in an event-by-event calculation of all relevant scales using the given reference scale-squared μ_0^2 .

6.1.8 Basic jets

Section basicjets	Description
inclusive	This logical parameter chooses whether the calculated cross-section should be inclusive in the number of jets found at NLO. An <i>exclusive</i> cross-section contains the same number of jets at next-to-leading order as at leading order. An <i>inclusive</i> cross-section may instead contain an extra jet at NLO.
algorithm	This specifies the jet-finding algorithm that is used, and can take the values <code>ktal</code> (for the Run II k_T -algorithm), <code>ankt</code> (for the “anti- k_T ” algorithm [59]), <code>cone</code> (for a midpoint cone algorithm), <code>hqrk</code> (for a simplified cone algorithm designed for heavy quark processes) and <code>none</code> (to specify no jet clustering at all). The latter option is only a sensible choice when the leading order cross-section is well-defined without any jet definition: e.g. the single top process, $q\bar{q}' \rightarrow t\bar{b}$, which is finite as $p_T(\bar{b}) \rightarrow 0$.
ptjetmin,	These specify the values of $p_{T,\min}$ and $ \eta _{\max}$ for the jets that are found by the algorithm.
etajetmax	
etajetmin	Optional parameter for setting a minimum jet rapidity $ \eta _{\min}$.
ptjetmax	Optional parameter for setting maximum jet $p_{T,\max}$
Rcutjet	If the final state of the chosen process contains either quarks or gluons then for each event an attempt will be made to form them into jets. For this it is necessary to define the jet separation
	$\Delta R = \sqrt{\Delta\eta^2 + \Delta\phi^2} \quad (9)$
	so that after jet combination, all jet pairs are separated by $\Delta R > \text{Rcutjet}$.
userap	Optional parameter for using jet rapidity rather than pseudorapidity when performing jet cuts. Default is <code>.true..</code>

6.1.9 Mass cuts

Section masscuts	Description
m34min,	These parameters represent a basic set of mass cuts that are be applied to the calculated cross-section. The only events that contribute to the
m34max,	

6.1.10 Cuts

Section cuts	Description
<code>makecuts</code>	If this parameter is set to <code>.false.</code> , then no additional cuts are applied to the events (apart from those in Sections 6.1.8 and 6.1.9) and the remaining parameters in this section are ignored. Otherwise, events will be rejected according to a set of cuts that is specified below. Further options may be implemented by editing <code>src/User/gencuts_user.f90</code> .
<code>ptleptmin</code> , <code>etaleptmax</code>	These specify the values of $p_{T,\min}$ and $ \eta _{\max}$ for one of the leptons produced in the process. One can also introduce optional settings <code>ptleptmax</code> and <code>etaleptmin</code> .
<code>etaleptveto</code>	This should be specified as a pair of double precision numbers that indicate a rapidity range that should be excluded for the lepton that passes the above cuts.
<code>ptminmiss</code>	Specifies the minimum missing transverse momentum (coming from neutrinos).
<code>ptlept2min</code> , <code>etalept2max</code>	These specify the values of $p_{T,\min}$ and $ \eta _{\max}$ for the remaining leptons in the process. This allows for staggered cuts where, for instance, only one lepton is required to be hard and central. One can also introduce optional settings <code>ptlept2max</code> and <code>etalept2min</code> .
<code>etalept2veto</code>	This should be specified as a pair of double precision numbers (separated by a space) that indicate a rapidity range that should be excluded for the remaining leptons.

6.1.11 Cuts (continued)

Section cuts	Description
<code>m34transmin</code>	<p>For general processes, this specifies the minimum transverse mass of particles 3 and 4,</p> $\text{general : } 2p_T(3)p_T(4) \left(1 - \frac{\vec{p}_T(3) \cdot \vec{p}_T(4)}{p_T(3)p_T(4)} \right) > \text{m34transmin} \quad (10)$ <p>For the $W(\rightarrow \ell\nu)\gamma$ process the role of this cut changes, to become instead a cut on the transverse cluster mass of the $(\ell\gamma, \nu)$ system,</p> $W\gamma : m_T^2 = \left[\sqrt{m_{\ell\gamma}^2 + \vec{p}_T(\ell) + \vec{p}_T(\gamma) ^2} + p_T(\nu) \right]^2 - \vec{p}_T(\ell) + \vec{p}_T(\gamma) + \vec{p}_T(\nu) ^2$ $m_T > \text{m34transmin} \quad (11)$ <p>For the $Z\gamma$ process this parameter specifies a simple invariant mass cut,</p> $Z\gamma : m_{Z\gamma} > \text{m34transmin} \quad (12)$ <p>A final mode of operation applies to the $W\gamma$ process and is triggered by a negative value of <code>m34transmin</code>. This allows simple access to the cut that was employed in v6.0 of the code:</p> $W\gamma, \text{obsolete} : m_T^2 = [p_T(\ell) + p_T(\gamma) + p_T(\nu)]^2 - \vec{p}_T(\ell) + \vec{p}_T(\gamma) + \vec{p}_T(\nu) ^2$ $m_T > \text{m34transmin} \quad (13)$
<code>Rj1min</code>	<p>In each case the screen output indicates the cut that is applied.</p> <p>Using the definition of ΔR given above in Eq.9), requires that all jet-lepton pairs are separated by $\Delta R > \text{R(jet,lept)}_{\text{min}}$.</p>
<code>Rllmin</code>	<p>When non-zero, all lepton-lepton pairs must be separated by $\Delta R > \text{R(lept,lept)}_{\text{min}}$.</p>
<code>delyjjmin</code>	<p>This enforces a rapidity gap between the two hardest jets j_1 and j_2, so that: $\eta^{j_1} - \eta^{j_2} > \text{delyjjmin}$.</p>
<code>jetsopphem</code>	<p>If this parameter is set to <code>.true.</code>, then the two hardest jets are required to lie in opposite hemispheres, $\eta^{j_1} \cdot \eta^{j_2} < 0$.</p>
<code>lbjscheme</code>	<p>This integer parameter provides no additional cuts when it takes the value 0. When equal to 1 or 2, leptons are required to lie between the two hardest jets. With the ordering $\eta^{j_-} < \eta^{j_+}$ for the rapidities of jets j_1 and j_2: <code>lbjscheme</code> = 1 : $\eta^{j_-} < \eta^{\text{leptons}} < \eta^{j_+}$; <code>lbjscheme</code> = 2 : $\eta^{j_-} + \text{Rcutjet} < \eta^{\text{leptons}} < \eta^{j_+} - \text{Rcutjet}$.</p>
<code>ptbjetmin,</code> <code>etabjetmax</code>	<p>If a process involving b-quarks is being calculated, then these can be used to specify <i>stricter</i> values of p_T^{min} and $\eta ^{\text{max}}$ for b-jets. Similarly, values for <code>ptbjetmax</code> and <code>etabjetmin</code> can be specified.</p>

6.1.12 Photon

Note that all the photon cuts specified in this section of the input file, are applied even if `makecuts` is set to `.false..`

Section photon	Description
<code>fragmentation</code>	This parameter is a logical variable that determines whether the production of photons by a parton fragmentation process is included. If <code>fragmentation</code> is set to <code>.true..</code> , the code uses a standard cone isolation procedure (that includes LO fragmentation contributions in the NLO calculation). If <code>fragmentation</code> is set to <code>.false..</code> , the code implements a Frixione-style photon cut [55],

$$\sum_{i \in R_0} E_{T,i}^j < \epsilon_h E_T^\gamma \left(\frac{1 - \cos R_{i\gamma}}{1 - \cos R_0} \right)^n. \quad (14)$$

In this equation, R_0 , ϵ_h and n are defined by `cone_ang`, `epsilon_h` and `n_pow` respectively (see below). $E_{T,i}^j$ is the transverse energy of a parton, E_T^γ is the transverse energy of the photon and R is the separation between the photon and the parton using the usual definition

$$R = \sqrt{\Delta\phi_{i\gamma}^2 + \Delta\eta_{i\gamma}^2}. \quad (15)$$

	n is an integer parameter which by default is set to 1.
<code>fragmentation_set</code>	A length eight character variable that is used to choose the particular photon fragmentation set. Currently implemented fragmentation functions can be called with ‘BFGSet_I’, ‘BFGSetII’ [60] or ‘GdRG_LO’ [61].
<code>fragmentation_scale</code>	A double precision variable that will be used to choose the scale at which the photon fragmentation is evaluated.
<code>gammptmin</code>	This specifies the value of p_T^{\min} for the photon with the largest transverse momentum. Note that this cut, together with all the photon cuts specified in this section of the input file, are applied even if <code>makecuts</code> is set to <code>.false..</code> One can also add an entry for <code>gammptmax</code> to cut on a range.
<code>gammrapmax</code>	This specifies the value of $ y ^{\max}$ for any photons produced in the process. One can also add an entry for <code>gammrapmin</code> to cut on a range.
<code>gammpt2, gammpt3</code>	The values of p_T^{\min} for the second and third photons, ordered by p_T .
<code>Rgalmin</code>	Using the usual definition of R above, this requires that all photon-lepton pairs are separated by $R > \text{Rgalmin}$. This parameter must be non-zero for processes in which photon radiation from leptons is included.
<code>Rgagamin</code>	Using the usual definition of R above, this requires that all photon pairs are separated by $R > \text{Rgagamin}$.
<code>Rgajetmin</code>	Using the usual definition of R above, this requires that all photon-jet pairs are separated by $R > \text{Rgajetmin}$.
<code>cone_ang</code>	Fixes the cone size (R_0) for photon isolation. This cone is used in both forms of isolation.
<code>epsilon_h</code>	This cut controls the amount of radiation allowed in cone when <code>fragmentation</code> is set to <code>.true..</code> If <code>epsilon_h</code> < 1 then the photon is isolated using $\sum_{i \in R_0} E_T(\text{had}) < \epsilon_h p_T^\gamma$. Otherwise <code>epsilon_h</code> > 1 sets $E_T(\text{max})$ in $\sum_{i \in R_0} E_T(\text{had}) < E_T(\text{max})$.

<code>n_pow</code>	When using the Frixione isolation prescription, the exponent n in Eq. (14).
<code>fixed_coneenergy</code>	This is only operational when using the Frixione isolation prescription. If <code>fixed_coneenergy</code> is <code>.false.</code> then ϵ_h controls the amount of hadronic energy allowed inside the cone using the Frixione isolation prescription (see above, Eq. (14)) If <code>fixed_coneenergy</code> is <code>.true.</code> then this formula is replaced by one where $\epsilon_h E_T^\gamma \rightarrow \epsilon_h$.
<code>hybrid, R_inner</code>	If <code>hybrid</code> is set to <code>.true.</code> use a hybrid isolation scheme with Frixione isolation on an inner cone of radius <code>R_inner</code> .

6.1.13 Histograms

Section histogram	Description
<code>writetop</code>	Write output histograms suitable as input for top-drawer.
<code>writetxt</code>	Write output histograms as whitespace-separated columns.
<code>newstyle</code>	Use the new plotting infrastructure introduced in MCFM-10.0

6.1.14 Integration

Section integration	Description
<code>usesobol</code>	When <code>.true.</code> and the number of MPI processes is a power of two, the Sobol sequence is used, see ref. [62], otherwise the MT19937 pseudo random number generator.
<code>seed</code>	Initialization seed for MT19937 pseudo random number generator.
<code>precisiongoal</code>	Relative precision goal for the integration.
<code>readin</code>	When <code>.true.</code> the automatically written snapshot from a previous run will be read-in to resume the integration.
<code>writeintermediate</code>	When <code>.true.</code> histograms are written after each Vegas iteration.
<code>warmupprecisiongoal</code>	Sets the relative precision goal for the warmup run. Unless this precision is reached, the number of calls for the warmup is increased.
<code>warmupchisqgoal</code>	Sets the χ^2 per iteration goal for the warmup run. Unless the χ^2 /it. of the warmup is below this target, the number of calls for the warmup is increased.

6.2 Process specific options

6.2.1 Single Top

Section singletop	Description
c_phiq	Sets real Wilson coefficient of $Q_{\varphi q}^{(3,33)}$ for processes 164 and 169. See 13.40 and ref. [33].
c_phphi	Sets real and imaginary part of the $Q_{\varphi ud}^{33}$ Wilson coefficient.
c_tw	Sets real and imaginary part of the Q_{uW}^{33} Wilson coefficient.
c_bw	Sets real and imaginary part of the Q_{dW}^{33} Wilson coefficient.
c_tg	Sets real and imaginary part of the Q_{uG}^{33} Wilson coefficient.
c_bg	Sets real and imaginary part of the Q_{dG}^{33} Wilson coefficient.
lambda	Scale Λ , see 13.40 and ref. [33].
enable_lambda4	Enable contributions of order $1/\Lambda^4$ when set to <code>.true.</code> .
disable_sm	When set to <code>.true.</code> the pure SM contributions are disabled, and just the SM-EFT interference and EFT contributions are calculated.
mode_anomcoup	When set to <code>.true.</code> at LO one can reproduce results obtained without power counting as in the anomalous couplings approach, see 13.40 and ref. [33].
nnlo_enable_light, nnlo_enable_heavy_prod, nnlo_enable_heavy_decay, nnlo_enable_interf_lxh, nnlo_enable_interf_lxd, nnlo_enable_interf_hxd, nnlo_fully_inclusive	At NNLO there are several different contributions from vertex corrections on the light-quark line, heavy-quark line in production, and heavy-quark line in the top-quark decay. Additionally there are one-loop times one-loop interference contributions between all three contributions. For a fully inclusive calculation without decay <code>nnlo_fully_inclusive</code> has to be set to <code>'true.'</code> and the decay and decay interference parts have to be removed. Additionally jet requirements must be lifted. For further information see Section 13.39.

6.2.2 Anomalous W/Z couplings

Section anom_wz	Description
enable	Boolean flag to enable anomalous W-boson and Z-boson coupling contributions for certain processes. False has the same effect as setting all anomalous couplings to zero, but additionally skips computation of anomalous coupling code parts.
delg1_z	Δg_1^Z See section 13.24.
delk_z	$\Delta \kappa^Z$ See section 13.24.
delk_g	$\Delta \kappa^\gamma$ See sections 13.24 and 13.73.
lambda_z	Λ^Z See section 13.24.
lambda_g	Λ^γ See sections 13.24 and 13.73.
h1Z	h_1^Z Anomalous couplings for $Z\gamma$ process at NNLO. See section 13.74.
h1gam	h_1^γ See section 13.74.
h2Z	h_2^Z See section 13.74.

<code>h2gam</code>	h_2^γ See section 13.74.
<code>h3Z</code>	h_3^Z See section 13.74.
<code>h3gam</code>	h_3^γ See section 13.74.
<code>h4Z</code>	h_4^Z See section 13.74.
<code>h4gam</code>	h_4^γ See section 13.74.
<code>tevscale</code>	Form-factor scale, in TeV See section 13.24. No form-factors are applied to the anomalous couplings if this value is negative.

6.2.3 $W/Z+2$ jets

Section wz2jet	Description
Qflag	This only has an effect when running a $W + 2$ jets or $Z + 2$ jets process. When <code>.true.</code> , it includes the effect of four-quark processes. Please see section 13.10 below.
Gflag	This only has an effect when running a $W + 2$ jets or $Z + 2$ jets process. When <code>.true.</code> , it includes the effect of two-quark, two-gluon processes. Please see section 13.10 below.

6.2.4 H jetmass

Section hjetmass	Description
mtex	Sets the order $k = 0, 2, 4$ of the $1/m_t^k$ expansion for virtual corrections in the H +jet process 200. See section 13.43.

6.2.5 Anomalous H couplings

Section anom_higgs	Description
hwidth_ratio	For processes 123–126, 128–133 only, this variable provides a rescaling of the width of the Higgs boson. Couplings are rescaled such that the corresponding cross section close to the Higgs boson peak is unchanged. Further details of this procedure are given in arXiv:1311.3589 .
cttH,cWWH	See arXiv:1311.3589 .

6.2.6 Extra

Section extra	Description
debug	A logical variable which can be used during a debugging phase to mandate special behaviours. Passed by common block <code>common/debug/debug</code> .
verbose	A logical variable which can be used during a debugging phase to write special information. Passed in common block <code>common/verbose/verbose</code> .
new_pspace	A logical variable which can be used during a debugging phase to test alternative versions of the phase space. Passed in common block <code>common/new_pspace/new_pspace</code> .
spira	A logical variable. If <code>spira</code> is <code>.true.</code> , we calculate the width of the Higgs boson by interpolating from a table calculated using the NLO code of M. Spira. The default value is <code>.true.</code> . Otherwise the LO value valid for low Higgs masses only is used.
noglu	A logical variable. The default value is <code>.false.</code> . If set to <code>.true.</code> , no processes involving initial gluons are included.
ggonly	A logical variable. The default value is <code>.false.</code> . If set to <code>.true.</code> , only the processes involving initial gluons in both hadrons are included.
gqonly	A logical variable. The default value is <code>.false.</code> . If set to <code>.true.</code> , only the processes involving an initial gluon in one hadron and an initial quark or antiquark in the other hadron (or vice versa) are included.

<code>omitgg</code>	A logical variable. The default value is <code>.false..</code> If set to <code>.true.</code> , the gluon-gluon initial state is not included.
<code>clustering</code>	This logical parameter determines whether clustering is performed to yield jets. Only during a debugging phase should this variable be set to <code>.false..</code>
<code>colourchoice</code>	If <code>colourchoice=0</code> , all colour structures are included ($W, Z + 2$ jets). If <code>colourchoice=1</code> , only the leading colour structure is included ($W, Z + 2$ jets).
<code>rtsmin</code>	A minimum value of $\sqrt{s_{12}}$, which ensures that the invariant mass of the incoming partons can never be less than <code>rtsmin</code> .
<code>reweight</code>	Flag to set the use of the user-implemented reweighting procedure <code>reweight_user</code> in the routine <code>src/User/gencuts_user.f90</code> .

6.2.7 Dipoles

Section dipoles	Description
<code>aii</code>	A double precision variable which can be used to limit the kinematic range for the subtraction of initial-initial dipoles as suggested by Trocsanyi and Nagy [63]. The value <code>aii=1</code> corresponds to standard Catani-Seymour subtraction.
<code>aif</code>	A double precision variable which can be used to limit the kinematic range for the subtraction of initial-final dipoles as suggested by Trocsanyi and Nagy [63]. The value <code>aif=1</code> corresponds to standard Catani-Seymour subtraction.
<code>afi</code>	A double precision variable which can be used to limit the kinematic range for the subtraction of final-initial dipoles as suggested by Trocsanyi and Nagy [63]. The value <code>afi=1</code> corresponds to standard Catani-Seymour subtraction.
<code>aff</code>	A double precision variable which can be used to limit the kinematic range for the subtraction of final-final dipoles as suggested by Trocsanyi and Nagy [63]. The value <code>aff=1</code> corresponds to standard Catani-Seymour subtraction.
<code>bfi</code>	A double precision variable which can be used to limit the kinematic range for the subtraction of final-initial dipoles in the photon fragmentation case.
<code>bff</code>	A double precision variable which can be used to limit the kinematic range for the subtraction of final-final dipoles in the photon fragmentation case.

7 Histograms

7.1 Output

In addition to the direct output of the program to `stdout`, after all integration regions have completed the warmup stage and a subsequent sweep has been made for each contribution,

the program will produce additional output files as specified below. If a working directory was specified in the command line, then these output files will be written to that directory.

The standard output will detail the iteration-by-iteration best estimate of each contribution to the total cross-section, together with the accompanying error estimate. Estimates of the total cross-section, summing over all contributions, will be reported in the form:

```
Value of integral is    11.7521        0.58456E-02 nb
```

Other output files may be produced containing various histograms associated with the calculated process. The write-out of the different output files is controlled by the logical variable `nohistograms` in the `extra` section. The default value of this variable is `.false.`, but setting it to `true` may be useful for faster running if no histograms are required.

Histograms are written to a series of files with the generic naming structure:

```
procname_part_lhapdfset_scale_facscale_runstring_histoname.txt
```

where `procname` is a label assigned by the program corresponding to the calculated process; `histoname` is the name of the histogram specified in the plotting routine (see below) and the remaining labels are as input by the user in the file `input.ini`.

A default set of histograms is filled for each process. A snippet of the histogram output is repeated below:

```
# W rapidity
# underflow    0.0000000    0.0000000
# overflow     0.0000000    0.0000000
# sum    10453523.    7919.1419
# xmin xmax cross numerror
-6.0000000    -5.8000000    0.0000000    0.0000000
-5.8000000    -5.6000000    0.0000000    0.0000000
-5.6000000    -5.4000000    0.0000000    0.0000000
-5.4000000    -5.2000000    0.0000000    0.0000000
-5.2000000    -5.0000000    7.1413485    0.24680943
-5.0000000    -4.8000000    1289.2697    28.436126
-4.8000000    -4.6000000    11218.037    211.10230
-4.6000000    -4.4000000    36844.231    656.21780
```

The header lines provide the name of the histogram and the accumulated cross-section and uncertainty entering the bins (`sum`), as well as any underflow or overflow outside the bins (zero in this case). The following lines report the results in each bin, in the format: bin lower edge, bin upper edge, accumulated cross section, uncertainty. The units of the reported cross-sections are femtobarns.

To modify existing, or add new, histograms one must edit the plotting routine specified in each process description. These are found in the directory `src/User/` and correspond to the (default) value `.false.` for the flag `newstyle` in the `histogram` section.

Additional plotting infrastructure was included in the release of CuTe-MCFM, which is enabled by setting `histogram%newstyle = .true.` in the input file. At present this is only possible for the processes W^\pm , Z , H , $\gamma\gamma$, $Z\gamma$, ZH , $W^\pm H$, WW , $W^\pm Z$ and ZZ . It is the default for the CuTe-MCFM example input files. The predefined plotting routines that can be adjusted in this case are, for example for Z production, in the file `src/User/nplotter_Z_new.f90`, and similarly for the other processes.

A brief description of the two alternatives for the plotting routines is provided in the subsections below.

7.1.1 Traditional histograms

Traditional histograms are selected with `newstyle = .false.`

Modifying the plotting routines in the files `src/User/nplotter*.f` allows for modification of the pre-defined histograms and addition of any number of arbitrary observables. One can also edit the subroutine `nplotter_user` in the file `src/User/nplotter.f`, which is also called for every process in order to allow the user to bin their own histograms. Similar to the other routines, the routine is called as:

```
subroutine nplotter_user(p, wt,wt2, nd)
....
include 'mxpart.f'
....
real(dp), intent(in) :: p(mxpart,4),wt,wt2
integer, intent(in) :: nd
```

The variables passed to this routine are:

- `p(1,:)`: 4-momenta of incoming partons ($i = 1,2$), outgoing leptons and jets ($i = 3,4,...$) in the format `p(i,4)` with the particles numbered according to the input file and components labelled by `(px,py,pz,E)`.
- `wt`: weight of this event
- `wt2`: weight^2 of this event
- `nd`: an integer specifying the dipole number of this contribution (if applicable), otherwise equal to zero.

Extra histograms may be added to the plotting files in a fairly straightforward manner. Each histogram is filled by making a call to the routine `bookplot` and updating the histogram counter `n` by 1. For example, the pseudorapidity of particle 3 may be plotted using the following code fragment:

```
eta3=etarap(3,p)
call bookplot(n,tag,'eta3',eta3,wt,wt2,-4d0,4d0,0.1d0,'lin')
n=n+1
```


The first two arguments of the call should not be changed. The third argument is a string which is used as the title of the plot in the output files. The fourth argument carries the variable to be plotted, which must have been previously calculated. The arguments `wt` and `wt2` contain information about the phase-space weight and should not be changed. The last arguments tell the histogramming routine to use bins of size 0.1 which run from -4 to 4, and use a linear scale for the plot. A logarithmic scale may be used by changing the final argument to 'log'.

7.1.2 New style histograms

New style histograms are selected with `newstyle = .true.`

The routine `setup` first allocates the required space to store all histograms. For instance, space for 2 histograms is requested with:

```
allocate(histos(2))
```

Following this, the histograms can be defined either with uniform binning or custom bin sizes. For example, the line:

```
histos(1) = plot_setup_uniform(0._dp,500._dp,10._dp,'mZZ')
```

initializes the first histogram with bins from 0 to 500, of width 10, named `mZZ`. The second histogram could be initialized with:

```
histos(2) = plot_setup_custom([0d0,25d0,50d0,75d0,100d0,150d0,200d0], 'ptZZ')
```

This time the first argument sets up the array of bin edges – 7 edges to define 6 bins – and the histogram is named `ptZZ`.

After setup, the routine `book` is called for each phase space point. The plotting routine is provided the momentum configuration (`p`) and associated Vegas weight (`wt`). Given these, it returns the array of histograms (`ids`), calculated observables in the `vals` array, and Vegas weights in `wts`. For instance, for the example above this could be accomplished by:

```
ptZZ = ptfour(3,4,5,6,p)
mZZ = puremass(p(3,:)+p(4,:)+p(5,:)+p(6,:))
ids = histos
vals = [ptZZ, mZZ]
wts = [wt, wt]
```

The specification of weights for individual histograms allows the original Vegas weights to be reweighted for particular distributions, for instance with the output of the transition function in the case of resummed calculations.

7.2 User modifications to cuts and reweighting

The routine `gencuts_user` can be adjusted in the file `src/User/gencuts_user.f90` for additional cuts after the jet algorithm has performed the clustering.

In the same file the routine `reweight_user` can be modified to include a manual re-weighting for all integral contributions. This can be used to obtain improved uncertainties in, for example, tails of distributions. One example is included in the subdirectory `mcfm/src/User/examplesmcfm/src/User` where the `reweight_user` function approximately flattens the Higgs transverse momentum distribution, leading to equal relative uncertainties even in the tail at 1 TeV.

8 NNLO using non-local subtraction

We have performed NLO and NNLO calculations for the production of color singlet bosons using different methods and published the results in ref. [21]. NLO calculations can be performed by three methods, (subtraction, zero-jettiness slicing and q_T -slicing. NNLO calculations can be performed by zero-jettiness slicing and q_T -slicing.

8.1 Benchmark results at NNLO

We have included a suite of input files that have been set up to showcase all color-singlet processes that may be computed up to NNLO, located in:

```
Bin/2202.07738_nonlocal/lo
Bin/2202.07738_nonlocal/nlo
Bin/2202.07738_nonlocal/nnlo
```

or accessible via the process web-pages, (linked in the table below) These files reproduce the results presented in Ref. [21]. A list of the processes, input files and results (NNLO coefficient and running time) is shown in Table 28.

9 CuTe-MCFM

The logo for CuTe-MCFM is displayed in a bold, red, stylized font. The letters 'CuTe' are larger and more prominent than 'MCFM'. Small heart symbols are integrated into the design, appearing as part of the 'u' in 'CuTe' and between the 'M' and 'C' in 'MCFM'.

Final state	input file	precision	δ_{NNLO}	Time (CPU days)
H	input_H_qt.ini	0.01	10.13(0.09)pb	2.18
	input_H_scet.ini		10.09(0.09)pb	4.07
Z	input_Z_qt.ini	0.05	-388(20)pb	313
	input_Z_scet.ini		-371(18)pb	261
W^-	input_W-_qt.ini	0.03	-667(20)pb	268
	input_W-_scet.ini		-624(19)pb	213
W^+	input_W+_qt.ini	0.06	-358(21)pb	556
	input_W+_scet.ini		-275(16)pb	555
ZH	input_ZH_qt.ini	0.01	65.9(0.6)fb	19.4
	input_ZH_scet.ini		67.4(0.6)fb	19.1
$W^-H + W^+H$	input_WH_qt.ini	0.01	29.7(0.3)fb	271
	input_WH_scet.ini		29.4(0.3)fb	281
$e^-e^+\gamma$	input_eexa_qt.ini	0.03	133.8(4.0)fb	183
	input_eexa_scet.ini		128.7(3.8)fb	203
$e^-\bar{\nu}_e\gamma$	input_enexa_qt.ini	0.01	389.8(3.9)fb	26.1
	input_enexa_scet.ini		371.7(3.6)fb	50.0
$\nu_e e^+\gamma$	input_neexa_qt.ini	0.01	488.0(4.8)fb	29.1
	input_neexa_scet.ini		461.7(4.6)fb	47.1
$\gamma\gamma$	input_aa_qt.ini	0.01	13.98(0.13)pb	1.08
	input_aa_scet.ini		14.17(0.14)pb	0.92
$e^-\mu^+\bar{\nu}_e\nu_\mu$	input_emxnexnm_qt.ini	0.015	21.2(0.3)fb	325
	input_emxnexnm_scet.ini		21.6(0.3)fb	319
$e^-\bar{\nu}_e\mu^-\mu^+$	input_enexmmx_qt.ini	0.01	2.23(0.02)fb	82.7
	input_enexmmx_scet.ini		2.25(0.02)fb	76.6
$\bar{\nu}_e e^+\mu^-\mu^+$	input_neexmmx_qt.ini	0.01	3.13(0.03)fb	124
	input_neexmmx_scet.ini		3.14(0.03)fb	121
$e^-e^+\mu^-\mu^+$	input_eexmmx_qt.ini	0.01	2.99(0.03)fb	54.2
	input_eexmmx_scet.ini		3.03(0.03)fb	76.1

Table 28: Results have been obtained when requiring the given precision (precisiongoal in the input file) on the calculation of the NNLO coefficient (δ_{NNLO}).

9.1 N³LL and N⁴LL q_T^2 resummation for color-singlet processes in MCFM

Based on [arXiv:2009.11437](https://arxiv.org/abs/2009.11437) (Becher, Neumann '20).

The q_T resummation in CuTe-MCFM is available for color-singlet processes and based on a factorization theorem in SCET. It is fully differential in the Born kinematics and matches to large- q_T^2 fixed-order predictions at relative order α_s^2 . It provides an efficient way to estimate uncertainties from fixed-order truncation, resummation, and parton distribution functions. In addition to W , Z and H production, also the diboson processes $\gamma\gamma$, $Z\gamma$, ZH , WH , WW , WZ and ZZ are available, including decays.

While CuTe-MCFM can calculate q_T -resummed results without using pregenerated beam functions grids, we recommend that LHAPDF grid files are generated for the beam functions beforehand for a choice of a PDF set. This *significantly* accelerates the evaluation of the beam functions and the integration.

CuTe-MCFM ships with pregenerated beamfunction grids for the central values of `CT14nnlo` and `NNPDF31_nnlo_as_0118`, which are included in the `Bin/PDFs` directory. This path is automatically used as the preferred path for LHAPDF grid files. With these pregenerated grids the example input files work out of the box. For other PDF sets or when using PDF errors, the first run of CuTe-MCFM should be with the setting `makegrid=.true..` Additionally the input and output directories for the PDF grids have to be specified. For example the input directory is typically `/usr/local/share/LHAPDF/` (or the `PDFs/` directory relative to the mcfm executable in `Bin`) and the output directory should be a user-writable directory like `/home/user/gridout/` (or `PDFs/`). Note the trailing slashes.

When calling mcfm with `makegrid=.true.` only the beam function grids are written during that run, and mcfm exits afterwards. We recommend to use `PDFs/` as the gridout path, since this path is automatically added to the LHAPDF search paths, and you won't have to copy the generated grid directories to your LHAPDF grid directory or set the `LHAPDF_DATA_PATH` environment variable to the gridout path.

For example for the set `CT14nnlo` the grid directories `CT14nnlo_B00`, `CT14nnlo_B10`, `CT14nnlo_B11`, `CT14nnlo_B20`, `CT14nnlo_B21`, `CT14nnlo_B22` and `CT14nnlo_G10` are written and have to be copied to the directory where LHAPDF searches for the grid files. When the gridout path is chosen as `PDFs/` no further action is necessary. The LHAPDF grid file search path can be modified by setting the shell environment variable `LHAPDF_DATA_PATH` to the desired directory, but the `PDFs` directory is always used as the preferred directory.

The next run of mcfm should be done with `makegrid=.false.` and `usegrid=.true..`

Other important parameters for the resummation are `res_range`, determining the integration range of the purely resummed part, `resexp_range`, determining the integration range of the fixed-order expanded resummed part, and `fo_cutoff` which sets the lower q_T cutoff for the fixed-order part. Typically this cutoff should agree with the lower range of `resexp_range`. For example for Z production one can integrate up to m_Z with a cutoff of 1 GeV: `res_range = 0.0 90.0`, `resexp_range = 1.0 90.0`, `qt_cutoff = 1.0`.

For details regarding these parameters see the next section. The transition function is also discussed below.

9.2 Input file parameters

The `[resummation]` section has been added to the input file to control the resummation. The following keys are available:

Key	Description
<code>usegrid</code>	<code>.true.</code> or <code>.false.</code> determines whether pregenerated LHAPDF interpolation grids should be used for the resummation beam functions.
<code>makegrid</code>	If <code>.true.</code> , then MCFM runs in grid generation mode. This generates LHAPDF grid files in the directory <code>gridoutpath</code> from LHAPDF grids in the directory <code>gridinpath</code> . After the grid generation MCFM stops and should be run subsequently with <code>makegrid = .false.</code> and <code>usegrid = .true.</code> . When <code>lhapdf%dopdferrors=.true.</code> then also grids for the error sets are generated.
<code>gridoutpath</code>	Output directory for LHAPDF grid files, for example <code>/home/tobias/local/share/LHAPDF/</code>
<code>gridinpath</code>	Input directory for LHAPDF grid files, for example <code>/home/tobias/local/share/LHAPDF/</code>
<code>res_range</code>	Integration range of purely resummed part, for example <code>0.0 80.0</code> for q_T integration between 0 and 80 GeV.
<code>resexp_range</code>	Integration range of fixed-order expanded resummed part, for example <code>1.0 80.0</code> for q_T integration between 1 and 80 GeV.
<code>fo_cutoff</code>	Lower q_T cutoff q_0 for the fixed-order part, see eq. (??) below. Typically the value should agree with the lower range of <code>resexp_range</code> .
<code>transitions switch</code>	Parameter passed to the plotting routine to modify the transition function, see text.

We strongly recommend to calculate resummed results with pregenerated grids, see the previous section. The integration range for the purely resummed part can be controlled with the key `res_range` and should typically be between 0 and some upper value. For example for W^\pm , Z or H production this can just be the boson mass. For other processes there can be thresholds and this number must be selected more carefully to not run into numerical issues, see arXiv:2009.11437.

The setting `resexp_range` and `fo_cutoff` are relevant for the matching corrections. The values of the `resexp_range` determine the integration range for the fixed-order expansion of the resummed part. The minimum should typically be at least one GeV for numerical stability. For smaller values significantly more time goes into the integration, and the minimum number of Vegas calls might need to be increased. For single boson processes the maximum value can again be the boson mass, although it can be set to a value where the implemented transition function fully switches to zero. The fixed-order cutoff `fo_cutoff` determines the minimum q_T for the fixed-order calculation. This should typically agree with the lower range of the `resexp_range`.

Lastly, the parameter `transitions switch` is passed for convenience to the plotting routines where the transition function is implemented. It can be used for an easy control of the

transition region as described in the following.

9.3 Plotting routine and transition function

The following transition function is implemented for the example input files. For more details we refer to our publication. The fully matched cross-section is described in general by

$$\left. \frac{d\sigma^{N^3LL}}{dq_T} \right|_{\text{matched to NNLO}} = t(x) \left(\frac{d\sigma^{N^3LL}}{dq_T} + \Delta\sigma|_{q_T > q_0} \right) + (1 - t(x)) \frac{d\sigma^{\text{NNLO}}}{dq_T}$$

using a transition function $t(x)$. We have implemented a transition function t with $x = q_T^2/Q^2$ that smoothly switches between 1 and 0 like a sigmoid function.

Following a choice in CuTe, we first define

$$s(x; l, r, u) = \left(1 + \exp \left(\log \left(\frac{1-u}{u} \right) \frac{x-m}{w} \right) \right)^{-1}, \quad m = (r+l)/2, \quad w = (r-l)/2.$$

The function $s(x)$, parametrized by l, r, u , is defined to be $s(l) = 1 - u$ and $s(r) = u$. In terms of this sigmoid, our transition function $t(x; x^{\min}, x^{\max}, u)$, where $x = q_T^2/Q^2$, is then defined by

$$t(x; x^{\min}, x^{\max}, u) = \begin{cases} 1, & \text{for } x < x^{\min} \\ \frac{s(x; x^{\min}, x^{\max}, u)}{s(x^{\min}; x^{\min}, x^{\max}, u)}, & \text{otherwise} \end{cases}. \quad (16)$$

This ensures that below $x^{\min} = (q_T^{\min}/Q)^2$ only the naively matched result is used, and at x^{\max} for small $u \ll 1$ the transition function is approximately u . In practice it makes sense to set the transition function to zero below a small threshold like 10^{-3} without a noticeable discontinuity. This has the advantage that the deteriorating resummation and matching corrections do not impact the region of large q_T at all. Our example plotting routines use $x^{\min} = 0.001$, and $u = 0.001$, and the parameter x^{\max} corresponds to the value of `transitions witch` set in the input file. The transition function can be changed or completely replaced by just modifying the plotting routines. The following figure illustrates this transition function.

9.4 Modifying the plotting routines and transition function.

The plotting infrastructure has been completely rewritten for CuTe-MCFM, and we recommended to only use the new infrastructure from this point on by setting `histogram%newstyle = .true.` in the input file. This is the default for the CuTe-MCFM example input files.

For the processes $W^\pm, Z, H, \gamma\gamma, Z\gamma, ZH$ and $W^\pm H$ we include predefined plotting routines that can be adjusted. For example for Z production the plotting routine is in the file `src/User/nplotter_Z_new.f90`, and similarly for the other processes. The routine `setup` defines all histograms with custom or uniform binning and names. The number of used histograms needs to be allocated in this routine. The routine `book` is called for each phase space point. Through the boolean variable `abovecut` it is known whether the routine is called for “boosted $q_T = 0$ ” (resummed part and fixed-order expansion of resummed part) or for $q_T > 0$ (fixed-order). All provided example input files use the transition function as defined above, see also [arXiv:2009.11437](https://arxiv.org/abs/2009.11437).

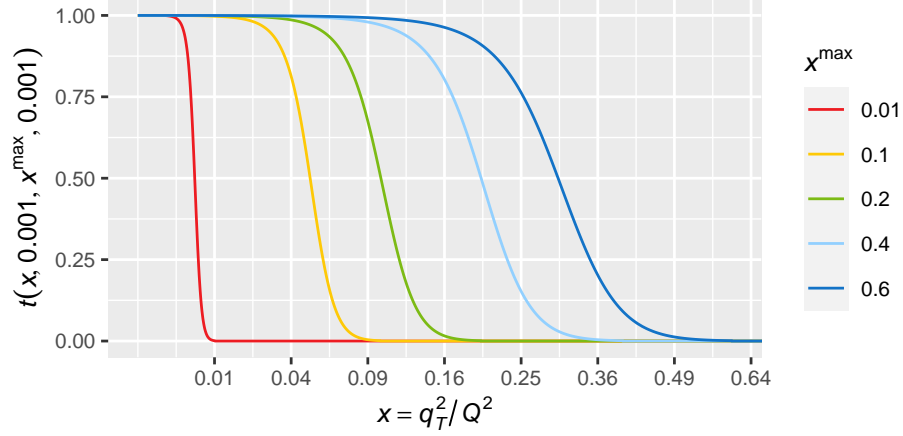


Figure 1: The transition function defined in eq. (16) for different values of the parameter x^{\max} which determines the position of the transition. The x -axis is displayed on a square-root scale to guide the eye on the quadratic q_T -dependence.

The plotting routine returns the calculated observables in the `vals` array, and Vegas weights in `wt`s. The transition function is implemented by reweighting the original Vegas weights with the output of the transition function. To disable the transition function, one sets `trans` to 1 before filling the `wt`s array.

Apart from modifying a default set of kinematical cuts in the input file, cuts can also be set in the file `src/User/gencuts_user.f90` in a fully flexible way based on the event's four momenta. Some commented out examples are included there.

Final state	input file	contribution	cross section
H	H/veto30nlo.ini	NLO	26.23 ± 0.01 pb
	H/veto30nnlo.ini	NNLO	28.97 ± 0.09 pb
	H/veto30nnll.ini	NNLL	24.89 ± 0.01 pb
	H/veto30n3ll.ini	N^3LL_p	24.29 ± 0.01 pb
	H/veto30nlomc.ini	NLO+NNLL MC	2.25 ± 0.01 pb
	H/veto30nnlomc.ini	NNLO+ N^3LL_p MC	3.89 ± 0.19 pb

Table 30: Benchmark results for jet-vetoed Higgs cross sections.

Final state	input file	contribution	cross section
W^+	W/vetowp30nlo.ini	NLO	3.048 ± 0.001 nb
	W/vetowp30nnlo.ini	NNLO	2.81 ± 0.003 nb
	W/vetowp30nnll.ini	NNLL	2.517 ± 0.002 nb
	W/vetowp30n3ll.ini	N^3LL_p	2.250 ± 0.002 nb
	W/vetowp30nlomc.ini	NLO+NNLL MC	0.561 ± 0.006 nb
	W/vetowp30nnlomc.ini	NNLO+ N^3LL_p MC	0.57 ± 0.02 nb
W^-	W/vetowm30nlo.ini	NLO	2.101 ± 0.001 nb
	W/vetowm30nnlo.ini	NNLO	1.979 ± 0.002 nb
	W/vetowm30nnll.ini	NNLL	1.796 ± 0.002 nb
	W/vetowm30n3ll.ini	N^3LL_p	1.600 ± 0.001 nb
	W/vetowm30nlomc.ini	NLO+NNLL MC	0.327 ± 0.003 nb
	W/vetowm30nnlomc.ini	NNLO+ N^3LL_p MC	0.33 ± 0.01 nb

Table 31: Benchmark results for jet-vetoed W^\pm cross sections.

10 Jet-vetoed cross sections

The jet veto scale p_T^{veto} can induce large logarithms if it is smaller than the hard process scale Q , which then mandates resummation. We consider processes where jets have been defined using sequential recombination jet algorithms [64] with distance measure

$$d_{ij} = \min(k_{Ti}^{2n}, k_{Tj}^{2n}) \frac{\Delta y_{ij}^2 + \Delta \phi_{ij}^2}{R^2}, \quad d_{iB} = k_{Ti}^{2n}, \quad (17)$$

where the choice $n = -1$ is the anti- k_T algorithm [59], $n = 0$ is the Cambridge-Aachen algorithm [65, 66], and $n = 1$ is the k_T algorithm [67, 68]. k_{Ti} denotes the transverse momentum of (pseudo-)particle i with respect to the beam direction, and Δy_{ij} and $\Delta \phi_{ij}$ are the rapidity and azimuthal angle differences of (pseudo-)particles i and j .

10.1 Benchmark results for jet-vetoed cross sections

Results for benchmark cross sections for a variety of single-boson processes taken from ref. [10] are shown in Tables 30–32 and for diboson processes in Tables 33–35. The input files are linked in the tables. The uncertainties indicated in these tables represent the numerical integration (Monte Carlo) uncertainty.

Final state	input file	contribution	cross section
Z	Z/veto30nlo.ini	NLO	668 ± 1 pb
	Z/veto30nnlo.ini	NNLO	628 ± 2 pb
	Z/veto30nnll.ini	NNLL	676 ± 2 pb
	Z/veto30n3ll.ini	N^3LL_p	596 ± 2 pb
	Z/veto30nlomc.ini	NLO+NNLL MC	-11 ± 1 pb
	Z/veto30nnlomc.ini	NNLO+ N^3LL_p MC	-7.7 ± 0.7 pb

Table 32: Benchmark results for jet-vetoed Z cross sections.

Final state	input file	contribution	cross section
WW	WW/veto30nlo.ini	NLO	234.0 ± 0.2 fb
	WW/veto30nnlo.ini	NNLO	242.7 ± 0.4 fb
	WW/veto30nnll.ini	NNLL	204.7 ± 0.2 fb
	WW/veto30n3ll.ini	N^3LL_p	205.2 ± 0.2 fb
	WW/veto30nlomc.ini	NLO+NNLL MC	25.8 ± 0.9 fb
	WW/veto30nnlomc.ini	NNLO+ N^3LL_p MC	19.8 ± 0.6 fb

Table 33: Benchmark results for jet-vetoed W^+W^- cross sections.

Final state	input file	contribution	cross section
W^+Z	WZ-atlas/vetowp25nlo.ini	NLO	20.11 ± 0.01 fb
	WZ-atlas/vetowp25nnlo.ini	NNLO	19.14 ± 0.02 fb
	WZ-atlas/vetowp25nnll.ini	NNLL	18.87 ± 0.01 fb
	WZ-atlas/vetowp25n3ll.ini	N^3LL_p	17.72 ± 0.01 fb
	WZ-atlas/vetowp25nlomc.ini	NLO+NNLL MC	0.17 ± 0.06 fb
	WZ-atlas/vetowp25nnlomc.ini	NNLO+ N^3LL_p MC	0.07 ± 0.01 fb
W^-Z	WZ-atlas/vetowm25nlo.ini	NLO	13.54 ± 0.01 fb
	WZ-atlas/vetowm25nnlo.ini	NNLO	12.82 ± 0.01 fb
	WZ-atlas/vetowm25nnll.ini	NNLL	12.66 ± 0.01 fb
	WZ-atlas/vetowm25n3ll.ini	N^3LL_p	11.77 ± 0.01 fb
	WZ-atlas/vetowm25nlomc.ini	NLO+NNLL MC	0.21 ± 0.04 fb
	WZ-atlas/vetowm25nnlomc.ini	NNLO+ N^3LL_p MC	0.12 ± 0.01 fb

Table 34: Benchmark results for jet-vetoed WZ cross sections.

Final state	input file	contribution	cross section
ZZ	ZZ/veto30nlo.ini	NLO	12.17 ± 0.01 fb
	ZZ/veto30nnlo.ini	NNLO	12.88 ± 0.01 fb
	ZZ/veto30nnll.ini	NNLL	11.90 ± 0.01 fb
	ZZ/veto30n3ll.ini	N^3LL_p	11.85 ± 0.01 fb
	ZZ/veto30nlomc.ini	NLO+NNLL MC	-0.22 ± 0.01 fb
	ZZ/veto30nnlomc.ini	NNLO+ N^3LL_p MC	-0.17 ± 0.01 fb

Table 35: Benchmark results for jet-vetoed ZZ cross sections.

11 Z production at N³LO and N⁴LL

Based on [arXiv:2207.07056](https://arxiv.org/abs/2207.07056) (Neumann, Campbell '22).

This page describes how to obtain Z-boson predictions at the level of up to N⁴LL+N³LO and at a fixed order of up to N³LO. The highest order predictions are then at the level of α_s^3 up to missing N³LO PDFs, which both affect the logarithmic accuracy and the fixed-order accuracy.

Warning: Please note that predictions at the level of α_s^3 are computationally very expensive due to the Z+jet NNLO matching corrections calculated with a small (5 GeV) cutoff. Our production plots typically run on 128 NERSC Perlmutter nodes for 12 hours, about 100k CPU hours. If you do not have these resources and are mostly interested in the region of small q_T (less than about 40 GeV), the matching to fixed order can be performed at the level of α_s^2 . This changes results by about 10% above 40 GeV (missing α_s^3 /Z+jet NNLO corrections at large q_T), but typically just at the level of 2% below 30 GeV, depending on cuts.

For Z production one can start with the input file `Bin/input_Z.ini` that has a set of default cuts for Z production, i.e. a mass window of the lepton pair around m_Z (`m34min` and `m34max` are set), and lepton minimum transverse momenta (`ptleptmin` and `ptlept2min`, both the same, i.e. symmetric cuts).

After choosing a set of PDFs (`lhpdf%lhpdfset`), beamfunctions grids should be pre-generated by running MCFM with `resummation%makegrid=.true..`

11.1 N⁴LL + matching at α_s^2 fixed-order (NLO Z+jet)

The fully matched result consists of the purely resummed part, the fixed-order Z+jet calculation and the fixed-order expansion of the resummation to remove overlap. At N³LL'+NNLO these three parts can be computed together automatically with `general%part=resNNLOp`, or with `general%part=resNNLO` at N³LL+NNLO (`general%part=resNLO` at NNLL+NLO). At the level of N⁴LL+N³LO the matching is with NNLO Z+jet predictions and, due to the computational requirements, these three parts are kept separate and have to be assembled manually.

11.1.1 Purely resummed N⁴LL

The purely resummed N⁴LL part can be obtained by running with `part = resonlyN3LO`. Similarly the N³LL resummation is obtained with `part = resonlyNNLO` and N³LL' with `part = resonlyNNLOp` (see overview of configuration options). Scale variation of hard, low and rapidity scale can be enabled with `scales%doscalevar = .true..`

The resummation part will be cut off at large transverse momenta through a transition function defined in the plotting routine. We recommend to use the default transition function with a parameter $(q_T^2/Q^2) = 0.4$ or 0.6 . The default plotting routine generates histograms with both choices that allows for estimating a matching uncertainty.

Since the resummation becomes also invalid and numerically unstable for $q_T > m_Z$, we select the resummation integration range between 0 and 80 GeV with `resummation%res_range=0 80`.

11.1.2 Fixed-order expansion of the resummed result

The fixed-order expansion of the resummed result (removing overlap with fixed-order Z+jet at NLO) (in the following called `resexp`) can be obtained by running `part = resexpNNLO`. We recommend a lower cutoff of 1 GeV, setting `resexp_range = 1.0 80.0` in the `resummation` section.

This part makes use of the transition function to ensure that this part is turned off at large q_T . Therefore the range is also limited to 80 GeV.

11.1.3 Fixed-order Z+jet at NLO

The fixed-order α_s^2 corrections (in the following called `resabove`) can be obtained by running `part = resaboveNNLO`. We recommend a cutoff of 1 GeV, setting `fo_cutoff = 1.0` in the `resummation` section. This cutoff disables matching corrections below 1 GeV and must agree with the lower value of `resexp_range`.

11.1.4 Combination and scale uncertainties

After running all three parts separately, the generated histograms can be added manually in a plotting program. The matching corrections consist of fixed-order result + fixed-order expansion of the resummed result. At α_s^2 a manual combination should agree with an automatic combination through `part = resNNLO`, for example.

To obtain uncertainties from scale variation the following procedure should be followed. The scales in the matching corrections must match, i.e. `resexp_scalevar_01` should be added to `resabove_scalevar_01`, and `resexp_scalevar_02` should be added to `resexp_scalevar_02`. Note that the scale variation histograms only give the difference to the central value. So the minimum of the scale varied matching corrections consist of:

```
min(resabove + resabove_scalevar_01 + resexp + resexp_scalevar_01,
resabove + resabove_scalevar_02 + resexp + resexp_scalevar_02)
```

Similarly the maximum can be taken, both giving an envelope of uncertainties. Note that in the resummation and its fixed-order expansion we have not decoupled the scale in the PDFs from other scales. Therefore when combining `resexp` with `resabove`, only the simultaneous variation of factorization scale and renormalization scale upwards and downwards can be used for the scale variation, corresponding to "`_01`" and "`_02`".

Finally the `scalevar_maximum` and `scalevar_minimum` histograms of the purely resummed result should be considered as an additional envelope. For this part the envelope of all scale variations is taken. The variation of the rapidity scale plays an important role and can be enabled by setting `scalevar_rapidity = .true.` in the `[resummation]` section. It gives

two important additional variations to the 2, 6, or 8-point variation of hard and resummation scale in the resummed part.

11.2 Adding α_s^3 matching corrections (Z+jet NNLO coefficient)

To obtain the matching corrections at α_s^3 we compute just the α_s^3 *coefficient* and add it to the previously obtained lower order results.

11.2.1 Fixed-order Z+jet NNLO coefficient

To obtain the fixed-order α_s^3 corrections please run with `part = resaboveN3LO`. We recommend a matching cutoff of 5 GeV, setting `fo_cutoff = 5.0` in the `resummation` section and consequently a jettiness cutoff of `taucut=0.08` in the `nnlo` section. It is possible to run with a larger `fo_cutoff` keeping the same `taucut` value, but either a smaller `fo_cutoff` or a larger `taucut` value will require a new validation of results.

11.2.2 Fixed-order Z+jet NNLO coefficient

To obtain the fixed-order α_s^3 corrections please run the Z+jet process (`nproc=41`) with `part=nnlocoeff` in the `[general]` section with a fixed q_T cutoff, i.e. by setting `pt34min = 5.0` in the `[masscuts]` section. The Z+jet calculation is based on jettiness slicing, which requires a jettiness cutoff. For a q_T cutoff of 5 GeV (for resummation this is the matching-corrections cutoff) we recommend a jettiness cutoff of `taucut=0.08` in the `[nnlo]` section. It is possible to run with a larger q_T cutoff, keeping the same `taucut` value, but either a smaller q_T cutoff or a larger `taucut` value will require a new validation of results. See [arXiv:2207.07056](https://arxiv.org/abs/2207.07056) for technical details.

11.2.3 α_s^3 fixed-order expansion coefficient of the resummed result

The α_s^3 fixed-order expansion coefficient of the resummed result (removing overlap with fixed-order Z+jet at NNLO) can be obtained by running `part = resexpN3LO`. **NOTE** that this only returns the N³LO expansion *coefficient*, to match with the fixed-order `nnlocoeff` part. Similarly, to match with the fixed-order part, we recommend a cutoff of 5 GeV, setting `resexp_range = 5.0 80.0` in the `resummation` section.

11.2.4 Combination

Similar to the lower order, the matching corrections α_s^3 coefficient can be added to lower order α_s^2 results.

11.3 Fixed order N³LO

To compute fixed-order N³LO cross-sections with q_T subtractions one needs to calculate the fixed-order Z+jet NNLO coefficient with a q_T cutoff, as outlined above. The below-cut contribution can be obtained via `part=n3locoeff` in the `[general]` section for Z production, i.e. `nproc=31`, where the `qtcut` value in the `[nnlo]` section has to match the `pt34min` value chosen for the Z+jet NNLO calculation.

We recommend to calculate the fixed-order NNLO coefficient first, as it is instructional to understand the procedure at N³LO. This proceeds by combining NLO Z+jet result with a `pt34min` value with the `part=nnloVWcoeff` part (below-cut at NNLO), where `qtcut` has to be set to match the `pt34min` value. The result of this manual procedure must agree with the automatic calculation, i.e. calculating Z with `part=nnlo` or `part=nnlocoeff`. Please pay particular attention to the difference of calculating the NNLO (α_s^2) and N³LO (α_s^3) coefficients and the full result.

12 C++ matrix element interface

Since version 10.1, MCFM offers a dedicated C++ interface to access its analytic one-loop amplitudes. Please cite ref. [69] in addition to the main MCFM references when using the C++ interface.

12.1 Processes with C++ interface

The following Standard-Model processes are available:

Process	Order EW	Order QCD
$pp \rightarrow \ell^+ \ell^-$	2	1
$pp \rightarrow \ell^+ \ell^- j$	2	2
$pp \rightarrow \ell^+ \ell^- jj$	2	3
$pp \rightarrow \ell^\pm \nu_\ell$	2	1
$pp \rightarrow \ell^\pm \nu_\ell j$	2	2
$pp \rightarrow \ell^\pm \nu_\ell jj$	2	3
$pp \rightarrow h$	1	2
$pp \rightarrow hj$	1	3
$pp \rightarrow hjj$	1	4
$pp \rightarrow hh$	2	2
$pp \rightarrow \ell^+ \ell^- h$	3	1
$pp \rightarrow \ell^+ \ell^- hj$	3	2
$pp \rightarrow \ell^\pm \nu_\ell h$	3	1
$pp \rightarrow \ell^\pm \nu_\ell hj$	3	2
$pp \rightarrow \gamma j$	1	2
$pp \rightarrow \gamma jj$	1	3
$pp \rightarrow \gamma \gamma$	2	1
$gg \rightarrow \gamma \gamma$	2	1
$pp \rightarrow \gamma \gamma j$	2	2
$pp \rightarrow \gamma \gamma \gamma$	3	1
$pp \rightarrow \gamma \gamma \gamma \gamma$	4	1
$pp \rightarrow \ell^+ \ell^- \gamma$	3	1
$pp \rightarrow \ell^\pm \nu_\ell \gamma$	3	1
$pp \rightarrow \nu_\ell \bar{\nu}_\ell \gamma$	3	1
$pp \rightarrow \ell^+ \ell'^- \nu_\ell \bar{\nu}_{\ell'}$	4	1

Process	Order EW	Order QCD
$pp \rightarrow \ell^+ \ell^- \nu_{\ell'} \bar{\nu}_{\ell'}$	4	1
$pp \rightarrow \ell^+ \ell^- \ell'^+ \ell'^-$	4	1
$pp \rightarrow \ell^+ \ell^- \ell^+ \ell^-$	4	1
$pp \rightarrow \ell^+ \ell^- \ell'^{\pm} \nu_{\ell'}$	4	1
$pp \rightarrow \ell^{\pm} \nu_{\ell} \nu_{\ell'} \bar{\nu}_{\ell'}$	4	1
$pp \rightarrow t \bar{t}$	0	3
$pp \rightarrow jj$	0	3

In addition, the following HEFT processes are available (requires model=heft):

Process	Order EW	Order QCD
$pp \rightarrow h$	1	2
$pp \rightarrow hj$	1	3
$pp \rightarrow hjj$	1	4

All processes are crossing invariant.

Further processes may be implemented in the future. Please contact the authors if interested in a specific process.

12.2 Installation

To use the C++ interface, please enable compiling MCFM as a library by adding the following flag

```
cmake .. -DWITH_LIBRARY
```

This will create a shared library `libMCFM.so` in the `lib/` directory.

12.3 Usage

Examples showing the basic usage of the interface and how to fill the complete list of parameters with default values are given in `src/BLHA/text.cxx` and `src/BLHA/params.cxx`, respectively.

The MCFM C++ interface is constructed as a C++ class

```
CXX_Interface mcfm;
```

included in the header

```
#include "MCFM/CXX_Interface.h"
```

It must be initialized on a `std::map` of `std::string`, containing all (standard-model) parameters

```
bool CXX_Interface::Initialize(std::map<std::string,std::string>& parameters);
```

Prior to use, each process has to be initialized in the interface

```
int CXX_Interface::InitializeProcess(const Process_Info &pi);
```

which takes a `Process_Info` object as input, which in turn contains the defining parameters of a given process, i.e. the PDG IDs, number of incoming particles, and QCD and EW coupling orders

```
Process_Info(const std::vector<int> &ids, const int nin, const int oqcd, const int oew);
```

Phase space points are defined using the `FourVec` struct, which represents four-vectors in the ordering (E, p_x, p_y, p_z)

```
FourVec(double e, double px, double py, double pz);
```

Given a list of four-vectors in this format, one-loop matrix elements can be calculated either using the process ID returned by the `InitializeProcess` method

```
void CXX_Interface::Calc(int procID, const std::vector<FourVec> &p, int oqcd);
```

or using a `Process_Info` struct:

```
void CXX_Interface::Calc(const Process_Info &pi, const std::vector<FourVec> &p, int oqcd);
```

In the same way, the result of this calculation can be accessed either via the process ID

```
const std::vector<double>& CXX_Interface::GetResult(int procID);
```

or using the `Process_Info` struct:

```
const std::vector<double> &CXX_Interface::GetResult(const Process_Info &pi)
```

The result is returned as a list of Laurent series coefficients in the format

$$(\mathcal{O}(\varepsilon^0), \mathcal{O}(\varepsilon^{-1}), \mathcal{O}(\varepsilon^{-2}), \text{Born}) .$$

However, by default only the $\mathcal{O}(\varepsilon^0)$ coefficient, i.e. the finite part, is returned.

The calculation of the pole terms and the Born can be enabled by setting the following switch to 1

```
void CXX_Interface::SetPoleCheck(int check);
```


12.4 Tests

A set of programs to test MCFM's amplitudes against [OpenLoops](#), [Recola](#), and [MadLoop](#) can be compiled. For example to compile the OpenLoops test program an additional OpenLoops directory `-DOLDIR=$HOME/OpenLoops` must be specified that contains the header files in the `include` subdirectory. For Recola and MadLoops the variables `RCLDIR` and `MLDIR` must be specified, respectively.

13 Notes on specific processes

The processes described in the file `process.DAT` include appropriate boson decays when the parameter `removebr` is set to `.false..` In many cases a more simple calculation can be performed by setting this parameter to `.true.`, in which case these decays are not performed. Technically the full calculation including the decays is still performed but cuts are not performed on the decay products and the branching ratio is divided out, thus yielding the cross section before decay. In the notes below we indicate the simpler processes thus obtained. When running in this mode, the parameter `zerowidth` should be set to `.true.` for consistency. However in certain circumstances, for the sake of comparison, it may be useful to run with it set to `.false..`

13.1 W -boson production, processes 1,6

These processes represent the production of a W boson which subsequently decays leptonically. This process can be calculated at LO, NLO, and NNLO. NLO calculations can be performed by dipole subtraction, zero-jettiness slicing and q_T -slicing. NNLO calculations can be performed by zero-jettiness slicing and q_T -slicing.

When `removebr` is true, the W boson does not decay.

13.2 EW corrections to W -boson production, processes 2,7

These processes compute the electroweak corrections to the production of a W boson which subsequently decays leptonically. The electron is taken to be massless. The electroweak corrections involve both real and virtual corrections. If particle 5 is present it is a photon. The calculation must be performed at NLO, i.e. `part=nlo`.

13.3 Photon-induced corrections to W -boson production, processes 3,8

These processes compute the production of a W boson, (which subsequently decays leptonically), through the reaction $q + \gamma \rightarrow e + \nu + q$. The calculation must be performed at NLO. Since the reaction has an initial photon, it is important to have an accurate parton distribution function for the photon in the proton, e.g. `LUXqed17_plus_PDF4LHC15_nnlo_30`.

13.4 $W + \text{jet}$ production, processes 11,16

This process is calculable at leading LO and next-to-leading order NLO. These processes represent the production of a W boson which subsequently decays leptonically, in association with a single jet. When `removebr` is true, the W boson does not decay.

13.5 $W + b$ production, processes 12,17

These processes represent the production of a W boson which subsequently decays leptonically, in association with a single bottom quark, exploiting the weak transitions $c \rightarrow b$ and $u \rightarrow b$. This is produced at leading order by an initial state which contains a charm quark (or the CKM suppressed u quark) and a gluon, e.g $c(-p_1) + g(p_2) \rightarrow W^+ (\rightarrow \nu(p_3) + e^+(p_4)) + b(p_5)$ and $u(-p_1) + g(p_2) \rightarrow W^+ (\rightarrow \nu(p_3) + e^+(p_4)) + b(p_5)$ or the charge conjugate processes for W^- . This process is somewhat analogous to single top production.

The effect of the bottom quark mass is included throughout the calculation. For this case the CKM matrix elements V_{cb} and V_{ub} , (if they are equal to zero in the input data file, `mdata.f`) are set equal to 0.041 and 0.00347 respectively. Otherwise the non-zero values specified in `mdata.f` are used. The calculation of this process may be performed at LO and NLO.

When `removebr` is true, the W boson does not decay.

13.6 $W + c$ production, processes 13,18

These processes represent the production of a W boson which subsequently decays leptonically, in association with a charm quark. This is produced at leading order by an initial state which contains a strange anti-quark (or Cabibbo suppressed d anti-quark) and a gluon, e.g $\bar{d}(-p_1) + g(p_2) \rightarrow W^+ (\rightarrow \nu(p_3) + e^+(p_4)) + \bar{c}(p_5)$ and $\bar{u}(-p_1) + g(p_2) \rightarrow W^+ (\rightarrow \nu(p_3) + e^+(p_4)) + \bar{c}(p_5)$ or the charge conjugate process for W^- . This process is somewhat analogous to single top production.

The effect of the charm quark mass is included throughout the calculation. The calculation of this process may be performed both at LO and NLO.

When `removebr` is true, the W boson does not decay.

13.7 $W + c$ production ($m_c = 0$), processes 14,19

These processes are identical to 13 and 18 except for the fact that the charm quark mass is neglected. The calculation can currently be performed at LO only.

13.8 $W + b\bar{b}$ production, processes 20,25

This process is calculable at leading LO and next-to-leading order NLO. These processes represent the production of a W boson which subsequently decays leptonically, in association with a $b\bar{b}$ pair. The effect of the bottom quark mass is included throughout the calculation. This calculation may be performed at NLO, thanks to the incorporation of the virtual corrections from ref. [13]. When `removebr` is true, the W boson does not decay.

To select final states in which one of the b -quarks may be unobserved the user can employ processes 401-408 instead. These processes use the same matrix elements but make specific requirements on the kinematics of the b -quarks and QCD radiation.

13.9 $W + b\bar{b}$ production ($m_b = 0$), processes 21,26

This process is calculable at leading LO and next-to-leading order NLO. These processes are identical to 20 and 25 except for the fact that the bottom quark mass is neglected. Processes `nproc=20,25` with a massive b -quark should be used in preference. However processes `nproc=21,26` run considerably faster than the corresponding processes with the mass for the b quark, (`nproc=20,25`). In circumstances where both b quarks are at large transverse momentum, the inclusion of the mass for the b -quark is not mandatory and a good estimate of the cross section may be obtained by using these processes.

When `removebr` is true, the W boson does not decay.

13.10 $W + 2$ jets production, processes 22,27

This process represents the production of a W boson and 2 jets, where the W boson decays leptonically. The calculation may be performed up to NLO, as detailed below. Virtual amplitudes are taken from ref. [17]. For more details on this calculation, please see Refs. [15, 16].

For these processes (and also for $Z + 2$ jet production, `nproc=44,46`) the next-to-leading order matrix elements are particularly complex and may be divided into two groups. The division is according to the lowest order diagrams from which they originate:

1. Diagrams involving two external quark lines and two external gluons, the “**Gflag**” contribution. The real diagrams in this case thus involve three external gluons.
2. Diagrams where all four external lines are quarks, the “**Qflag**” contribution. The real diagrams in this case involve only one gluon.

By specifying `Gflag` and `Qflag` in the file `input.ini` one may select one of these options at a time. The full result may be obtained by straightforward addition of the two individual pieces, with no meaning attached to either piece separately. The default is that both of these are set to `.true.` simultaneously.

Virtual amplitudes are taken from ref. [17].

When `removebr` is true, the W boson does not decay.

13.11 $W + 3$ jets production, processes 23,28

This process represents the production of a W boson and 3 jets, where the W boson decays leptonically. The calculation may be performed at LO only.

When `removebr` is true, the W boson does not decay.

13.12 $W + b\bar{b} + \text{jet}$ production ($m_b = 0$), processes 24,29

These processes represent the production of a W boson which subsequently decays leptonically, in association with a $b\bar{b}$ pair and an additional jet. The effect of the bottom quark mass is neglected throughout and the calculation may be performed at LO only. The corresponding LO processes with a mass for the b -quark are given in `nproc=431,436` and should be used in preference to these processes.

When `removebr` is true, the W boson does not decay.

13.13 Z -boson production, processes 31–33

These processes represent the production of a Z boson which subsequently decays either into electrons (`nproc=31`), neutrinos (`nproc=32`) or bottom quarks (`nproc=33`). Where appropriate, the effect of a virtual photon is also included. As noted above, for `nproc=31` and `nproc=33` the constraint `m34min > 0` is obligatory. The calculation may be performed at LO, NLO and NNLO [11, 21] although the NLO and NNLO calculation of process 33 does not include radiation from the bottom quarks (i.e. radiation occurs in the initial state only).

This process can be calculated at LO, NLO, and NNLO. NLO calculations can be performed by subtraction, zero-jettiness slicing and q_T -slicing. NNLO calculations can be performed by zero-jettiness slicing and q_T -slicing.

To calculate the total cross section to on-shell Z bosons, we take process (`nproc=32`), (no γ^* contribution) and set (`zerowidth=.true.`) and (`removebr=.true.`). When `removebr` is true in process 31, the Z boson does not decay.

13.14 Z -boson production decaying to jets, processes 34–35

These processes are calculable at leading LO and next-to-leading order NLO, `nproc=34` gives $Z(\rightarrow 3 \times (d(p_5) + \bar{d}(p_6)))$ and `nproc=35` gives $Z(\rightarrow 2 \times (u(p_5) + \bar{u}(p_6)))$. Radiation from the final state quarks is not included in this process.

13.15 $t\bar{t}$ production mediated by Z/γ^* -boson exchange, process 36

These processes represent the production of a virtual Z boson or photon which subsequently decays into $t\bar{t}$. The leptonic decays of the top quarks are included. Switching `zerowidth` from `.true.` to `.false.` only affects the W bosons from the top quark decay. Note that `m34min` > 0 is obligatory due to the inclusion of the virtual photon diagrams. The calculation may be only be performed at LO. This is a small contribution, but in $p\bar{p}$ -collisions gives a forward backward asymmetry.

13.16 Lepton pair production through photonic initial states, process 310

This process is calculable at leading order LO. This process represents the production of a lepton pair through an electroweak process involving two photons in the initial state, $\gamma\gamma \rightarrow e^-e^+$. Since the reaction has initial photons, it is important to have an accurate parton distribution function for the photon in the proton, e.g. LUXqed17_plus_PDF4LHC15_nnlo_30.

13.17 Z + jet production, processes 41–43

These processes represent the production of a Z boson and a single jet, where the Z subsequently decays either into electrons (`nproc=41`), neutrinos (`nproc=42`) or bottom quarks (`nproc=43`). Where appropriate, the effect of a virtual photon is also included. The calculation may be performed at LO and NLO and NNLO[9] although the NLO, (NNLO) calculation of process 43 does not include radiation from the bottom quarks. The one-loop virtual amplitudes are taken from the appendix IV of ref. [17].

When `removebr` is true in process 41, the Z boson does not decay.

13.18 $Z + 2$ jets production, processes 44, 46

These processes represents the production of a Z boson and 2 jets, including also the effect of a virtual photon (`nproc=44` only). The Z/γ^* decays to an e^+e^- pair (`nproc=44`) or into three species of neutrino (`nproc=46`). Virtual amplitudes are taken from ref. [17]. For more details on this calculation, please see Refs. [15, 16].

The calculation may be performed up to NLO. For $Z + 2$ jet production the next-to-leading order matrix elements are particularly complex and so they have been divided into two groups. The division is according to the lowest order diagrams from which they originate:

1. Diagrams involving two external quark lines and two external gluons, the “**Gflag**” contribution. The real diagrams in this case thus involve three external gluons.
2. Diagrams where all four external lines are quarks, the “**Qflag**” contribution. The real diagrams in this case involve only one gluon.

By specifying `Gflag` and `Qflag` in the file `input.ini` one may select one of these options at a time. The full result may be obtained by straightforward addition of the two individual pieces, with no meaning attached to either piece separately. The default is that both of these are set to `.true.` simultaneously.

When `removebr` is true, the Z boson does not decay.

13.19 $Z + 3$ jets production, processes 45, 47

These processes represent the production of a Z boson and 3 jets, including also the effect of a virtual photon when the Z decays to electrons (`nproc=45`), but not when it decays to neutrinos. The Z/γ^* decays to an e^+e^- pair (`nproc=45`) or into three species of neutrino (`nproc=47`). The calculation may be performed at LO only.

When `removebr` is true, the Z boson does not decay.

13.20 $Z + b\bar{b}$ production, $m_b \neq 0$, process 50

These processes represent the production of a Z boson (or virtual photon) which subsequently decays leptonically, in association with a $b\bar{b}$ pair. The effect of the bottom quark mass is included throughout the calculation. The calculation may be performed at LO only, because the one-loop calculation with massive quarks has not yet been performed.

When `removebr` is true, the Z boson does not decay.

13.21 $Z + b\bar{b}$ production ($m_b = 0$), processes 51–53

Process 51 is identical to 50 except for the fact that the bottom quark mass is neglected. This allows the calculation to be performed up to NLO. The other processes 52 and 53, also with massless b -quarks account for the decays into neutrinos (`nproc=52`) and bottom quarks (`nproc=53`). Note that the NLO calculation of process 53 does not currently include radiation from the bottom quarks produced in the decay.

When `removebr` is true in process 51, the Z boson does not decay.

13.22 $Z + b\bar{b} + \text{jet}$ production ($m_b = 0$), process 54

This process represents the production of a Z boson (and virtual photon) which subsequently decays leptonically, in association with a $b\bar{b}$ pair and an additional jet. The effect of the bottom quark mass is neglected throughout and the calculation may be performed at LO only.

When `removebr` is true, the Z boson does not decay.

13.23 $Z + c\bar{c}$ production ($m_c = 0$), process 56

Process 56 is the equivalent of 51, with the bottom quarks replaced by charm. Although the charm mass is neglected, the calculation contains diagrams with two gluons in the initial state and a Z coupling to the heavy quark line – hence the dependence upon the quark flavour.

When `removebr` is true in process 56, the Z boson does not decay.

13.24 Di-boson production, processes 61–89

These processes represent the production of a diboson pair $V_1 V_2$, where V_1 and V_2 may be either a W or Z/γ^* . All the processes in this section may be calculated at NLO with the exception of `nproc=69`. There are various possibilities for the subsequent decay of the bosons, as specified in the sections below. Amplitudes for the $V_1 V_2$ process at $O(\alpha_s)$ are taken from ref. [70]. We also include singly resonant diagrams at NLO for all processes in the case `zerowidth = .false..` For more details on this calculation, please see Refs. [19, 20].

For processes 62, 63, 64, 65, 74 and 75 the default behaviour is that the hadronic decay products of the bosons are clustered into jets using the supplied jet algorithm parameters, but no cut is applied on the number of jets. This behaviour can be altered by changing the value of the variable `notag` in the file `src/User/setnotag.f`.

Calculations of processes 61, 71, 76, 81 and 82 can be performed at NLO by subtraction, zero-jettiness slicing and q_T -slicing. They can be computed at NNLO using zero-jettiness slicing and q_T -slicing, as described in 'Non-local slicing approaches for NNLO QCD in MCFM', [21]. For processes 61, 81 and 86 the NNLO corrections include glue-glue initiated box diagrams which first contribute at order α_s^2 . Two loop results for virtual diagrams at $O(\alpha_s^2)$ are taken from [7].

13.24.1 WW production, processes 61-65, 69

For WW production, both W 's can decay leptonically (`nproc=61`) or one may decay hadronically (`nproc=62` for W^- and `nproc=64` for W^+). Corresponding to processes 62, 64, processes 63, 65 implement radiation in decay from the hadronically decaying W 's. Process 69 implements the matrix elements for the leptonic decay of both W 's but where no polarization information is retained. It is included for the sake of comparison with other calculations. Processes 62 and 64 may be run at NLO with the option `todk`, including radiation in the decay of the hadronically decaying W . Processes 63 and 65 give the effect of radiation in the decay alone by taking the sum of the choices `virt` and `real`, or equivalently `tota`.

Note that, in processes 62 and 64, the NLO corrections include radiation from the hadronic decays of the W .

When `removebr` is true in processes 61 and 69, the W bosons do not decay.

Process 61 can be calculated at NNLO. The NNLO calculations include contributions from the process $gg \rightarrow WW$ that proceeds through quark loops. The calculation of loops containing the third quark generation includes the effect of the top quark mass (but $m_b = 0$), while the first two generations are considered massless. For numerical stability, a small cut on the

transverse momentum of the W bosons is applied: $p_T(W) > 0.05$ GeV for loops containing massless (first or second generation) quarks, $p_T(W) > 2$ GeV for (t, b) loops. This typically removes less than 0.1% of the total cross section. The values of these cutoffs can be changed by editing `src/WW/gg_ww.f` and recompiling.

13.24.2 WZ production, processes 71–80

This process is calculable at LO, NLO and NNLO and has been treated in several papers, [11, 19–21]. For WZ production, the W is chosen to decay leptonically. The Z (or virtual photon, when appropriate) may decay into electrons (`nproc=71,76`), neutrinos (`nproc=72,77`), a pair of bottom quarks (`nproc=73,78`), three generations of down-type quarks (`nproc=74,79`) or two generations of up-type quarks (`nproc=75,80`). In process 78 the mass of the b -quark is neglected. These processes will be observed in the final state as W -boson + two or three jets. In processes 72 and 77, a sum is performed over all three species of neutrinos.

When `removebr` is true in processes 71 and 76, neither the W or the Z boson decays.

13.24.3 WZ with interference, processes 711 and 761

This process can be calculated at LO, NLO, and NNLO. NLO calculations can be performed by subtraction, zero-jettiness slicing and q_T -slicing. NNLO calculations can be performed by zero-jettiness slicing and q_T -slicing.

Full account is taken in this process of the interference between diagrams generated by the exchange of two positrons. This leads to a more complicated resonance structure in the phase space.

13.24.4 ZZ production, processes 81–84, 90

The Z 's can either both decay leptonically (`nproc=81`), one can decay leptonically while the other decays into neutrinos (`nproc=82`) or bottom quarks (`nproc=83`), or one decays into neutrinos and the other into a bottom quark pair (`nproc=84`). In process 83 the mass of the b -quark is neglected. Note that, in processes 83–84, the NLO corrections do not include radiation from the bottom quarks that are produced by the Z decay. In process 90 the two Z bosons decay to identical charged leptons, and interference effects between the decay products of the two Z bosons are included. In all cases these processes also include the contribution from a virtual photon.

When `removebr` is true in process 81, neither of the Z bosons decays.

This process has been treated in several papers, [11, 19–21]. Processes 81 and 82 can be calculated at NNLO. The NNLO calculation includes contributions from the process $gg \rightarrow ZZ$ that proceeds through quark loops. The calculation of loops containing the third quark generation includes the effect of both the top and the bottom quark mass ($m_t, m_b \neq 0$), while the first two generations are considered massless. For numerical stability, a small cut on the transverse momentum of the Z bosons is applied: $p_T(Z) > 0.1$ GeV. This typically removes less than 0.1% of the total cross section. The values of these cutoffs can be changed by editing `src/ZZ/getggZZamps.f` and recompiling.

13.24.5 Anomalous WWZ

It is possible to specify anomalous trilinear couplings for the W^+W^-Z and $W^+W^-\gamma$ vertices that are relevant for WW and WZ production. To run in this mode, one must set `zerowidth` equal to `.true.` and modify the appropriate lines for the couplings in `input.ini` (see below). Note that, at present, the effect of anomalous couplings is not included in the gluon-gluon initiated contributions to the WW process.

The anomalous couplings appear in the Lagrangian, $\mathcal{L} = \mathcal{L}_{SM} + \mathcal{L}_{anom}$ as follows (where \mathcal{L}_{SM} represents the usual Standard Model Lagrangian and \mathcal{L}_{anom} is taken from Ref. [71]):

$$\mathcal{L}_{anom} = ig_{WWZ} \left[\Delta g_1^Z (W_{\mu\nu}^* W^\mu Z^\nu - W_{\mu\nu} W^{*\mu} Z^\nu) + \Delta \kappa^Z W_\mu^* W_\nu Z^{\mu\nu} + \frac{\lambda^Z}{M_W^2} W_{\rho\mu}^* W_\nu^\mu Z^{\nu\rho} \right] + ig_{WW\gamma} \left[\Delta \kappa^\gamma W_\mu^* W_\nu \gamma^{\mu\nu} + \frac{\lambda^\gamma}{M_W^2} W_{\rho\mu}^* W_\nu^\mu \gamma^{\nu\rho} \right],$$

where $X_{\mu\nu} \equiv \partial_\mu X_\nu - \partial_\nu X_\mu$ and the overall coupling factors are $g_{WW\gamma} = -e$, $g_{WWZ} = -e \cot \theta_w$. This is the most general Lagrangian that conserves C and P separately and electromagnetic gauge invariance requires that there is no equivalent of the Δg_1^Z term for the photon coupling.

In order to avoid a violation of unitarity, these couplings are often included only after suppression by dipole form factors,

$$\Delta g_1^Z \rightarrow \frac{\Delta g_1^Z}{(1 + \hat{s}/\Lambda^2)^2}, \quad \Delta \kappa^{Z/\gamma} \rightarrow \frac{\Delta \kappa_1^{Z/\gamma}}{(1 + \hat{s}/\Lambda^2)^2}, \quad \lambda^{Z/\gamma} \rightarrow \frac{\Delta \lambda^{Z/\gamma}}{(1 + \hat{s}/\Lambda^2)^2},$$

where \hat{s} is the vector boson pair invariant mass and Λ is an additional parameter giving the scale of new physics, which should be in the TeV range. These form factors should be produced by the new physics associated with the anomalous couplings and this choice is somewhat arbitrary. The use of the form factors can be disabled as described below. The file `input.ini` contains the values of the 6 parameters which specify the anomalous couplings. If the input file contains a negative value for the form-factor scale then the suppression factors described above are not applied.

13.24.6 $WW+ZZ$ interfering, process 8211

This process calculable at leading LO and next-to-leading order NLO. This process describes a specific final state which is accesible both from the decay to two W 's and two Z 's. The two processes can thus interfere.

This process has been treated in several papers, [11, 19–21].

13.25 WH production, processes 91-100, 900

This process can be calculated at LO, NLO, and NNLO. These processes represent the production of a W boson which subsequently decays leptonically, in association with a Standard Model Higgs boson that decays into a tau pair (`nproc=91, 96`), decays into a b -quark pair (`nproc=92, 97`), a pair of photons (`nproc=93, 98`), or a pair of W -bosons (`nproc=94, 99`), a pair of Z bosons (`nproc=95, 100`). Note that in the cases of Higgs decay to $W,(Z)$ pairs, below the $W,(Z)$ pair threshold one of the $W,(Z)$ bosons is virtual and therefore one must set `zerowidth=.false..` The calculation may be performed at NNLO for these processes.

Radiation from the bottom quarks in the decay, an NLO effect, is included in (`nproc=920, 970`). `nproc=900` may be used to compute the sum over both W charges in one run (with the decay products 3 and 4 representing lepton and antilepton respectively). This sum is performed by adjusting the CKM matrix to allow both charges of the W boson.

When `removebr` is `.true.`, neither the W boson nor the Higgs decays.

For more information on this process see refs. [11, 21, 22]. NLO calculations can be performed by subtraction, zero-jettiness slicing and q_T -slicing. NNLO calculations can be performed by zero-jettiness slicing and q_T -slicing.

13.26 ZH production, processes 101-110

These processes represent the production of a Z boson (or virtual photon) in association with a Standard Model Higgs boson that decays into a bottom quark pair (`nproc=101-103`), or decays into a pair of photons (`nproc=104-105`) or a pair of W bosons (`nproc=106-108`), or a pair of Z bosons (`nproc=109`), or a pair of τ 's (`nproc=110`).

The Z subsequently decays into either an e^+e^- pair (`nproc=101, 106, 109`), neutrinos (`nproc=102, 107`) or a bottom quark pair (`nproc=103, 108`). The calculation may be performed at NLO, although radiation from the bottom quarks in the decay of the Higgs (or the Z , for processes 103, 108) is not included. Radiation from the bottom quarks in the decay of the Higgs is included in (`nproc=1010`).

When `removebr` is true in processes 101, 106, 109, neither the Z boson nor the Higgs decays.

For more information on this process see refs. [11, 21, 22]. NLO calculations can be performed by subtraction, zero-jettiness slicing and q_T -slicing. NNLO calculations can be performed by zero-jettiness slicing and q_T -slicing.

13.27 Higgs production, ($m_t = \infty$), processes 111-121

This process is calculable at leading LO, at next-to-leading order NLO, and at next-to-next-to-leading order NNLO.

These processes represent the production of a Standard Model Higgs boson that decays either into a bottom quark pair (`nproc=111`), a pair of tau's (`nproc=112`), a W^+W^- pair that further decays leptonically (`nproc=113`) a W^+W^- pair where the W^- decays hadronically

(`nproc=114,115`) or a ZZ pair (`nproc=116-118`). In addition, the loop-level decays of the Higgs into a pair of photons (`nproc=119`) and the $Z\gamma$ decay are included (`nproc=120,121`).

For the case of W^+W^- process `nproc=115` gives the contribution of radiation from the hadronically decaying W^- . Process 114 may be run at NLO with the option `todk`, including radiation in the decay of the hadronically decaying W^- .¹ For the case of a ZZ decay, the subsequent decays can either be into a pair of muons and a pair of electrons (`nproc=116`), a pair of muons and neutrinos (`nproc=117`) or a pair of muons and a pair of bottom quarks (`nproc=118`).

At LO the relevant diagram is the coupling of two gluons to the Higgs via a top quark loop. This calculation is performed in the limit of infinite top quark mass, so that the top quark loop is replaced by an effective operator. This corresponds to the effective Lagrangian,

$$\mathcal{L} = \frac{1}{12\pi v} G_{\mu\nu}^a G_a^{\mu\nu} H, \quad (18)$$

where v is the Higgs vacuum expectation value and $G_{\mu\nu}^a$ the gluon field strength tensor. The calculation may be performed at NLO, although radiation from the bottom quarks in the decay of processes 111 and 118 is not yet included.

When `removebr` is true in processes 111,112,113,118, the Higgs boson does not decay.

Process 119 implements the decay of the Higgs boson into two photons via loops of top quarks and W -bosons. The decay is implemented using the formula Eq.(11.12) from ref. [72]. When `removebr` is true in process 119 the Higgs boson does not decay.

Processes 120 and 121 implement the decay of the Higgs boson into an lepton-antilepton pair and a photon. As usual the production of a charged lepton-antilepton pair is mediated by a Z/γ^* (process 120) and the production of three types of neutrinos $\sum \nu\bar{\nu}$ by a Z -boson (process 121). These processes are implemented using a generalization of the formula of [73]. (Generalization to take into account off-shell Z -boson and adjustment of the sign of C_2 in their Eq.(4)).

13.28 $H \rightarrow W^+W^-$ production, ($m_t = \text{finite}$), processes 123-127

These processes represent the production of a Higgs boson that decays to W^+W^- , with subsequent decay into leptons. For process 123, the exact form of the triangle loop coupling a Higgs boson to two gluons is included, with both top and bottom quarks circulating in the loop. This is to be contrasted with process 113 in which only the top quark contribution is included in the effective coupling approach.

Process 124 includes only the effect of the interference of the Higgs and $gg \rightarrow W^+W^-$ amplitudes, as described in ref. [23]. The calculation is available at LO only. LO corresponds to $O(\alpha_s^2)$ in this case. The calculation of loops containing the third quark generation includes the effect of the top quark mass (but $m_b = 0$), while the first two generations are considered massless. For numerical stability, a small cut on the transverse momentum of the W bosons is applied: $p_T(W) > 0.05$ GeV for loops containing massless (first or second generation) quarks, $p_T(W) > 2$ GeV for (t, b) loops. This typically removes less than 0.1% of the cross

¹We have not included the case of a hadronically decaying W^+ ; it can be obtained from processes `nproc=114,115` by performing the substitutions $\nu \rightarrow e^-$ and $e^+ \rightarrow \bar{\nu}$.

section. The values of these cutoffs can be changed by editing `src/HWW/gg_WW_int.f` and recompiling.

Process 125 includes all gg -initiated diagrams that have a Higgs boson in the s -channel, namely the square of the s -channel Higgs boson production and the interference with the diagrams that do not contain a Higgs boson, (i.e. $gg \rightarrow W^+W^- \rightarrow \nu_e e^+ e^- \bar{\nu}_e$), i.e. $|M_H|^2 + 2|M_H^* M_{WW}|$.

The result for the square of the box diagrams alone, i.e. the process $gg \rightarrow W^+W^- \rightarrow \nu_e e^+ e^- \bar{\nu}_e$, may be obtained by running process `nproc=61` with `part=virt` and `ggonly=.true.`

Process 126 calculates the full result for this process from gg -initiated diagrams. This includes diagrams that have a Higgs boson in the s -channel, the continuum W^+W^- diagrams described above and their interference, i.e. $|M_H + M_{WW}|^2$.

Process 127 calculates the full result for this process for gg -initiated box diagrams alone, $gg \rightarrow W^+W^-$, i.e. $|M_{WW}|^2$.

13.29 $H \rightarrow ZZ \rightarrow e^- e^+ \mu^- \mu^+$ production, ($m_t = \text{finite}$), processes 128-133

These processes represent the production of a Higgs boson that decays to ZZ , with subsequent decay into charged leptons. For process 128, the exact form of the triangle loop coupling a Higgs boson to two gluons is included, with both top and bottom quarks circulating in the loop. This is to be contrasted with process 116 in which only the top quark contribution is included in the effective coupling approach.

Process 129 includes only the effect of the interference of the Higgs and $gg \rightarrow ZZ$ amplitudes. The calculation is available at LO only. LO corresponds to $O(\alpha_s^2)$ in this case. The calculation of loops containing the third quark generation includes the effect of both the top quark mass and the bottom quark, while the first two generations are considered massless. For numerical stability, a small cut on the transverse momentum of the Z bosons is applied: $p_T(Z) > 0.05$ GeV. This typically removes less than 0.1% of the cross section. The values of these cutoffs can be changed by editing `src/ZZ/getggZZamps.f` and recompiling.

Process 130 includes all gg -initiated diagrams that have a Higgs boson in the s -channel, namely the square of the s -channel Higgs boson production and the interference with the diagrams that do not contain a Higgs boson, (i.e. $gg \rightarrow Z/\gamma^* + Z/\gamma^* \rightarrow e^- e^+ \mu^- \mu^+$), i.e. $|M_H|^2 + 2|M_H^* M_{ZZ}|$.

Process 131 calculates the full result for this process from gg -initiated diagrams. This includes diagrams that have a Higgs boson in the s -channel, the continuum $Z/\gamma^* + Z/\gamma^*$ diagrams described above and their interference, i.e. $|M_H + M_{ZZ}|^2$.

Process 132 gives the result for the square of the box diagrams alone, i.e. the process $gg \rightarrow Z/\gamma^* + Z/\gamma^* \rightarrow e^- e^+ \mu^- \mu^+$, i.e. $|M_{ZZ}|^2$.

Process 133 calculates the interference for the qg initiated process.

For those processes that include contributions from the Higgs boson, the form of the Higgs propagator may be changed by editing the file `src/Need/sethparams.f`. If the logical variable `CPscheme` is changed from the default value `.false.` to `.true.` then the Higgs propagator is computed using the “bar-scheme” that is implemented in the HTO code of G. Passarino [74,

[75](#)]. The value of the Higgs boson width has been computed with v1.1 of the HTO code, for Higgs masses in the interval $50 < m_H < 1500$ GeV. These values are tabulated, in 0.5 GeV increments, in the file `Bin/hto_output.dat`. The widths for other masses in this range are obtained by linear interpolation.

13.30 $e^-e^+\nu_e\bar{\nu}_e$ production, processes 1281, 1311, 1321

These processes compute cross sections relevant for the final state $e^-e^+\nu_e\bar{\nu}_e$, i.e. with charged leptons and neutrinos from the same (electron) doublet. As a result they receive contributions from diagrams with resonant ZZ propagators and resonant WW propagators. Process 1281 only includes amplitudes containing a Higgs boson (c.f. processes 123 and 128). Process 1321 only includes continuum (box-diagram) amplitudes (c.f. processes 127 and 132). Process 1311 includes both amplitudes and the effects of the interference between them (c.f. processes 126 and 131).

13.31 $e^-e^+\nu\bar{\nu}$ production, processes 1282, 1312, 1322

These processes compute cross sections relevant for the final state $e^-e^+\nu\bar{\nu}$, i.e. an electron pair and a sum over all three flavours of neutrino. For muon and tau neutrinos, only ZZ diagrams contribute. For electron neutrinos there are contributions from diagrams with resonant ZZ propagators and resonant WW propagators. Process 1282 only includes amplitudes containing a Higgs boson (c.f. processes 123 and 128). Process 1322 only includes continuum (box-diagram) amplitudes (c.f. processes 127 and 132). Process 1312 includes both amplitudes and the effects of the interference between them (c.f. processes 126 and 131).

13.32 $H + b$ production, processes 136–138

These processes represent the production of a Standard Model Higgs boson that decays into a pair of bottom quarks, in association with a further bottom quark. The initial state at lowest order is a bottom quark and a gluon. The calculation may be performed at NLO, although radiation from the bottom quarks in the Higgs decay is not included. For more details on this calculation, please see Ref. [\[27\]](#).

For this process, the matrix elements are divided up into a number of different sub-processes, so the user must sum over these after performing more runs than usual. At lowest order one can proceed as normal, using `nproc=136`. For a NLO calculation, the sequence of runs is as follows:

- Run `nproc=136` with `part=virt` and `part=real` (or, both at the same time using `part=tota`);
- Run `nproc=137` with `part=real`.

The sum of these yields the cross-section with one identified b -quark in the final state. To calculate the contribution with two b -quarks in the final state, one should use `nproc=138` with `part=real`.

When `removebr` is `.true.`, the Higgs boson does not decay.

13.33 $t\bar{t}$ production with 2 semi-leptonic decays, processes 141–145

These processes describe $t\bar{t}$ production including semi-leptonic decays for both the top and the anti-top. Since version 6.2 we have updated this to use the one-loop amplitudes of ref. [29]. The code for the virtual amplitudes now runs about three times faster than earlier versions where the virtual amplitudes of ref. [76] were used. Switching `zerowidth` from `.true.` to `.false.` only affects the W bosons from the top quark decay, because our method of including spin correlations requires the top quark to be on shell.

Process 141 includes all corrections, i.e. both radiative corrections to the decay and to the production. This process is therefore the basic process for the description of top production where both quarks decay semi-leptonically. When `removebr` is true in process 141, the top quarks do not decay. When one wishes to calculate observables related to the decay of the top quark, `removebr` should be false in process 141. The LO calculation proceeds as normal. At NLO, there are two options:

- `part=virt`, `real` or `tota`: final state radiation is included in the production stage only
- `part = todk`: radiation is included in the decay of the top quark also and the final result corresponds to the sum of real and virtual diagrams. Note that these runs automatically perform an extra integration, so will take a little longer.

Process 142 includes only the corrections in the semileptonic decay of the top quark. Thus it is of primary interest for theoretical studies rather than for physics applications. Because of the method that we have used to include the radiation in the decay, the inclusion of the corrections in the decay does not change the total cross section. This feature is explained in section 6 of ref. [28].

In the case of process 145, there are no spin correlations in the decay of the top quarks. The calculation is performed by multiplying the spin summed top production cross section, by the decay matrix element for the decay of the t and the \bar{t} . These processes may be used as a diagnostic test for the importance of the spin correlation.

13.34 $t\bar{t}$ production with decay and a gluon, process 143

This process is only calculable at leading order LO. This process describes lowest order $t\bar{t} + g$ production including two leptonic decays $t \rightarrow b\ell\nu$. When `removebr` is true, the top quarks do not decay. This LO process only includes radiation in production.

13.35 $t\bar{t}$ production with one hadronic decay, processes 146–151

This process is calculable at leading LO and next-to-leading order NLO. These processes describe the hadronic production of a pair of top quarks, with one quark decaying hadronically and one quark decaying semi-leptonically. For processes 146–148, the top quark decays semi-leptonically whereas the anti-top quark decays hadronically. For processes 149–151, the top quark decays hadronically whereas the anti-top quark decays semi-leptonically. The base processes for physics are process 146 and 149 which include radiative corrections in both production and decay. Switching `zerowidth` from `.true.` to `.false.` only affects the W bosons from the top quark decay, because our method of including spin correlations requires

the top quark to be on shell. When one wishes to calculate observables related to the decay of the top quark, `removebr` should be false in processes 146 and 149. The LO calculation proceeds as normal. At NLO, there are two options:

- `part=virt`, `real` or `tota` : final state radiation is included in the production stage only
- `part = todk` : radiation is included in the decay of the top quark also and the final result corresponds to the sum of real and virtual diagrams. Note that these runs automatically perform an extra integration, so will take a little longer.

Processes 147 and 150 include only the radiative corrections in the decay of the top quark without including the radiative corrections in the hadronic decay of the W -boson. Because of the method that we have used to include the radiation in the decays, the inclusion of the corrections in this stage of the decay does not change the total cross section. Process 148 (151) includes only the radiative corrections in the hadronic decay of the W -boson coming from the anti-top (top). The inclusion of the corrections in this stage of the decay increases the partial width by the normal α_s/π factor.

13.36 $Q\bar{Q}$ production, processes 157–159

These processes are calculable at leading LO and next-to-leading order NLO. These processes calculate the production of heavy quarks (157 for top, 158 for bottom and 159 for charm) up to NLO using the matrix elements of ref. [30]. No decays are included.

13.37 $t\bar{t}$ + jet production, process 160

This process calculates the production of top quarks and a single jet at LO, without any decay of the top quarks.

13.38 Single-top-quark production and decay at NNLO, process 1610

This calculation is based on ref. [77]. See also ref. [78] for the role of double-DIS scales and the relevancy for PDFs.

This process can be run by using process number 1610. The resulting histograms and cross-sections are printed for a strict fixed-order expansion as well as for a naive addition of all contributions. The fixed-order expansion assembles pieces according to the following formula. Please see ref. [77] for more details.

$$\begin{aligned}
d\sigma_{\text{LO}} &= \frac{1}{\Gamma_t^{(0)}} d\sigma^{(0)} \otimes d\Gamma_t^{(0)}, \\
d\sigma_{\delta\text{NLO}} &= \frac{1}{\Gamma_t^{(0)}} \left[d\sigma^{(1)} \otimes d\Gamma_t^{(0)} + d\sigma^{(0)} \otimes \left(d\Gamma_t^{(1)} - \frac{\Gamma_t^{(1)}}{\Gamma_t^{(0)}} d\Gamma_t^{(0)} \right) \right], \\
d\sigma_{\delta\text{NNLO}} &= \frac{1}{\Gamma_t^{(0)}} \left[d\sigma^{(2)} \otimes d\Gamma_t^{(0)} + d\sigma^{(1)} \otimes \left(d\Gamma_t^{(1)} - \right. \right. \\
&\quad \left. \left. + d\sigma^{(0)} \otimes \left(d\Gamma_t^{(2)} - \frac{\Gamma_t^{(2)}}{\Gamma_t^{(0)}} d\Gamma_t^{(0)} - \frac{\Gamma_t^{(1)}}{\Gamma_t^{(0)}} \left(d\Gamma_t^{(1)} - \frac{\Gamma_t^{(1)}}{\Gamma_t^{(0)}} d\Gamma_t^{(0)} \right) \right) \right) \right].
\end{aligned}$$

At each order a corresponding top-decay width is used throughout all parts. The NNLO width is obtained from ref. [79] and at LO and NLO from ref. [80]. These widths agree with numerical results obtained from our calculation of course.

This process can be run with a fixed scale or with dynamic DIS (DDIS) scales by setting `dynamicsscale = DDIS`, `renscale = 1.0` and `facscale = 1.0`.

At NNLO there are several different contributions from vertex corrections on the light-quark line, heavy-quark line in production, and heavy-quark line in the top-quark decay. Additionally there are one-loop times one-loop interference contributions between all three contributions. These contributions can be separately enabled in the `singletop` block:

```
[singletop]
  nnlo_enable_light = .true.
  nnlo_enable_heavy_prod = .true.
  nnlo_enable_heavy_decay = .true.
  nnlo_enable_interf_lxh = .true.
  nnlo_enable_interf_lxd = .true.
  nnlo_enable_interf_hxd = .true.
  nnlo_fully_inclusive = .false.
```

For a fully inclusive calculation without decay the last setting has to be set to `.true.` and the decay and decay interference parts have to be removed. Additionally jet requirements must be lifted, see below.

When scale variation is enabled with DDIS scales then automatically also a variation around the fixed scale $\mu = m_t$ is calculated for comparison.

This process uses a fixed diagonal CKM matrix with $V_{ud} = V_{cs} = V_{tb} = 1$. The setting `removebr=.true.` removes the $W \rightarrow \nu e$ branching ratio.

This process involves complicated phase-space integrals and we have pre-set the initial integration calls for precise differential cross-sections with fiducial cuts. The number of calls can be tuned overall with the multiplier setting `integration%globalcallmult`. For total fully inclusive cross-sections the number of calls can be reduced by a factor of ten by setting `integration%globalcallmult = 0.1`, for example.

For scale variation uncertainties and PDF uncertainties we recommend to start with the default number of calls and a larger number of warmup iterations `integration%iterbatchwarmup=10`,

for example. For the warmup grid no scale variation or PDF uncertainties are calculated and this ensures a good Vegas integration grid that can be calculated fast. The setting `integration%callboost` modifies the number of calls for subsequent integration iterations after the warmup. For example setting it to 0.1 reduces the calls by a factor of ten. This is typically enough to compute the correlated uncertainties for a previously precisely determined central value.

At NNLO the default value for τ_{cut} is 10^{-3} , which is the value used for all the plots in our publication. We find that cutoff effects are negligible at the sub-permille level for this choice. We strongly recommend to not change this value.

Using the plotting routine with b-quark tagging The calculation has been set up with b-quark tagging capabilities that can be accessed in both the `gencuts_user.f90` routine and the plotting routine `nplotter_singletop_new.f90`. The plotting routine is prepared to generate all histograms shown in our publication in ref. [77]. By default the top-quark is reconstructed using the leading b-quark jet and the exact W-boson momentum, but any reconstruction algorithm can easily be implemented.

The version of the `gencuts_user.f90` file used for the plots in our paper [77] is available as `gencuts_user_singletop_nnlo.f90`. It can be used as a guide on how to access the b-quark tagging in the `gencuts_user` routine.

See also `nplotter_ktopanom.f` (used for the NLO off-shell calculation in ref. [33] for a reconstruction of the W-boson. It is based on requiring an on-shell W-boson and selecting the solution for the neutrino z -component that gives the closest on-shell top-quark mass by adding the leading b-quark jet.

Calculating fully inclusive cross-sections When calculating a fully inclusive cross-section without top-quark decay please set `zerowidth = .true.`, `removebr = .true.` in the general section of the input file; `inclusive = .true.`, `ptjetmin = 0.0`, `etajetmax = 99.0` in the basicjets section; `makecuts = .false.` in the cuts section; also set `nnlo_enable_heavy_decay = .false.` and `nnlo_enable_interf_lxd = .false.`, `nnlo_enable_interf_hxd = .false.` and `nnlo_fully_inclusive = .true.` in the singletop section.

These settings ensure that neither the decay nor any production times decay interference contributions are included. The last setting makes sure that only the right pieces in the fixed-order expansion of the cross-section are included. It also ensures that the b-quark from the top-quark decay is not jet-tagged and just integrated over.

Notes on runtimes and demo files Running the provided input file `input_singletop_nnlo_Tevatron_total.ini` with `-integration%globalcallmult=0.1` and without histograms takes about 4-5 CPU days. So depending on the number of cores, this can be run on a single desktop within a few hours.

Running the input file `input_singletop_nnlo_LHC_fiducial.ini` with the default set of calls and histograms takes about 3 CPU months (about 3 wall-time hours on our cluster with 45 nodes). For the fiducial

cross-section (without precise histograms) a setting of `-integration%globalcallmult=0.2` can also be used.

Note that `-extra%nohistograms = .true.` has been set in these demonstration files, so no further histograms from `nplotter_singletop_new.f90` are generated.

The input file `input_singletop_nnlo_LHC_fiducial.ini` together with the file `gencuts_user_singletop_nnlo.f90`, replacing `src/User/gencuts_user.f90` reproduces the fiducial cross-sections in ref. [77] table 6.

13.39 Single-top-quark production and decay at NNLO, process 1650

This calculation is based on ref. [77]. This process constitutes the real correction needed for the complete NNLO order calculation. In other words it is the plus-one-jet process evaluated at NLO.

13.40 Off-shell single top production in SM and SMEFT, processes 164,169

The processes 164 and 169 represent off-shell single-top-quark and anti-top-quark production, respectively. The calculations are performed in the complex-mass scheme. Both the SM and contributions from the SMEFT can be calculated. For more details on this calculation, please refer to ref. [33].

Dynamical double deep inelastic scattering scales can be consistently used at NLO by setting `dynamicsscale` to ‘DDIS’ and `scale=facscale` to 1d0. In this way the momentum transfer along the W -boson Q^2 is used as the scale for the light-quark-line corrections $\mu^2 = Q^2$, and $\mu^2 = Q^2 + m_t^2$ for the heavy-quark-line corrections. These scales are also consistently used for the non-resonant contributions, with QCD corrections on the ud -quark line, and separate QCD corrections on the bottom-quark line.

The new block ‘Single top SMEFT, nproc=164,169’ in the input file governs the inclusion of SMEFT operators and corresponding orders. The scale of new physics Λ can be separately set, and has a default value of 1000 GeV. The flag `enable 1/lambda4` enables the $1/\Lambda^4$ contributions, where operators $Q_{\varphi ud}^{33}$, Q_{dW}^{33} , Q_{dG}^{33} and Q_{4R} can contribute for the first time. For the non-Hermitian operators we allow complex Wilson coefficients. We also have a flag to disable the pure SM contribution, leaving only contributions from SMEFT operators either interfered with the SM amplitudes or as squared contributions at $1/\Lambda^4$. This can be used to directly and quickly extract kinematical distributions and the magnitudes of pure SMEFT contributions.

To allow for easier comparisons with previous anomalous couplings results, and possibly estimate further higher order effects, we allow for an anomalous couplings mode at LO by enabling the corresponding flag. The relations between our operators and the anomalous couplings are

$$\begin{aligned}
\delta V_L &= \mathcal{C}_{\varphi q}^{(3,33)} \frac{m_t^2}{\Lambda^2}, \text{ where } V_L = 1 + \delta V_L, \\
V_R &= \mathcal{C}_{\varphi ud}^{33} \frac{m_t^2}{\Lambda^2}, \\
g_L &= -4 \frac{m_W m_t}{\Lambda^2} \cdot \mathcal{C}_{dW}^{33}, \\
g_R &= -4 \frac{m_W m_t}{\Lambda^2} \cdot \mathcal{C}_{uW}^{33},
\end{aligned}$$

where m_W is the W -boson mass, and $m_W = \frac{1}{2}g_W v$ has been used to derive this equivalence. Note that the minus sign for g_L and g_R is different from the literature. See also the publication [33] for more information.

For comparisons with on-shell results one needs to add up the contributions from processes 161 at NLO and from the virt and real contributions from 162, see above.

The analysis/plotting routine is contained in the file ‘src/User/nplotter_ktopanom.f’, where all observables presented in this study are implemented, and the W -boson/neutrino reconstruction is implemented and can be switched on or off.

13.41 Wt production, processes 180–187

These processes represent the production of a W boson that decays leptonically in association with a top quark. The lowest order diagram involves a gluon and a bottom quark from the PDF, with the b -quark radiating a W boson and becoming a top quark. The calculation can be performed up to NLO. For more details on this calculation, please see Ref. [34].

Processes 180 and 185 produce a top quark that does not decay, whilst in processes 181 and 186 the top quark decays leptonically. Consistency with the simpler processes (180,185) can be demonstrated by running process 181,186 with `removebr` set to true.

At next-to-leading order, the calculation includes contributions from diagrams with two gluons in the initial state, $gg \rightarrow Wtb$. The p_T of the additional b quark is vetoed according to the value of the parameter `ptmin_bjet` which is specified in the input file. The contribution from these diagrams when the p_T of the b quark is above `ptmin_bjet` is zero. The values of this parameter and the factorization scale (`facscale`) set in the input file should be chosen carefully. Appropriate values for both (in the range 30-100 GeV) are discussed in the associated paper [34].

When one wishes to calculate observables related to the decay of the top quark, `removebr` should be false. The LO calculation proceeds as normal. At NLO, there are two options:

- `part=virt`, `real` or `tota`: final state radiation is included in the production stage only
- `part = todk`: radiation is included in the decay of the top quark also and the final result corresponds to the sum of real and virtual diagrams. This process can only be performed at NLO with `zerowidth = .true`. This should be set automatically. Note that these runs automatically perform an extra integration, so will take a little longer.

The contribution from radiation in the decay may be calculated separately using processes 182,187. These process numbers can be used with `part=virt,real` only. To ensure consistency, it is far simpler to use 181,186 and this is the recommended approach.

13.42 Di-jet production, processes 190–191

Process 190 represents di-jet production through strong interactions. It may be calculated to LO only.

Process 191 is an ancillary process that is used in the calculation of weak one-loop corrections to di-jet production. This process is calculable at leading LO and next-to-leading order NLO. When computed at LO it gives the contribution of weak ($O(\alpha^2)$) and mixed weak-strong ($O(\alpha\alpha_s)$) mediated processes to di-jet production. Please refer to Ref. [35] for details.

13.43 $H + \text{jet}$ production, $m_t = \text{finite}$, process 200

This process represents the production of a Higgs boson in association with a single jet based on refs. [40, 41, 81–84]. Decay modes are currently unsupported/untested. The top-quark mass is taken into account exactly for the Born and real-emission parts, as well as for the singular part of the virtual corrections. The real emission calculation is based on the one-loop, Higgs boson + 4 parton calculations with full quark mass effects of ref. [40, 41].

The finite part of the two-loop virtual corrections can be computed in different ways by setting the input file parameter `mtex`.

- In a low energy asymptotic expansion in $1/m_t^k$ up to order $k = 2, 4$ by setting `mtex` to 2 or 4 in the input file. This is recommended for transverse momenta up to $\simeq 225$ GeV.
- In a high energy expansion by setting `mtex`=100 in the input file. This is recommended for transverse momenta beyond 450 GeV.
- In a rescaling approach where the finite part of the two-loop virtual amplitude in the effective field theory ($m_t = \infty$) is rescaled pointwise by the ratio of the one-loop amplitude computed with full m_t dependence to the one-loop amplitude for $m_t = \infty$. This mode is the default mode and enabled with `mtex`=0 in the input file. This is the recommended approach for the intermediate energy region and for estimating top-mass uncertainties in the transition regions between these approaches.

This process is therefore calculable at leading LO and at next-to-leading order NLO (using an approximation for the two loop matrix element). Full NLO calculations (with the exact two-loop matrix element) have been performed in refs. [85–87].

13.44 $H + \text{jet}$ production, processes 201–210

These processes represent the production of a Higgs boson in association with a single jet, with the subsequent decay of the Higgs to either a pair of bottom quarks (processes 201,203,206) or to a pair of tau's (202,204,207), or to a pair of W 's which decay leptonically (208), or to a pair of Z 's which decay leptonically (209), or to a pair of photons (210).

13.44.1 $m_t = \text{finite}$, 201,202,206,207

The Higgs boson couples to a pair of gluons via a loop of heavy fermions which, in the Standard Model, is accounted for almost entirely by including the effect of the top quark alone. For processes 201,202,206,207, the matrix elements include the full dependence on the top quark mass. The calculation can only be performed at LO. The LO full m_t dependence calculation implements results of refs.[83, 84]. However, the Higgs boson can either be the Standard Model one (processes 201,202) or a pseudoscalar (206,207). Note that the pseudoscalar case corresponds, in the heavy top limit, to the effective Lagrangian,

$$\mathcal{L} = \frac{1}{8\pi v} G_{\mu\nu}^a \tilde{G}_a^{\mu\nu} A, \quad (19)$$

where $\tilde{G}_a^{\mu\nu} = i\epsilon^{\mu\nu\alpha\beta} G_{\alpha\beta}^a$. The interaction differs from the scalar case in by a factor of $3/2$ and hence the rate is increased by a factor of $(3/2)^2$.

13.44.2 $m_t = \infty$, 203,204,208,209,210

For processes 203,204,208,209,210, the calculation is performed in the limit of infinite top quark mass, so that NLO and NNLO results can be obtained. The virtual one-loop matrix elements have been implemented from refs [88] and [89]. Phenomenological results have previously been given in refs. [90],[88] and [91]. Note that the effect of radiation from the bottom quarks in process 203 is not included. NNLO corrections have only been implemented for processes 204 and 210, using the 1-jettiness slicing approach described in ref. [92]. When `removebr` is true in processes 201, 203, 206, 208, 209 and 210, the Higgs boson does not decay.

13.45 Higgs production via WBF, processes 211–217

These processes provide predictions for the production of a Higgs boson in association with two jets via weak-boson fusion (WBF). The Higgs boson subsequently decays to either a pair of bottom quarks (processes 211, 216), to a pair of tau's (212, 217), to a pair of W bosons (213), to a pair of Z bosons (214), or to a pair of photons (215). For more details on this calculation, please see Ref. [36].

Calculations can be performed up to NLO for processes 211–215. In addition to this, processes 216 and 217 provide the lowest order calculation of the WBF reaction which radiates an additional jet.

When `removebr` is true, the Higgs boson does not decay.

13.46 $e^-e^+\nu_\mu\bar{\nu}_\mu$ -pair production via WBF, processes 220,2201,222,2221

The *weak* processes (`nproc=220,222`) occur in $O(\alpha^6)$, whereas the *strong* processes (`nproc=2201,2221`) occur in $O(\alpha^4\alpha_S^2)$. These processes can currently only be calculated at lowest order.

$$\begin{aligned}
220 \quad & f(p_1) + f(p_2) \rightarrow Z(e^-(p_3), e^+(p_4))Z(\mu^-(p_5), \mu^+(p_6)) + f(p_7) + f(p_8), [WBF] \\
222 \quad & f(p_1) + f(p_2) \rightarrow Z(e^-(p_3), e^+(p_4))Z(\nu_\mu(p_5), \bar{\nu}_\mu(p_6)) + f(p_7) + f(p_8) [WBF] \\
2201 \quad & f(p_1) + f(p_2) \rightarrow Z(e^-(p_3), e^+(p_4))Z(\mu^-(p_5), \mu^+(p_6)) + f(p_7) + f(p_8) [strong] \\
2221 \quad & f(p_1) + f(p_2) \rightarrow Z(e^-(p_3), e^+(p_4))Z(\nu_\mu(p_5), \bar{\nu}_\mu(p_6)) + f(p_7) + f(p_8) [strong]
\end{aligned}$$

13.47 $\tau^+\tau^-$ production, process 221

This process provides predictions for the production of a tau lepton pair mediated by γ^*/Z , with subsequent leptonic decays. The calculation is available at LO only. The relevant matrix elements are adapted from the ones in ref. [93].

When `removebr` is true, the tau leptons do not decay.

13.48 $\nu_e e^+ \mu^- \mu^+$ -pair production via WBF, processes 223,2231

The *weak* process (`nproc=223`) occurs in $O(\alpha^6)$, whereas the *strong* process occurs (`nproc=2231`) in $O(\alpha^4\alpha_S^2)$. These processes can currently only be calculated at lowest order.

$$\begin{aligned}
223 \quad & f(p_1) + f(p_2) \rightarrow W^+(\nu_e(p_3), e^+(p_4))Z(\mu^-(p_5), \mu^+(p_6)) + f(p_7) + f(p_8) [weak] \\
2231 \quad & f(p_1) + f(p_2) \rightarrow W^+(\nu_e(p_3), e^+(p_4))Z(\mu^-(p_5), \mu^+(p_6)) + f(p_7) + f(p_8) [strong]
\end{aligned}$$

13.49 $e^- \bar{\nu}_e \nu_\mu \mu^+$ -pair production via WBF, processes 224,2241

The *weak* process (`nproc=224`) occurs in $O(\alpha^6)$, whereas the *strong* process (`nproc=2241`) occurs in $O(\alpha^4\alpha_S^2)$. These processes can currently only be calculated at lowest order.

$$\begin{aligned}
224 \quad & f(p_1) + f(p_2) \rightarrow W^-(e^-(p_3), \bar{\nu}_e(p_4))W^+(\nu_\mu(p_5), \mu^+(p_6)) + f(p_7) + f(p_8) [WBF] \\
2241 \quad & f(p_1) + f(p_2) \rightarrow W^-(e^-(p_3), \bar{\nu}_e(p_4))W^+(\nu_\mu(p_5), \mu^+(p_6)) + f(p_7) + f(p_8) [strong]
\end{aligned}$$

13.50 $e^- \bar{\nu}_e \mu^- \mu^+$ -pair production via WBF, processes 225,2251

The *weak* process occurs in $O(\alpha^6)$, whereas the *strong* process occurs in $O(\alpha^4\alpha_S^2)$. These processes can currently only be calculated at lowest order.

$$\begin{aligned}
225 \quad & f(p_1) + f(p_2) \rightarrow W^-(e^-(p_3), \bar{\nu}_e(p_4))Z(\mu^-(p_5), \mu^+(p_6)) + f(p_7) + f(p_8) [weak] \\
2251 \quad & f(p_1) + f(p_2) \rightarrow W^-(e^-(p_3), \bar{\nu}_e(p_4))Z(\mu^-(p_5), \mu^+(p_6)) + f(p_7) + f(p_8) [strong]
\end{aligned}$$

13.51 $e^-e^+\bar{\nu}_e\nu_e$ -pair production via WBF, processes 226

This *weak* process occurs at $O(\alpha^6)$, and contains contributions, from both WW and ZZ production. This process can currently only be calculated at lowest order.

$$226 \quad f(p_1) + f(p_2) \rightarrow e^-(p_3) + e^+(p_4) + \nu_e(p_5) + \bar{\nu}_e(p_6) + f(p_7) + f(p_8)[WBF]$$

13.52 $\nu_e e^+ \nu_\mu \mu^+$ -pair production via WBF, processes 228,2281

The *weak* process (`nproc=228`) occurs in $O(\alpha^6)$, whereas the *strong* process occurs (`nproc=2281`) in $O(\alpha^4\alpha_S^2)$. These processes can currently only be calculated at lowest order.

$$228 \quad f(p_1) + f(p_2) \rightarrow W^+(\nu_e(p_3), e^+(p_4))W^+(\nu_\mu(p_5), \mu^+(p_6)) + f(p_7) + f(p_8)[WBF]$$

$$2281 \quad f(p_1) + f(p_2) \rightarrow W^+(\nu_e(p_3), e^+(p_4))W^+(\nu_\mu(p_5), \mu^+(p_6)) + f(p_7) + f(p_8)[strong]$$

13.53 $e^-\bar{\nu}_e\mu^-\bar{\nu}_\mu$ -pair production via WBF, processes 229,2291

The *weak* process (`nproc=229`) occurs in $O(\alpha^6)$, whereas the *strong* process occurs (`nproc=2291`) in $O(\alpha^4\alpha_S^2)$. These processes can currently only be calculated at lowest order.

$$229 \quad f(p_1) + f(p_2) \rightarrow W^-(e^-(p_3), \bar{\nu}_e(p_4))W^-(\mu^-(p_5), \bar{\nu}_\mu(p_6)) + f(p_7) + f(p_8)[WBF]$$

$$2291 \quad f(p_1) + f(p_2) \rightarrow W^-(e^-(p_3), \bar{\nu}_e(p_4))W^-(\mu^-(p_5), \bar{\nu}_\mu(p_6)) + f(p_7) + f(p_8)[strong]$$

13.54 t -channel single top with an explicit b -quark, processes 231–240

These represent calculations of the t -channel single top (231) and anti-top (231) processes in a scheme with four flavours of quark in the proton, so that b -quarks are not present in the proton. The b -quark is instead explicitly included in the final state. For more details on this calculation, please see Ref. [32].

Processes 232 and 236 represent t -channel single top production in association with a further jet and may be calculated at LO only.

Processes 233 and 238 are the complete four-flavour scheme t -channel single top production processes. These are therefore the processes that should be used for most physics applications. When one wishes to calculate observables related to the decay of the top quark, `removebr` should be false in processes 233 and 236. The LO calculation proceeds as normal. At NLO, there are two options:

- `part=virt`, `real` or `tota` : final state radiation is included in the production stage only
- `part = todk` : radiation is included in the decay of the top quark also and the final result corresponds to the sum of real and virtual diagrams. Note that these runs automatically perform an extra integration, so will take a little longer.

Processes 234 and 239 give the extra contribution due to radiation in top decay. These processes are mainly of theoretical interest.

Processes 235 and 240 are the leading order single top processes with an extra radiated parton. These processes do not include jets produced in the decay process.

13.55 W^+W^+ +jets production, processes 251,252

These processes represent the production of two W^+ bosons in association with two (process 251) or three (process 252) jets. The lowest order at which two positively charged W bosons can be produced is with two jets. This process is only implemented for leptonic decays of the W particles. The calculation is available at LO only. The calculation and code are from ref. [39]. `removebr` is not implemented and has no effect.

13.56 $WZ + 2$ jet production, process 253-254

These processes represent the production of W and Z bosons in association with two jets. This process is only implemented for leptonic decays of the W and Z particles. The calculation is available at LO only.

13.57 $WZ + b +$ jet production, process 255-256

These processes represent the production of W and Z bosons in association with two jets, one of which contains a b -quark. This process is only implemented for leptonic decays of the W and Z particles. The calculation is available at LO only.

13.58 $WZ + 2b$ production, process 259-260

These processes represent the production of W and Z bosons in association with two b -quark jets. This process is only implemented for leptonic decays of the W and Z particles. The calculation is available at LO only.

13.59 $Z + Q$ production, processes 261–267

These processes represent the production of a Z boson that decays into a pair of electrons, in association with a heavy quark, Q . For more details on this calculation, please see Ref. [94].

For processes 261, 262, 266 and 267 the initial state at lowest order is the heavy quark and a gluon and the calculation may be performed at NLO. As for $H + b$ production, the matrix elements are divided into two sub-processes at NLO. Thus the user must sum over these after performing more runs than usual. At lowest order one can proceed as normal, using `nproc=261` (for $Z + b$) or `nproc=262` (for $Z + c$). For a NLO calculation, the sequence of runs is as follows:

- Run `nproc=261` (or 262) with `part=virt` and `part=real` (or, both at the same time using `part=tota`);
- Run `nproc=266` (or 267) with `part=real`.

The sum of these yields the cross-section with one identified heavy quark in the final state when `inclusive` is set to `.false.` . To calculate the rate for at least one heavy quark, `inclusive` should be `.true.`.

For processes 263 and 264, the calculation uses the matrix elements for the production of a Z and a heavy quark pair and demands that one of the heavy quarks is not observed. It may either lie outside the range of p_T and η required for a jet, or both quarks may be contained in the same jet. Due to the extra complexity (the calculation must retain the full dependence on the heavy quark mass), this can only be computed at LO.

When `removebr` is true, the Z boson does not decay.

13.60 Higgs+2 jet, processes 269

13.61 $H + 2$ jet production, ($m_t = \infty$), processes 270–274

These processes represent the production of a Standard Model Higgs boson in association with two jets. The Higgs boson subsequently decays to either a pair of photons (`nproc=270`), a bottom quark pair (`nproc=271`), a pair of tau's (`nproc=272`), a pair of leptonically decaying W 's (`nproc=273`) or a pair of leptonically decaying Z 's (`nproc=274`).

The matrix elements are included in the infinite top mass limit using the effective Lagrangian approach.

When `removebr` is true, the Higgs boson does not decay.

13.62 $H + 3$ jet production, ($m_t = \infty$), processes 275–279

These processes represent the production of a Standard Model Higgs boson in association with three jets. The Higgs boson subsequently decays to either a bottom quark pair (`nproc=275`), or a pair of tau's (`nproc=276`) or a pair of W 's that decay leptonically into a single generation of leptons (`nproc=278`) or a pair of Z 's that decay leptonically into a single generation of leptons (`nproc=279`). The matrix elements are included in the infinite top mass limit using an effective Lagrangian approach. These calculations can be performed at LO only.

When `removebr` is true, the Higgs boson does not decay.

13.63 Direct γ production, processes 280–282

These processes represent the production a real photon. Since this process includes a real photon, the cross section diverges when the photon is very soft or in the direction of the beam. Thus in order to produce sensible results, the input file must supply values for both `gamptmin` and `gamrapmax`. This will ensure that the cross section is well-defined.

Currently the code computes this process up to NLO accuracy. The extension to NNLO [95–97] has not yet been made public.

13.64 Direct $\gamma +$ heavy flavour production, processes 283–284

These processes represent the production a real photon with a b quark or a c quark. Since this process includes a real photon, the cross section diverges when the photon is very soft or in the direction of the beam. Thus in order to produce sensible results, the input file must supply values for both `gammptmin` and `gammrapmax`. This will ensure that the cross section is well-defined.

The calculation of process 283–284 is only available at leading order.

13.65 $g(-p_1) + g(-p_2) \rightarrow \gamma(p_3) + \gamma(p_4)$

This process computes the contribution of light-quark loops to the process $gg \rightarrow \gamma\gamma$. It is calculable at leading LO and next-to-leading order NLO. The calculation and a phenomenological analysis are described in Ref. [43]. This process includes the one-loop gluon-gluon contribution as given in ref. [98].

13.66 $g(-p_1) + g(-p_2) \rightarrow \gamma(p_3) + \gamma(p_4)$, (top loops at LO)

This process calculable at leading LO and next-to-leading order NLO.

This process computes the contribution of quark loops ($n_f = 5$ light quarks and top quarks) to the process $gg \rightarrow \gamma\gamma$. It is calculable at leading LO and next-to-leading order NLO, although the effect of top-quark loops are only included at LO. The calculation and a phenomenological analysis are described in Ref. [43].

13.67 Diphoton production

Process 285 represents the production of a pair of real photons. Since this process includes two real photons, the cross section diverges when one of the photons is very soft or in the direction of the beam. Thus in order to produce sensible results, the input file must supply values for both `ptminphoton` and `etamaxphoton`. This will ensure that the cross section is well-defined.

The calculation of process 285 may be performed using either the Frixione algorithm or standard cone isolation. Since version 10.1 also a fixed cone size can be specified as well as a simple hybrid cone isolation, see ref. [99].

This process also includes the one-loop gluon-gluon contribution as given in ref. [98]. The production of a photon via parton fragmentation is included at NLO and can be run separately by using the `frag` option in part. This option includes the contributions from the integrated photon dipole subtraction terms and the LO QCD matrix element multiplied by the fragmentation function.

The phase space cuts for the final state photons are defined in `input.ini`, for multiple photon processes such as 285 – 287 the p_T 's of the individual photons (hardest, second hardest and third hardest or softer) can be controlled independently. The remaining cuts on $R_{\gamma j}$, η_γ etc.

are applied universally to all photons. Users wishing to alter this feature should edit the file `photon_cuts.f` in the directory `src/User`.

This process can be calculated at LO, NLO, and NNLO. NLO calculations can be performed by subtraction, zero-jettiness slicing and q_T -slicing. NNLO calculations can be performed by zero-jettiness slicing and q_T -slicing. Input files for these 6 possibilities are given in the link below.

The fixed-order NNLO calculation has been implemented in ref. [43]. Transverse momentum resummation at the level of $N^3LL + NNLO$ has been implemented in ref. [100]. By including the three-loop hard [101] and beam functions [102],[103],[104] it has been upgraded to N^3LL' in ref. [99].

13.68 Transverse momentum resummation

Transverse momentum resummation can be enabled for process 285 at highest order $N^3LL' + NNLO$ with ‘part=resNNLOp’. The setting ‘part=resNNLO’ resums to order $N^3LL + NNLO$ (α_s^2 accuracy in improved perturbation theory power counting) and ‘part=resNLO’ to order $N^3LL + NLO$. Note that process 285 with resummation only includes the $q\bar{q}$ channel. The gg channel enters at an increased relative level of α_s , so has to be added with process number 2851 at order ‘part=resNLO’ for overall $N^3LL' + NNLO$ precision. For an overall consistent precision of $N^3LL + NNLO$ the gg channel can be added with ‘part=resLO’.

Note that at fixed-order the gg channel is included at NNLO automatically at the level of α_s^2 .

The fixed-order NNLO calculation has been implemented in ref. [43]. Transverse momentum resummation at the level of $N^3LL + NNLO$ has been implemented in ref. [100]. By including the three-loop hard [101] and beam functions [102],[103],[104] it has been upgraded to N^3LL' in ref. [99].

13.69 $g(-p_1) + g(-p_2) \rightarrow \gamma(p_3) + \gamma(p_4) + f(p_5)$

Process 2861 represents the process $gg \rightarrow \gamma\gamma g$ mediated by a loop of light quarks. This process is calculable at leading order LO, $O(\alpha_s^3)$.

The calculation is described in Ref. [105].

13.70 $\gamma\gamma$ +jet production, process 286

Process 286, corresponding to the production of a pair of real photons in association with a jet, can be computed at NLO. Since this process includes two real photons, the cross section diverges when one of the photons is very soft or in the direction of the beam. Thus in order to produce sensible results, the input file must supply values for both `gammptmin` and `gammrapmax`. This will ensure that the cross section is well-defined.

The calculation of process 286 may be performed at NLO using either the Frixione algorithm [55] or standard cone isolation. This process also includes the one-loop gluon-gluon contribution as given in ref. [98]. The production of a photon via parton fragmentation is

included at NLO and can be run separately by using the **frag** option in **part**. This option includes the contributions from the integrated photon dipole subtraction terms and the LO QCD matrix element multiplied by the fragmentation function.

The phase space cuts for the final state photons are defined in **input.ini**, for multiple photon processes such as 285 - 287 the p_T 's of the individual photons (hardest, second hardest and third hardest or softer) can be controlled independently. The remaining cuts on $R_{\gamma j}$, η_γ etc. are applied universally to all photons. Users wishing to alter this feature should edit the file **photon_cuts.f** in the directory **src/User**.

The calculation is described in Ref. [105].

13.71 $\gamma\gamma\gamma$ production, process 287

Process 287 represents the production of three real photons. The cross section diverges when one of the photons is very soft or in the direction of the beam. Thus in order to produce sensible results, the input file must supply values for both **gamptmin** and **gamrapmax**. This will ensure that the cross section is well-defined.

The calculation of process 285 may be performed at NLO using either the Frixione algorithm [55] or standard cone isolation. The production of a photon via parton fragmentation is included at NLO and can be run separately by using the **frag** option in **part**. This option includes the contributions from the integrated photon dipole subtraction terms and the LO QCD matrix element multiplied by the fragmentation function. The phase space cuts for the final state photons are defined in **input.ini**, for multiple photon processes such as 285 - 287 the p_T 's of the individual photons (hardest, next-to hardest and softest) can be controlled independently. The remaining cut on $R_{\gamma j}$, η_γ etc. are applied universally to all photons. Users wishing to alter this feature should edit the file **photon_cuts.f** in the directory **src/User**.

13.72 $\gamma\gamma\gamma\gamma$ production, process 289

Process 289 represents the production of four real photons. The cross section diverges when one of the photons is very soft or in the direction of the beam. Thus in order to produce sensible results, the input file must supply values for both **gamptmin** and **gamrapmax**. This will ensure that the cross section is well-defined.

The calculation of process 289 may be performed at NLO using either the Frixione algorithm [55] or standard cone isolation. The production of a photon via parton fragmentation is included at NLO and can be run separately by using the **frag** option in **part**. This option includes the contributions from the integrated photon dipole subtraction terms and the LO QCD matrix element multiplied by the fragmentation function. The phase space cuts for the final state photons are defined in **input.ini**, for multiple photon processes such as 285 - 289 the p_T 's of the individual photons (hardest, next-to hardest and softest) can be controlled independently. The remaining cut on $R_{\gamma j}$, η_γ etc. are applied universally to all photons. Users wishing to alter this feature should edit the file **photon_cuts.f** in the directory **src/User**.

Note that for this process the second softest and softest photons are forced to have equal minimum p_T , defined by the **[gamptmin(3rd)]** variable in the input file.

13.73 $W\gamma$ production, processes 290-299, 2941, 2991

These processes represent the production of a W boson which subsequently decays leptonically, in association with a real photon. Since this process includes a real photon, the cross section diverges when the photon is very soft or in the direction of the beam. Thus in order to produce sensible results, the input file must supply values for both `gammptmin` and `gammrapmax`. Moreover, when the parameters `zerowidth` and `removebr` are set to `.false.` the decay $W \rightarrow \ell\nu$ will include photon radiation from the lepton, so that a non-zero $R(\gamma, \ell)_{min}$ (`Rgalmin`) should also be supplied. This will ensure that the cross section is well-defined. Virtual amplitudes are taken from ref. [70].

The calculation of processes 290 and 295 may be performed at NLO and NNLO using the Frixione algorithm [55] or standard isolation. The phenomenology of these processes at NNLO has been treated in ref. [12]. The one-loop virtual diagrams are taken from [70] and the two-loop virtual diagrams are taken from [106]. For processes 290 and 295 the role of `mtrans34cut` changes to become a cut on the transverse mass on the M_{345} system, i.e. the photon is included with the leptons in the cut.

Processes 292 and 297 represent the $W\gamma$ +jet production processes. They may be computed to NLO.

Processes 294 and 299 represent the photon-induced reactions, $p + \gamma \rightarrow e\nu\gamma j$ and should be computed at NLO. Processes 2941 and 2991 represent the photon-induced reactions, $p + \gamma \rightarrow e\nu\gamma jj$ and should be computed at NLO.

13.73.1 Anomalous $WW\gamma$ couplings

Processes 290-297 may also be computed including the effect of anomalous $WW\gamma$ couplings, making use of the amplitudes calculated in Ref. [107]. Including only dimension 6 operators or less and demanding gauge, C and CP invariance gives the general form of the anomalous vertex [107],

$$\begin{aligned} \Gamma_{WW\gamma}^{\alpha\beta\mu}(q, \bar{q}, p) = & \bar{q}^\alpha g^{\beta\mu} \left(2 + \Delta\kappa^\gamma + \lambda^\gamma \frac{q^2}{M_W^2} \right) - q^\beta g^{\alpha\mu} \left(2 + \Delta\kappa^\gamma + \lambda^\gamma \frac{\bar{q}^2}{M_W^2} \right) \\ & + (\bar{q}^\mu - q^\mu) \left[-g^{\alpha\beta} \left(1 + \frac{1}{2} p^2 \frac{\lambda^\gamma}{M_W^2} \right) + \frac{\lambda^\gamma}{M_W^2} p^\alpha p^\beta \right], \end{aligned} \quad (20)$$

where the overall coupling has been chosen to be $-|e|$. The parameters that specify the anomalous couplings, $\Delta\kappa^\gamma$ and λ^γ , are specified in the input file as already discussed in Section 13.24. If the input file contains a negative value for the form-factor scale Λ then no suppression factors are applied to the anomalous couplings. Otherwise, the couplings are included in MCFM only after suppression by dipole form factors,

$$\Delta\kappa^\gamma \rightarrow \frac{\Delta\kappa_1^\gamma}{(1 + \hat{s}/\Lambda^2)^2}, \quad \lambda^\gamma \rightarrow \frac{\Delta\lambda^\gamma}{(1 + \hat{s}/\Lambda^2)^2}, \quad (21)$$

where \hat{s} is the $W\gamma$ pair invariant mass.

The Standard Model cross section is obtained by setting $\Delta\kappa^\gamma = \lambda^\gamma = 0$.

13.74 $Z\gamma$, production, processes 300, 305

Processes 300 and 305 represent the production of a Z boson (or virtual photon for process 300) in association with a real photon based on ref. [108]. The Z/γ^* subsequently decays into either an e^+e^- pair (`nproc=300`) or neutrinos (`nproc=305`). Since these processes include a real photon, the cross section diverges when the photon is very soft or in the direction of the beam. Thus in order to produce sensible results, the input file must supply values for both `gammptmin` and `gammrapmax`. Moreover, when the parameters `zerowidth` and `removebr` are set to `.false.` the decay $Z \rightarrow e^-e^+$ (`nproc=300`) will include photon radiation from both leptons, so that a non-zero $R(\gamma, \ell)_{min}$ (`Rgalmin`) should also be supplied. This will ensure that the cross section is well-defined. The calculation of processes 300 may be performed at NNLO using the Frixione algorithm [55] or standard isolation. The one-loop virtual diagrams are taken from [70] and the two-loop virtual diagrams are taken from [106].

For the process 300 the role of `mtrans34cut` changes to become a cut on the invariant mass on the M_{345} system, i.e. the photon is included with the leptons in the cut.

13.74.1 Anomalous $ZZ\gamma$ and $Z\gamma\gamma$ couplings

Processes 300-305 may also be computed including the effect of anomalous couplings between Z bosons and photons. Note that, at present, the effect of anomalous couplings is not included in the gluon-gluon initiated contributions.

The anomalous $Z\gamma Z$ vertex (not present at all in the Standard Model), considering operators up to dimension 8, is given by [107],

$$\Gamma_{Z\gamma Z}^{\alpha\beta\mu}(q_1, q_2, p) = \frac{i(p^2 - q_1^2)}{M_Z^2} \left(h_1^Z (q_2^\mu g^{\alpha\beta} - q_2^\alpha g^{\mu\beta}) \right. \\ \left. + \frac{h_2^Z}{M_Z^2} p^\alpha (p \cdot q_2 g^{\mu\beta} - q_2^\mu p^\beta) - h_3^Z \varepsilon^{\mu\alpha\beta\nu} q_{2\nu} - \frac{h_4^Z}{M_Z^2} \varepsilon^{\mu\beta\nu\sigma} p^\alpha p_\nu q_{2\sigma} \right)$$

where the overall coupling has been chosen to be $|e|$ (and $\epsilon^{0123} = +1$). The non-standard $Z_\alpha(q_1)\gamma_\beta(q_2)\gamma_\mu(p)$ momentum-space vertex can be obtained from this equation by setting $q_1^2 \rightarrow 0$ and replacing $h_i^Z \rightarrow h_i^\gamma$. The parameters that specify the anomalous couplings, h_i^Z and h_i^γ (for $i = 1 \dots 4$), are specified in the input file as, e.g. `h1(Z)` and `h1(gamma)`. If the input file contains a negative value for the form-factor scale Λ then no suppression factors are applied to these anomalous couplings. Otherwise, the couplings are included in MCFM only after suppression by dipole form factors,

$$h_{1,3}^{Z/\gamma} \rightarrow \frac{h_{1,3}^{Z/\gamma}}{(1 + \hat{s}/\Lambda^2)^3}, \quad h_{2,4}^{Z/\gamma} \rightarrow \frac{h_{2,4}^{Z/\gamma}}{(1 + \hat{s}/\Lambda^2)^4}, \quad (22)$$

where \hat{s} is the $Z\gamma$ pair invariant mass. Note that these form factors are slightly different from those discussed in Sections 13.24 and 13.73. The form factors can be modified in `src/Need/set_anomcoup.f`.

The Standard Model cross section is obtained by setting $h_i^Z = h_i^\gamma = 0$ for $i = 1 \dots 4$.

13.75 $Z\gamma\gamma$ production processes, 301, 306

Processes 301 and 306 represent the production of a Z boson (or virtual photon for process 301) in association with two photons. The Z/γ^* subsequently decays into either an e^+e^- pair (`nproc=301`) or neutrinos (`nproc=306`). Since these processes include real photons, the cross section diverges when either of the photons is very soft or in the direction of the beam. Thus in order to produce sensible results, the input file must supply values for both `gammptmin` and `gammrapmax`. Moreover, when the parameters `zerowidth` and `removebr` are set to `.false.`, the decay $Z \rightarrow e^-e^+$ (`nproc=301`) will include photon radiation from both leptons, so that a non-zero $R(\gamma, \ell)_{min}$ (`Rgalmin`) should also be supplied. This will ensure that the cross section is well-defined. Anomalous couplings are not currently implemented for these processes.

13.76 $Z\gamma j$, production, processes 302, 307

Processes 302 and 307 represent the production of a Z boson (or virtual photon) in association with a real photon and at least one jet. The Z/γ^* subsequently decays into either an e^+e^- pair (`nproc=302`) or neutrinos (`nproc=307`). Since these processes include a real photon and a jet, the cross section diverges when the photon or jet is very soft or in the direction of the beam. Thus in order to produce sensible results, the input file must supply values for both `gammptmin` and `gammrapmax`, and `ptjetmin` and `etajetmax`. Moreover, when the parameters `zerowidth` and `removebr` are set to `.false.`, the decay $Z \rightarrow e^-e^+$ (`nproc=302`) will include photon radiation from both leptons, so that a non-zero $R(\gamma, \ell)_{min}$ (`Rgalmin`) should also be supplied. This will ensure that the cross section is well-defined. The calculation of processes 302 and 307 may be performed at NLO using the Frixione algorithm [55] or standard isolation. Anomalous couplings are not currently implemented for these processes.

13.77 $Z\gamma\gamma j$ and $Z\gamma jj$, 303, 304, 308 and 309

These processes are available at LO only. The Z/γ^* subsequently decays into either an e^+e^- pair (`nproc=303,304`) or neutrinos (`nproc=308,309`). Since these processes include a real photon and a jet, the cross section diverges when a photon or a jet is very soft or in the direction of the beam. Thus in order to produce sensible results, the input file must supply values for both `gammptmin` and `gammrapmax`, and `ptjetmin` and `etajetmax`. Moreover, when the parameters `zerowidth` and `removebr` are set to `.false.`, the decay $Z \rightarrow e^-e^+$ (`nproc=303, 304`) will include photon radiation from both leptons, so that a non-zero $R(\gamma, \ell)_{min}$ (`Rgalmin`) should also be supplied. This will ensure that the cross section is well-defined. Anomalous couplings are not currently implemented for these processes.

13.78 $W + Q + \text{jet}$ production processes 311–326

These processes represent the production of a W boson that decays leptonically, in association with a heavy quark, Q and an additional light jet. In processes 311 and 316, Q is a bottom quark, whilst processes 321 and 326 involve a charm quark. In these processes the quark Q occurs as parton PDF in the initial state. The initial state in these processes consists of a light quark and a heavy quark, with the light quark radiating the W boson. These calculations may be performed at LO only.

When `removebr` is true, the W boson does not decay.

13.79 $W + c + \text{jet}$ production, processes 331, 336

These processes represent the production of a W boson that decays leptonically, in association with a charm quark and an additional light jet.

In contrast to processes 321 and 326 described above, the initial state in this case consists of two light quarks, one of which is a strange quark which radiates the W boson. The calculation may be performed at LO only.

When `removebr` is true, the W boson does not decay.

13.80 $Z + Q + \text{jet}$ production, processes 341–357

These processes represent the production of a Z boson that decays into a pair of electrons, in association with a heavy quark, Q and an untagged jet. For more details on this calculation, please see Ref. [109].

For processes 341 and 351 the initial state at lowest order is the heavy quark and a gluon and the calculation may be performed at NLO. Thus in these processes the quark Q occurs as parton PDF in the initial state. As for $H + b$ and $Z + Q$ production, the matrix elements are divided into two sub-processes at NLO. Thus the user must sum over these after performing more runs than usual. At lowest order one can proceed as normal, using `nproc=341` (for Zbj) or `nproc=351` (for Zcj). For a NLO calculation, the sequence of runs is as follows:

- Run `nproc=341` (or 351) with `part=virt` and `part=real` (or, both at the same time using `part=tota`);
- Run `nproc=342` (or 352) with `part=real`.

The sum of these yields the cross-section with one identified heavy quark and one untagged jet in the final state when `inclusive` is set to `.false.`. To calculate the rate for at least one heavy quark and one jet (the remaining jet may be a heavy quark, or untagged), `inclusive` should be `.true.`.

Processes 346, 347 and 356, 357 are the lowest order processes that enter the above calculation in the real contribution. They can be computed only at LO.

When `removebr` is true, the Z boson does not decay.

13.81 $c\bar{s} \rightarrow W^+$, processes 361–363

These processes represent the production of a W^+ from a charm and anti-strange quark at LO. The W^+ boson decays into a neutrino and a positron.

The NLO corrections to this LO process include a contribution of the form, $g\bar{s} \rightarrow W^+\bar{c}$. For process 361 this contribution is calculated in the approximation $m_c = 0$ at NLO. In order to perform the NLO calculation for a non-zero value of m_c , one must instead sum the results of processes 362 and 363 for `part=tota`.

Process (W^+/W^-)	<code>inclusive=.false.</code>	<code>inclusive=.true.</code>
401/406	(b) or (\bar{b})	$+(b, \bar{b})$ or (b, j) or (\bar{b}, j)
402/407	(B)	$+(B, j)$
403/408	(b, \bar{b})	(no extra configurations)

Table 38: The different final states allowed in the calculation of processes 401–408. A jet containing both b and \bar{b} quarks is denoted by B and a light (quark or gluon) jet by j . The inclusive (right-hand) column also allows the final states in the exclusive (middle) column.

13.82 $W\gamma\gamma$ production, processes 370–371

These processes represent the production of a W boson which subsequently decays leptonically, in association with two real photons. Since this process includes real photons, the cross section diverges when the photon is very soft or in the direction of the beam. Thus in order to produce sensible results, the input file must supply values for both `gammptmin` and `gammrapmax`. Moreover, when the parameters `zerowidth` and `removebr` are set to `.false.` the decay $W \rightarrow \ell\nu$ will include photon radiation from the lepton, so that a non-zero `R(photon,lept)_min` should also be supplied. This will ensure that the cross section is well-defined.

These processes may be computed at leading order only.

13.83 $W + Q$ production in the 4FNS, processes 401–408

These processes represent the production of a W boson and one or more jets, at least one of which is a b -quark, calculated in the 4-flavour number scheme (4FNS). This implies that contributions that explicitly contain a b -quark in the initial state are not included. These processes all use the same matrix elements as processes 20 and 25 (see section 13.8), but make different cuts on the final state. The final state is specified by the process number and the value of the flag `inclusive`, as shown in Table 38. An additional flag is hard-coded into the file `src/Cuts/filterWbbmas.f` to control the inclusion of the 3-jet configuration, (b, \bar{b}, j) when `inclusive` is set to `.true.`. By default, the statement `veto3jets = .false.` is included in this file. If this flag is set to `.true.` then the (b, \bar{b}, j) contribution is not included in processes 401, 402, 406, 407.

As usual, jets may be unobserved as a result of them falling outside the p_T and rapidity ranges specified in the input file. In addition, the number of jets may be different from the number of partons in the matrix element calculation as a result of merging in the jet algorithm.

13.84 $W + Q$ production in the 5FNS, processes 411, 416

These processes represent production of a W boson in association with a b -jet, computed in the 5-flavour number scheme, i.e. a b -quark is present in the initial state. The lowest order processes are the same as in processes 311, 316. The results at NLO are not physical cross sections since part of the corrections are not included in order to avoid double-counting with

the 4FNS process (processes 401 and 406). To obtain combined 4FNS+5FNS predictions, the user should select process 421 (W^+) or 426 (W^-).

13.85 $W + Q$ production in combined 4FNS/5FNS, processes 421, 426

These processes represent the production of a W boson and one or more jets, at least one of which is a b -quark, calculated by combining the 4- and 5-flavour results of processes 401, 411 (for 421) and 406, 416 (for 426). The selection of the final state is the same as for processes 401 and 406, as described in Section 13.83. The procedure for combining the two calculations is described in refs. [110, 111].

13.86 $W + b\bar{b}$ jet production, processes 431,436

These processes represent the production of a W boson which subsequently decays leptonically, in association with a $b\bar{b}$ pair and an additional jet. The effect of the bottom quark mass is included (in contrast to the massless approximation used in processes 24, 29) and the calculation may be performed at LO only.

When `removebr` is true, the W boson does not decay.

13.87 Diboson+jet production, processes 461–487

These processes represent the production of a vector boson pair in association with a jet. They are the counterparts of the corresponding diboson process (`nproc-400`) described above, but also including a jet in the final state. They may be computed to NLO. Amplitudes are taken from refs. [44–46].

13.88 $W + t\bar{t}$ processes 500–516

These processes represent the production of a W^\pm boson which subsequently decays leptonically, in association with a $t\bar{t}$ pair. In all except processes 500 and 510 the decays of the top and anti-top quark are included. Processes 501,502 and 511,512 refer to the semileptonic decay of the top and antitop quarks, with the latter process in each pair giving the radiation in the decay of the top and antitop. Process 503 (513) refers to the semileptonic decay of the top (antitop) and the hadronic decay of the antitop (top). Processes 506(516) gives the semileptonic decay of the antitop(top) and the hadronic decay of the top(antitop). Processes 506(516) do not give same sign lepton events, so they may be of less phenomenological importance. For this reason we have not yet included radiation in the decay for these processes.

For processes 503, 506, 513 and 516 the default behaviour is that the hadronic decay products are clustered into jets using the supplied jet algorithm parameters, but no cut is applied on the number of jets. This behaviour can be altered by changing the value of the variable `notag` in the file `src/User/setnotag.f`.

The top quarks are always produced on-shell, which is a necessity for a gauge invariant result from this limited set of diagrams, but all spin correlations are included. Switching `zerowidth`

from `.true.` to `.false.` only affects the W bosons (both the directly produced one and from the top quark decay). Processes 501 and 511 may be run at NLO with the option `todk`, including radiation in the decay of the top quark, see section 13.33.

13.89 $Zt\bar{t}$ production, processes 529–533

These processes represent the production of a Z boson in association with a pair of top quarks. These processes are only available at LO. For process 529, neither the top quarks nor the Z -boson decays. In processes 530–533, the top quarks are always produced on-shell, which is a necessity for a gauge invariant result from this limited set of diagrams. Switching `zerowidth` from `.true.` to `.false.` only affects the Z and the W bosons from the top quark decay. In process 530 the Z boson decays into an electron pair, whilst in 531 the decay is into a massless bottom quark pair. In process 532–533 the Z boson decays into an electron pair, whilst one or other of the top quark or top anti-quark decays hadronically.

For processes 532 and 533 the default behaviour is that the hadronic decay products are clustered into jets using the supplied jet algorithm parameters, but no cut is applied on the number of jets. This behaviour can be altered by changing the value of the variable `notag` in the file `src/User/setnotag.f`.

When `removebr` is true in process 530, the top quarks and the Z boson do not decay.

13.90 Ht and $H\bar{t}$ production, processes 540–557

These processes describe the production of a single top quark (540, 544, 550, 554) or antiquark (541, 547, 551, 557) by W exchange in the t -channel, in association with a Higgs boson. These processes can be performed at NLO. For processes 540, 541, 550, 551, the top quark does not decay, but the Higgs boson decays to $b\bar{b}$, (540, 541), or to $\gamma\gamma$, (550, 551). Processes 544, 547 and 554, 557 include the decay of the top quark and antiquark in the approximation in which the top quark is taken to be on shell allowing a clean separation between production and decay. For more details on this calculation, please see Ref. [48].

It is possible to study the effects of anomalous couplings of the Higgs boson to the top quark and W bosons. These are parametrized by $c_{t\bar{t}H} = g_{t\bar{t}H}/g_{t\bar{t}H}^{SM}$ and $c_{WWH} = g_{WWH}/g_{WWH}^{SM}$ respectively, so that $c_{t\bar{t}H} = c_{WWH} = 1$ in the SM. Different couplings may be chosen by modifying the variables `cttH` and `cWWH` in the `anom_higgs` section of the input file.

13.91 Zt and $Z\bar{t}$ production, processes 560–569

These processes describe the production of a single top quark (or antiquark) by W exchange in the t -channel, in association with a Z boson. Processes 560, 561, 564, 567 can be performed at NLO. Processes 560–563 are for stable top quarks, whereas processes 564–569 include the decay of the top quark and antiquark in the approximation in which the top quark is taken to be on shell allowing a clean separation between production and decay. For more details on this calculation, please see Ref. [48].

For processes 564 and 567 the default behaviour is that the hadronic decay products are clustered into jets using the supplied jet algorithm parameters, but no cut is applied on the number of jets. This behaviour can be altered by changing the value of the variable `notag` in the file `src/User/setnotag.f`.

13.92 HH production, processes 601–602

These processes represent the production of a pair of Higgs bosons. The production proceeds through gluon-fusion one-loop diagrams involving loops of top quarks. The formulae implemented in the code are taken from ref. [49], where the two Higgs bosons are treated as being on-shell. To enforce this condition, the code sets `zerowidth` to true, overriding the value set in the input file. The calculation can be performed at LO only, (i.e. one-loop order only). Two decays of the Higgs bosons are currently foreseen, although other decays can easily be implemented. In process 601, one Higgs boson decays to a pair of b -quarks, and the other decays to a pair of τ 's. In process 602, one Higgs boson decays to a pair of b -quarks, and the other decays to a pair of photons.

13.93 WH production, process 609

This process represents the production of W and H bosons in association with a jet, with the subsequent decay $H \rightarrow \tau^+ \tau^-$. Both charges of the W boson are summed over and, as a result, the decay products of the W boson, particles 3 and 4, represent lepton and antilepton respectively (i.e. they do not correspond to a neutrino and charged lepton). It is primarily of interest as a component part of the NNLO contributions to WH production. For further information see ref. [22]. This process is calculable at leading LO and next-to-leading order NLO.

13.94 Associated production of WH and a jet, processes 610-618

These processes represent the production of W^\pm and H bosons in association with a jet, with various decays of the Higgs boson provided. They are primarily of interest as a component part of the NNLO contributions to WH production. For further information see ref. [22]. This process is calculable at leading LO and next-to-leading order NLO.

13.95 Associated production of ZH and a jet, processes 620-623

These processes represent the production of Z and H bosons in association with a jet, with various decays of the Higgs boson provided. They are primarily of interest as a component part of the NNLO contributions to ZH production. For further information see ref. [22]. This process is calculable at leading LO and next-to-leading order NLO.

13.96 $Ht\bar{t}$ production, processes 640–667

These processes represent the production of a Higgs boson in association with a pair of top quarks. The calculation can be performed at LO only.

For process 640, neither the top quarks nor the Higgs boson decays. In processes 641–647, the top quarks are always produced on-shell, which is a necessity for a gauge invariant result from this limited set of diagrams. Switching `zerowidth` from `.true.` to `.false.` only affects the Higgs and the W bosons from the top quark decay. In process 641 both the top quarks decay leptonically and the Higgs boson decays into a pair of bottom quarks. Consistency with the simpler process (640) can be demonstrated by running process 641 with `removebr` set to true. In process 644 the top quark decays leptonically and the anti-top quark decays hadronically and the Higgs boson decays into a pair of bottom quarks. In process 647 the anti-top quark decays leptonically and the top quark decays hadronically and the Higgs boson decays into a pair of bottom quarks.

Processes 651–657 correspond to processes 641–647 but with the Higgs decaying to two photons. Processes 661–667 correspond to processes 641–647 but with the Higgs decaying to two W -bosons which subsequently decay leptonically.

14 New features in MCFM-10

14.1 Downloads of earlier versions, MCFM-10

- [MCFM-10.2.2.tar.gz](#) (May 19th, 2022, updated November 4th, 2022)
- [MCFM-10.1.tar.gz](#) (January 10th, 2022)
 - C++ interface to tree and one-loop amplitudes as a replacement of OpenLoops and Recola [\[2107.04472\]](#)
 - t-channel single-top-quark production at NNLO [\[2012.01574\]](#), see also [\[2109.10448\]](#)
 - q_T^2 resummation for Diphoton production at $N^3LL'+NNLO$ [\[2107.12478\]](#)
- [MCFM-10.0.1.tar.gz](#) (March 29th, 2021, updated May 27th, 2021)
 - $N^3LL+NNLO$ q_T^2 resummation for the single boson processes W^+, W^-, Z and H and diboson processes $\gamma\gamma, Z\gamma, ZH\gamma\gamma, Z\gamma, ZH$ and WH . See the [CuTe-MCFM](#) site for further details.
 - Support for histograms with custom binning.
 - Streamlined compilation process into single CMake script.

14.2 New features in MCFM-10.2

Version 10.2 of the code introduces the ability to compute diboson processes to NNLO. It also allows all NNLO calculations to be performed using two variants of slicing: using 0-jettiness (as in previous versions) or q_T (new). Benchmark results are reported in Section 8.

This version also extends the capabilities of the interface to allow a calculation of one-loop amplitudes representing diboson+jet production with a variety of W and Z boson decays, including all appropriate interferences. The calculation of diboson amplitudes (without the presence of an additional jet) has also been extended to include additional processes that include interference contributions. The new scattering amplitudes available are:

```
d u~ e- ve~ e+ e-
u d~ e+ ve e+ e-
u u~ e- e+ ve ve~
d u~ e- ve~ a g
u d~ e+ ve a g
u u~ e- e+ a g
u u~ e- ve~ mu+ vmu g
d u~ e- ve~ mu+ mu- g
u d~ e+ ve mu+ mu- g
u u~ e- e+ mu+ mu- g
u u~ e- e+ e- e+ g
u u~ e- e+ vmu vmu~ g
u u~ e- e+ ve ve~ g
```

where, in addition, all relevant combinations of quark flavors are included.

A description of the new features added in recent releases (v9.0 onwards) is given in Section 15.

14.3 New features in MCFM-10.0

For using the q_T resummation of CuTe-MCFM please refer to `cute-mcfm.pdf` and ref. [100].

New plotting infrastructure. MCFM-10.0 implements a new plotting infrastructure that allows for much easier setup and custom-binned histograms. The new style histograms can be enabled by setting `newstyle = .true.` in the `[histogram]` section of the input file. An example for Z production with resummation and custom binning is given in `src/User/nplotter_Z_new.f90`. Each plotter implements a new Fortran module with a function `setup()` that is called once at the beginning of MCFM to set up the histogram binnings. The function `book(p,wt,ids,vals,wts)` is called for each phase space point, calculates the observables based on the jet four-momenta in `p` and returns them in the `vals` array. The `wts` array is typically filled with `wt` for each observable, but can be modified to return a different weight to the histogramming routine. This is used in the example file to implement a transition function for the resummed and fixed-order components.

To adopt a new process to the new histograms, the file `src/Mods/mod_SetupPlots.f90` can be modified. More precisely, the function `setup_plots` needs to import the plotting module of the process, call the setup routine for the process, and set the `pbook` pointer to the actual book routine of the new plotting module.

15 New features in MCFM-9

15.1 Download of MCFM-9

- [MCFM-9.1.tar.gz](#) (April 7th, 2020)
 - New implementation of $H+2j$ virtual matrix elements with mass effects.
- [MCFM-9.0.tar.gz](#) (released September 25th, 2019)
 - Overhaul of the code offering many new features such as an efficient calculation of scale and PDF uncertainties and a robust estimate of residual slicing-dependence (for NNLO calculations). For a detailed description of many of the improvements, please refer to the companion publication [arXiv:1909.09117 \[hep-ph\]](#).

15.2 Description of MCFM-9

In this section we present the new and modified features in MCFM-9.0 and describe how to use them on a technical level. This serves mostly as a quick-start for users already familiar with MCFM. With all re-implemented and newly implemented components we strive for Fortran 2008 compliance, making explicit use of its features. Following the Fortran standard furthermore allows us to achieve compatibility with not just the GNU compiler. In previous versions of MCFM the licensing was unclear, since none was specified. We now license all code under the GNU GPL 3 license². For supporting material we recommend studying the release paper of MCFM-9.0 in ref. [\[62\]](#), from which this section is taken.

Improved input file mechanism. We have implemented a new input file mechanism based on the configuration file parser `config_fortran` [\[112\]](#). This INI-like file format no longer depends on a strict ordering of configuration elements, allows easy access to configuration elements through a single global configuration object, and makes it easy to add new configuration options of scalar and array numerical and string types. Using the parser package also allows one to override or specify all configuration options as command line arguments to MCFM, for example running MCFM like `./mcfm_omp input.ini -general%nproc=200 -general%part=nlo`. This is useful for batch parameter run scripts. Settings can also be overridden with additional input files that specify just a subset of options.

²See <https://www.gnu.org/licenses/gpl-3.0.en.html>.

New histogramming. We replaced the previous Fortran77 implementation of histograms, that used routines from 1988 by M. Mangano, with a new suite of routines. The new histogram implementation allows for any number of histograms with any number of bins, each of which is dynamically allocated. Furthermore, everything is also handled in a fully multi-threaded approach with the integration. For each OMP thread temporary histograms are allocated which are then reduced to a single one after each integration iteration, so that no OMP locks (critical regions) are required.

New Vegas integration, part-adaptive and resumable. The previous implementation of the Vegas routine was based on Numerical Recipes code. We have re-implemented Vegas and the surrounding integration routines. All parts of a NLO or NNLO calculation are now chosen adaptively based on the largest absolute numerical uncertainty. A precision goal can be set in the input file as well as a χ^2/it goal and a precision goal for the warmup run. If the goals for the warmup are not reached, the warmup repeats with twice the number of calls. With the setting `writeintermediate` one can control whether histograms are written in intermediate stages during the integration. Enabling the setting `readin` allows one to resume the integration from any point from a previous run. Snapshots saving the whole integration state are saved automatically. When resuming, the only parameter that the user can safely officially change is the `precisiongoal`. Further tweak configuration options to control the stages of the integration have been introduced, which can provide benefits over the default settings in certain situations.

The section `integration` in the configuration file allows for tweaks in the following way. The precision goal can be adjusted by setting `precisiongoal` to a relative precision that should be reached. Similarly, the settings `warmupprecisiongoal` and `warmupchisqgoal` control the minimum relative precision and χ^2/it for the warmup phase of `iterbatchwarmup` (default 5) iterations. If the warmup criterion fails, the number of calls is increased by a factor of two. The calls per iteration get increased by a factor of `callboost` (default 4) after the warmup. From then on the number of calls per iteration is increased by a factor of `itercallmult` (default 1.4) for a total of `iterbatch1` iterations. After these first `iterbatch1` iterations, the increase happens for every `iterbatch2` iterations. The setting `maxcallsperiter` controls the cap for the number of calls per iteration. The number of Vegas grid subdivisions can be controlled with `ndmx` (default 100).

The purpose of these settings is a fine control in certain situations. For example to compute expensive PDF uncertainties, one wants a relatively precise warmup run (where additional PDF sets are not sampled) and as few calls as necessary afterwards: For the plots in this paper we thus chose a relative warmup precision goal of 10%, and set `callboost` to 0.25. This means that the first `iterbatch1` iterations after the warmup run only with a quarter of the calls than during the warmup. This precision is sufficient to compute precise PDF uncertainties, when making use of the strong correlations as in MCFM-9.0. Any further iterations come in batches of `iterbatch2`, which we set to 1. It allows for a quick switching to parts of the NNLO cross section that have the largest uncertainty. For normal applications one wants to boost the number of calls after the warmup significantly, so a default value of `callboost=4` is chosen.

We provide default settings for the initial number of calls per iteration for all components of a NNLO calculation. They can be overridden with the following settings in the `integration` section: `initcallslord`, `initcallsnlovirt`, `initcallsnloreal`, `initcallsnlofrag` for parts

of a NLO calculations, `initcallssnlobelow`, `initcallssnloabove` for parts of a SCET based NLO calculation, and `initcallsnnlobelow`, `initcallsnnlovirtabove`, as well as `initcallsnnlorealabove` for the parts of the NNLO coefficient.

Low discrepancy sequence. MCFM-8.0 and prior relied on a linear congruential generator implementation from Numerical Recipes for the generation of a pseudo-random sequence. With newer versions the MT19937 implementation of the C++ standard library is used, and with this version of MCFM we include an implementation of the Sobol low discrepancy sequence based on the code `sobseq` [113] with initialization numbers from ref. [114]. The Sobol sequence is used by default and can be toggled using the flag `usesobol = .true.` in the `integration` section of the input file, see ref. [62]. When running in MPI mode, the number of nodes has to be a power of two for the Sobol sequence, because we use it in a strided manner. Otherwise the code will automatically fall back to using the MT19937 sequence with seed value `seed` in the integration section of the input file. A `seed` value of 0 denotes a randomly initialized seed.

Fully parallelized OMP+MPI use of LHAPDF. In previous versions of MCFM calls to LHAPDF were forced to access from only a single OMP thread through a lock. This is because the interface was based on the old LHAGLUE interface, part of LHAPDF. We have written an interface to LHAPDF from scratch based on the new object oriented treatment of PDFs in LHAPDF 6. For each OMP thread we initialize a copy of the used PDF members which can be called fully concurrently. The amount of PDF sets with or without PDF uncertainties is only limited by the available system memory. The memory usage of MCFM can then range from roughly 20MB when only one central PDF grid is being used, to ~ 7.4 GB when 32 OMP threads fully load all members of the PDF sets `CT14nnlo`, `MMHT2014nnlo68c1`, `ABMP16als118_5_nnlo`, `NNPDF30_nnlo_as_0118`, `NNPDF31_nnlo_as_0118` and `PDF4LHC15_nnlo_30` for PDF uncertainties. The total number of members for these grids is 371, each loaded for every of the 32 OMP threads.

Since each OMP thread allocates its own copy of PDF members and histograms we have no need to introduce any OMP locks. On the other hand the memory usage increases and one runs into being CPU cache or DRAM bandwidth bound earlier. In practice, we find that this is still faster than having OMP locks, which directly decrease the speedup in the spirit of Amdahl's law. Ideally the LHAPDF library should be improved to allow for thread-safe calls with just one memory allocation.

Histograms for additional values of τ_{cut} , μ_R , μ_F and multiple PDFs. When using the automatic scale variation, in addition to the normal histograms, additional histograms with filenames `_scale_XY_` are generated, where X is a placeholder for the renormalization scale variation and Y for the factorization scale variation. X and Y can either be u for an upwards variation by a factor of two, d for a downwards variation by a factor of two, or just - if no change of that scale was made. The envelope of maximum and minimum can then easily be obtained.

For the sampling of additional values of τ_{cut} for NLO and NNLO calculations using jettiness subtractions, additional histograms with filenames `_taucut_XXX_` are written. Here XXX is a placeholder for the chosen τ_{cut} values in the optional array `taucutarray`, if specified, or one of

the five automatically chosen values. These additional files only contain the *differences* to the nominal choice of τ_{cut} , so that $\Delta\sigma(\tau_{\text{cut,nominal}}) - \Delta\sigma(\tau_{\text{cut,i}})$ is stored. If `taucutarray` has not been specified, the automatic choice of additional τ_{cut} values is enabled based on the default nominal τ_{cut} for the process or the users choice of the nominal τ_{cut} value as specified in `taucut`. In addition a file with `_taucutfit_` is generated, which in addition to the fitted corrections and its uncertainty includes columns for the maximum relative integration uncertainty for the additionally sampled τ_{cut} values and the reduced χ^2 of the fit. The fit, together with the individual τ_{cut} histograms, allows the user to assess the systematic τ_{cut} error and possibly improve results.

When multiple PDF sets are chosen, additional files with the names of the PDF sets are generated. In case PDF uncertainties are enabled, the histograms also include the upper and lower bounds of the PDF uncertainties.

User cuts, histograms and re-weighting. Modifying the plotting routines in the files `src/User/nplotter*.f` allows for modification of the pre-defined histograms and addition of any number of arbitrary observables. The routine `gencuts_user` can be adjusted in the file `src/User/gencuts_user.f90` for additional cuts after the jet algorithm has performed the clustering. In the same file the routine `reweight_user` can be modified to include a manual re-weighting for all integral contributions. This can be used to obtain improved uncertainties in, for example, tails of distributions. One example is included in the subdirectory `examples`, where the `reweight_user` function approximately flattens the Higgs transverse momentum distribution, leading to equal relative uncertainties even in the tail at 1TeV.

Compatibility with the Intel compiler and benchmarks Previous versions of MCFM were developed using `gfortran` as a compiler. MCFM contained code that did not follow a specific Fortran standard, and was only compatible with using `gfortran`. We fixed code that did not compile or work with the recent Intel Fortran compiler `ifort` 19.0.1. This does not mean that we claim to be strictly standards compliant with a specific Fortran version, but we aim to be compliant with Fortran 2008. We now fully support GCC versions newer than 7 and Intel compilers newer than 19. There might still be compatibility issues with other Fortran compilers, but we are happy to receive bug reports for any issues regarding compilation, that are not due to a lack of modern Fortran 2008 features. To use the Intel compiler one has to change the `USEINTEL` flag in the files `Install` and `makefile` to `YES`.

To see whether MCFM can make use of potential Intel compiler improvements over the GNU compiler collection (GCC) we benchmarked the double real emission component of Higgs production at NNLO. We perform tests on our cluster with Intel Xeon 64-bit X5650 2.67 GHz Westmere CPUs, where two six-core CPUs are run in a dual-socket mode with a total of twelve cores. Similarly, we have an AMD 6128 HE Opteron 2GHz quad-socket eight-core setup, thus each having 32 cores per node.

We benchmark both the Intel and GCC compilers on both the Intel and AMD systems. On the Intel system we use 16 MPI processes each with 12 OMP threads, and on the AMD system we have 8 MPI processes using 32 OMP threads. With this we have the same total clockrate of 512GHz for each setup. For all benchmarks we find that the scaling is perfect up to this size, that is if we use half the number of MPI or OMP threads we double our run-time.

Table 39: Benchmark results on the Intel system with $10 \cdot 25\text{M}$ calls distributed over 16 MPI processes, each using 12 OMP threads. The GCC version is 9.1.0 and the Intel Fortran compiler 19.0.1

Compiler/flags	wall time $\pm 0.5\text{s}$
ifort -O3 -xsse4.2	90s
ifort -O2 -xsse4.2	86s
ifort -O2	90s
ifort -O1	103s
gfortran -O3 -march=westmere	101s
gfortran -O2 -march=westmere	105s
gfortran -O2	105s
gfortran -O1	110s

We first try both the Intel fortran compiler 19.0.1 and GCC 9.1.0 on the Intel system with the highest generic optimization flags `-O3 -xsse4.2` and `-O3 -march=westmere`, respectively. Furthermore, we lower the optimizations to `-O2` each and remove the processor specific optimization flags `-xsse4.2` and `-march=westmere`, respectively. All our benchmark run-times in the following are consistent within ± 0.5 seconds.

We do not support enabling unsafe math operations with `-ffast-math`, since the code relies on the knowledge of NaN values and checks on those. Such checks would be skipped with the meta flag `-ffast-math` which sets `-ffinite-math-only`.

The benchmark results in 39 show that using the Intel compiler, performance benefits of $\simeq 10 - 20\%$ can be achieved. Our goal here is not to go beyond this and check whether exactly equivalent optimization flags have been used in both cases. Enabling optimizations beyond `-O2` have little impact, but come with a penalty for the Intel compiler and with a slight benefit for gfortran. We also notice that processor specific optimizations play no significant role. This might also be in part due to the fact that MCFM does not offer much space for (automatic) vectorization optimizations. To summarize, the default optimization flags of `-O2` should be sufficient in most cases. We do not expect that the conclusions from these benchmarks change for different processes. On the other hand if computing PDF uncertainties, the majority of time is used by LHAPDF and different optimization flags for LHAPDF might play a role then. We performed the same benchmark with an older version of GCC, version 7.1.0 using `-O2` optimizations, and found that the run-times are the same as for the newer version.

Finally, we performed some benchmarks on our AMD setup and found that it is $\simeq 2.5$ times slower for the same total clockrate. Using the Intel compiler for the AMD setup decreased the performance by another $\simeq 30\%$. This is likely due to the fact that the Intel compiler already optimizes for the general Intel architecture.

These benchmarks try to give a general impression and might depend in detail on the process, the number of histograms and whether to compute PDF uncertainties, for example. Especially when computing PDF uncertainties the perfect scaling we tested here might break down since the computation can become memory bound. We discuss this caveat in more detail in 15.2.

Remarks on memory bound performance issues To get numerically precise predictions at the per mille level for NNLO cross sections, already hundreds of million of calls are necessary. Obtaining PDF uncertainties using those NNLO matrix elements significantly increases the computational time. In a simplified view, the total computational time composes as $N_{\text{calls}} \cdot (T + N_{PDF} \cdot T_{PDF})$, where T is the computational effort for the matrix element piece, and the PDF part is proportional to the time calling the PDF evolution N_{PDF} times and code related to performing the convolutions. For tree level matrix element evaluations, usually also $T \ll T_{PDF}$ holds, so the computational cost grows linearly with the number of PDFs.

This naive picture breaks down in practice when a lot of PDFs are sampled together with a lot of histograms or histogram bins. The total memory necessary to store all the histogram information grows like $N_{PDF} \cdot N_{\text{bins}} \cdot N_{\text{thr.}}$, where N_{PDF} is the number of PDF members, N_{bins} the number of histogram bins summed over all histograms and $N_{\text{thr.}}$ is the number of OMP threads. The factor $N_{\text{thr.}}$ enters since we have thread-local storage to avoid OMP locks. The values are stored in double precision, so the total memory used is $N_{PDF} \cdot N_{\text{bins}} \cdot N_{\text{thr.}} \cdot 8$ bytes.

Assuming for example, 300 PDF members, 10 histograms with each 20 bins and 12 threads, this sums up to 720kb of memory. For the virtual corrections and LO pieces, one has to update this amount of memory once for each call. For the real emission matrix elements one has to accumulate all dipole contributions, so this number additionally scales with the number of dipole contributions. All the histogram updates are usually fully vectorized for modern superscalar processors with SSE and/or AVX extensions. But if this used memory is too large and does not easily fit into the CPU core caches anymore, a transfer to and from DRAM happens, which now is the limiting factor and significantly slows down the computation. Because for that reason, one should work with a minimal number of necessary histograms when working with a lot of PDF members. This is especially important for cluster setups that are not optimized towards memory bound applications, non-NUMA systems. For example in our cluster we have relatively old AMD Opteron quad-socket eight-core nodes with little CPU cache, and with above numbers we are already limited in wall-time improvements with using ~ 16 cores. Then reducing the number of histograms will *significantly* improve the performance. In principle one can reduce the histogram precision to single precision and cut memory transfer and storage in half, while doubling the computational speed. This might lead to problems with accumulated rounding errors though, and we have not investigated this further, since in practice one can sufficiently limit the number of histograms or PDF sets.

16 Versions prior to MCFM-9

16.1 MCFM-8

- [MCFM-8.3.tar.gz](#) (released April 4th, 2019), v8.3 manual (PDF)
 - New processes for off-shell SM and SMEFT single-top-quark production
- [MCFM-8.2.tar.gz](#) (released February 8th, 2018)
 - Implementation of high-pt treatment of mass effects in H+jet process.
- [MCFM-8.1.tar.gz](#) (released December 19th, 2017)
 - Electroweak one-loop corrections for Z, top-pair and di-jet production.

- Z+photon process at NNLO including anomalous couplings.
- H+2 jet process with a finite top-quark mass (LO) and H+jet with finite top-quark mass effects (NLO)
- Support for boosted (as opposed to hadronic) definition of jettiness, which is now also used as default.
- Support for pt and rapidity ranges for most cuts in the input file.
- Native implementation of two PDF sets containing photons: mrstqed and CT14qed.
- [MCFM-8.0.tar.gz](#) (released May 25th, 2016; updated June 2nd to fix MMHT implementation)
 - Introduced NNLO capability for color-singlet processes.
 - Overall improvement in speed.

16.2 MCFM-7

- [MCFM-7.0.1.tar.gz](#) (released October 29th, 2015)
 - Fixed error in real calculation for some versions of gcc 4.x.
 - Updated output to support ROOT6.
- [MCFM-7.0.tar.gz](#) (released March 21st, 2015; updated June 11 for gfortran 4.9)
 - Code compiles with the OpenMP flag to automatically exploit all available threads.
 - Added four-photon process at NLO.
 - Inclusion of vector boson fusion/vector boson scattering processes at LO.
 - After Higgs discovery, added s-channel Higgs diagrams to the $gg \rightarrow VV$ processes.

16.3 MCFM-6

- [MCFM-6.8.tar.gz](#)
 - Added process for diphoton+jet production at NLO.
 - Added identical-particle interference effects for 4-lepton production and effect of WW/ZZ interference for 2-lepton, 2-neutrino production.
 - Added additional decay modes for WW and ZZ processes.
 - Fixed bug in triphoton process at NLO.
- [MCFM-6.7.tar.gz](#) (December 6th, 2013)
 - New implementation of $gg \rightarrow ZZ$ box contribution including massive loops.
 - Added processes for triphoton production at NLO, 1-loop Higgs pair production.
 - Fixed errors reported in native histograms and improved PDF uncertainty output.

- [MCFM-6.6.tar.gz](#) (April 1st, 2013)
 - Implementation of single top tH and tZ processes.
 - Implementation of dark matter mono-jet and mono-photon processes.
 - Inclusion of TensorReduction library for one-loop integrals.
- [MCFM-6.5.tar.gz](#) (March 5th, 2013)
- [mcfm-6.4.tar.gz](#) (December 22nd, 2012)
 - Corrected bug in implementation of one-loop amplitudes for H+2q+2g processes.
 - Enabled effect of removebr for process 307.
 - Fixed the implementation of a dynamic scale for single top + b processes.
 - Added a new scale choice for top production $(m_{345}^2 + p_T(345)^2)$.
 - Improved numerical stability in calculation of virtual contribution to process 201 and in calculation of real corrections to processes 180-187.
- [mcfm-6.3.tar.gz](#) (August 10th, 2012)
 - Added processes giving the radiation in the hadronic decay of the W+W- process.
 - Added processes giving the gg to H to WW process with radiation in the hadronic decay of the W.
 - Added processes giving the production and decay of t tbar W+/- including radiation in the semi-leptonic decay of the top and the anti-top.
 - Added processes giving the $H \rightarrow Z\gamma$ in the gluon fusion production process.
 - Added processes describing production of $Z + \gamma + \gamma$ and $Z + \gamma + \text{jet}$ at NLO.
- [mcfm-6.2.tar.gz](#) (April 10th, 2012)
 - Added processes that give results for the t-channel single top process in the four-flavour scheme with top decay;
 - Added process for Higgs + 2 jets, with Higgs decaying to $\gamma\gamma$;
 - Added processes for Wb production from charm quarks;
 - Added LO processes for Higgs + 3 jets with Higgs decaying to WW or ZZ;
 - Added LO process for identical fermions in ZZ decay;
 - corrected small bugs.
- [mcfm-6.1.tar.gz](#) (October 19th, 2011)
 - inclusion of massive (t,b) loops in $gg \rightarrow WW$ diagrams;
 - new process for computing effect of interference with Higgs diagrams for $gg \rightarrow WW$;
 - inclusion of direct photon production including fragmentation;
 - anomalous couplings for $W\gamma$ and $Z\gamma$ production;

- improved interface and output, corrected small bugs.
- [mcfm-6.0.tar.gz](#) (May 2nd, 2011)
 - NLO results for Wbb production including heavy quark mass effects;
 - inclusion of $W\gamma$, $Z\gamma$ and $\gamma\gamma$ processes with fragmentation;
 - gluon-initiated contributions to diboson processes;
 - small correction to Z+2 jet process and other bug fixes.

16.4 MCFM-5 and before

- [mcfm-5.8.tar.gz](#) (April 9th, 2010)
- [mcfm-5.7.tar.gz](#) (January 22nd, 2010)
- [mcfm-5.6.tar.gz](#) (July 31st, 2009)
- [mcfm-5.5.tar.gz](#) (June 5th, 2009)
- [mcfm-5.4.tar.gz](#) (March 12th, 2009)
- [mcfm-5.3.tar.gz](#) (October 21st, 2008)
- [mcfm-5.2.tar.gz](#) (July 12th, 2007)
- [mcfm-5.1.tar.gz](#) (June 1st, 2006)
- [mcfm-5.0.tar.gz](#) (April 25th, 2006)
- [mcfm-4.1.tar.gz](#) (January 17th, 2005)
- [mcfm-4.0.tar.gz](#) (October 15th, 2004)
 - Major revision of the code, which now includes single top processes.
- [mcfm-3.4.5.tar.gz](#) (December 23rd, 2003)
 - Minor update, addition of LO WW production with no polarization info, process 64.
- [mcfm-3.4.4.tar.gz](#) (September 3rd, 2003)
 - Minor update, mostly cosmetic changes.
- [mcfm-3.4.3.tar.gz](#) (July 2nd, 2003)
 - Bug fixes for input files using the 'tota' option at NLO.
- [mcfm-3.4.2.tar.gz](#) (June 6th, 2003)
 - Further minor improvements over version 3.4.1.
- [mcfm-3.4.1.tar.gz](#) (May 29th, 2003)
 - Minor improvements over version 3.4.
- [mcfm-3.4.tar.gz](#) (April 24th, 2003)

- Version 3.4 contains a number of new Higgs production processes at next-to-leading order.
- [mcfm-3.2.tar.gz](#) (October 1st, 2002)
- [mcfm-2.1.tar.gz](#) (December 14th, 2001)
 - An old version, preserved for historical value only.
- [mcfm-1.0.tar.gz](#)
 - An old version, preserved for historical value only.

References

- [1] G. Passarino and M.J.G. Veltman. “One Loop Corrections for $e^+ e^-$ Annihilation Into $\mu^+ \mu^-$ in the Weinberg Model”. *Nucl.Phys.* B160 (1979), p. 151. DOI: [10.1016/0550-3213\(79\)90234-7](#).
- [2] G.J. van Oldenborgh and J.A.M. Vermaseren. “New Algorithms for One Loop Integrals”. *Z.Phys.* C46 (1990), pp. 425–438. DOI: [10.1007/BF01621031](#).
- [3] Stefano Carrazza, R. Keith Ellis, and Giulia Zanderighi. “QCDLoop: a comprehensive framework for one-loop scalar integrals”. *Comput. Phys. Commun.* 209 (2016), pp. 134–143. DOI: [10.1016/j.cpc.2016.07.033](#). arXiv: [1605.03181 \[hep-ph\]](#).
- [4] R. Keith Ellis and Giulia Zanderighi. “Scalar one-loop integrals for QCD”. *JHEP* 02 (2008), p. 002. DOI: [10.1088/1126-6708/2008/02/002](#). arXiv: [0712.1851 \[hep-ph\]](#).
- [5] A. van Hameren. “OneLOop: For the evaluation of one-loop scalar functions”. *Comput. Phys. Commun.* 182 (2011), pp. 2427–2438. DOI: [10.1016/j.cpc.2011.06.011](#). arXiv: [1007.4716 \[hep-ph\]](#).
- [6] Yozo Hida, Xiaoye S. Li, and David H. Bailey. *Quad Double computation package*. <https://crd.lbl.gov/~dhbailey/mpdist/>. 2003–2018.
- [7] Thomas Gehrmann, Andreas von Manteuffel, and Lorenzo Tancredi. “The two-loop helicity amplitudes for $q\bar{q}' \rightarrow V_1 V_2 \rightarrow 4$ leptons”. *JHEP* 09 (2015), p. 128. DOI: [10.1007/JHEP09\(2015\)128](#). arXiv: [1503.04812 \[hep-ph\]](#).
- [8] L. Naterop, A. Signer, and Y. Ulrich. “handyG —Rapid numerical evaluation of generalised polylogarithms in Fortran”. *Comput. Phys. Commun.* 253 (2020), p. 107165. DOI: [10.1016/j.cpc.2020.107165](#). arXiv: [1909.01656 \[hep-ph\]](#).
- [9] Tobias Neumann and John Campbell. “Fiducial Drell-Yan production at the LHC improved by transverse-momentum resummation at $N^4\text{LL}+N^3\text{LO}$ ” (July 2022). arXiv: [2207.07056 \[hep-ph\]](#).
- [10] John M. Campbell et al. “Jet-veto resummation at $N^3\text{LL}_p+\text{NNLO}$ in boson production processes”. *in preparation* (2023). In preparation.
- [11] Radja Boughezal et al. “Color singlet production at NNLO in MCFM”. *Eur. Phys. J. C* 77.1 (2017), p. 7. DOI: [10.1140/epjc/s10052-016-4558-y](#). arXiv: [1605.08011 \[hep-ph\]](#).

- [12] John M. Campbell et al. “The $pp \rightarrow W(\rightarrow l\nu) + \gamma$ process at next-to-next-to-leading order”. *JHEP* 07 (2021), p. 079. DOI: [10.1007/JHEP07\(2021\)079](https://doi.org/10.1007/JHEP07(2021)079). arXiv: [2105.00954](https://arxiv.org/abs/2105.00954) [[hep-ph](#)].
- [13] Simon Badger, John M. Campbell, and R. K. Ellis. “QCD corrections to the hadronic production of a heavy quark pair and a W-boson including decay correlations”. *JHEP* 03 (2011), p. 027. DOI: [10.1007/JHEP03\(2011\)027](https://doi.org/10.1007/JHEP03(2011)027). arXiv: [1011.6647](https://arxiv.org/abs/1011.6647) [[hep-ph](#)].
- [14] R. Keith Ellis and Sinisa Veseli. “Strong radiative corrections to W b anti-b production in p anti-p collisions”. *Phys. Rev. D* 60 (1999), p. 011501. DOI: [10.1103/PhysRevD.60.011501](https://doi.org/10.1103/PhysRevD.60.011501). arXiv: [hep-ph/9810489](https://arxiv.org/abs/hep-ph/9810489).
- [15] John M. Campbell and R. Keith Ellis. “Next-to-Leading Order Corrections to $W^+ 2$ jet and $Z^+ 2$ Jet Production at Hadron Colliders”. *Phys. Rev. D* 65 (2002), p. 113007. DOI: [10.1103/PhysRevD.65.113007](https://doi.org/10.1103/PhysRevD.65.113007). arXiv: [hep-ph/0202176](https://arxiv.org/abs/hep-ph/0202176).
- [16] John M. Campbell, R. Keith Ellis, and David L. Rainwater. “Next-to-leading order QCD predictions for $W + 2$ jet and $Z + 2$ jet production at the CERN LHC”. *Phys. Rev. D* 68 (2003), p. 094021. DOI: [10.1103/PhysRevD.68.094021](https://doi.org/10.1103/PhysRevD.68.094021). arXiv: [hep-ph/0308195](https://arxiv.org/abs/hep-ph/0308195).
- [17] Zvi Bern, Lance J. Dixon, and David A. Kosower. “One loop amplitudes for $e^+ e^-$ to four partons”. *Nucl. Phys. B* 513 (1998), pp. 3–86. DOI: [10.1016/S0550-3213\(97\)00703-7](https://doi.org/10.1016/S0550-3213(97)00703-7). arXiv: [hep-ph/9708239](https://arxiv.org/abs/hep-ph/9708239) [[hep-ph](#)].
- [18] John M. Campbell and R. Keith Ellis. “Radiative corrections to Z b anti-b production”. *Phys. Rev. D* 62 (2000), p. 114012. DOI: [10.1103/PhysRevD.62.114012](https://doi.org/10.1103/PhysRevD.62.114012). arXiv: [hep-ph/0006304](https://arxiv.org/abs/hep-ph/0006304).
- [19] John M. Campbell and R. Keith Ellis. “An Update on vector boson pair production at hadron colliders”. *Phys. Rev. D* 60 (1999), p. 113006. DOI: [10.1103/PhysRevD.60.113006](https://doi.org/10.1103/PhysRevD.60.113006). arXiv: [hep-ph/9905386](https://arxiv.org/abs/hep-ph/9905386).
- [20] John M. Campbell, R. Keith Ellis, and Ciaran Williams. “Vector boson pair production at the LHC”. *JHEP* 07 (2011), p. 018. DOI: [10.1007/JHEP07\(2011\)018](https://doi.org/10.1007/JHEP07(2011)018). arXiv: [1105.0020](https://arxiv.org/abs/1105.0020) [[hep-ph](#)].
- [21] John M. Campbell, R. Keith Ellis, and Satyajit Seth. “Non-local slicing approaches for NNLO QCD in MCFM” (Feb. 2022). arXiv: [2202.07738](https://arxiv.org/abs/2202.07738) [[hep-ph](#)].
- [22] John M. Campbell, R. Keith Ellis, and Ciaran Williams. “Associated production of a Higgs boson at NNLO”. *JHEP* 06 (2016), p. 179. DOI: [10.1007/JHEP06\(2016\)179](https://doi.org/10.1007/JHEP06(2016)179). arXiv: [1601.00658](https://arxiv.org/abs/1601.00658) [[hep-ph](#)].
- [23] John M. Campbell, R. Keith Ellis, and Ciaran Williams. “Gluon-Gluon Contributions to $W^+ W^-$ Production and Higgs Interference Effects”. *JHEP* 10 (2011), p. 005. DOI: [10.1007/JHEP10\(2011\)005](https://doi.org/10.1007/JHEP10(2011)005). arXiv: [1107.5569](https://arxiv.org/abs/1107.5569) [[hep-ph](#)].
- [24] John M. Campbell, R. Keith Ellis, and Ciaran Williams. “Bounding the Higgs Width at the LHC: Complementary Results from $H \rightarrow WW$ ”. *Phys. Rev. D* 89.5 (2014), p. 053011. DOI: [10.1103/PhysRevD.89.053011](https://doi.org/10.1103/PhysRevD.89.053011). arXiv: [1312.1628](https://arxiv.org/abs/1312.1628) [[hep-ph](#)].
- [25] John M. Campbell, R. Keith Ellis, and Ciaran Williams. “Bounding the Higgs Width at the LHC Using Full Analytic Results for $gg \rightarrow e^- e^+ \mu^- \mu^+$ ”. *JHEP* 04 (2014), p. 060. DOI: [10.1007/JHEP04\(2014\)060](https://doi.org/10.1007/JHEP04(2014)060). arXiv: [1311.3589](https://arxiv.org/abs/1311.3589) [[hep-ph](#)].

- [26] John M. Campbell et al. “Interference effects for Higgs boson mediated Z -pair plus jet production”. *Phys. Rev. D* 90.9 (2014), p. 093008. DOI: [10.1103/PhysRevD.90.093008](https://doi.org/10.1103/PhysRevD.90.093008). arXiv: [1409.1897 \[hep-ph\]](https://arxiv.org/abs/1409.1897).
- [27] John M. Campbell et al. “Higgs-Boson Production in Association with a Single Bottom Quark”. *Phys. Rev. D* 67 (2003), p. 095002. DOI: [10.1103/PhysRevD.67.095002](https://doi.org/10.1103/PhysRevD.67.095002). arXiv: [hep-ph/0204093](https://arxiv.org/abs/hep-ph/0204093).
- [28] John M. Campbell and R. Keith Ellis. “Top-Quark Processes at NLO in Production and Decay”. *J. Phys.* G42.1 (2015), p. 015005. DOI: [10.1088/0954-3899/42/1/015005](https://doi.org/10.1088/0954-3899/42/1/015005). arXiv: [1204.1513 \[hep-ph\]](https://arxiv.org/abs/1204.1513).
- [29] Simon Badger, Ralf Sattler, and Valery Yundin. “One-Loop Helicity Amplitudes for $t\bar{t}$ Production at Hadron Colliders”. *Phys. Rev. D* 83 (2011), p. 074020. DOI: [10.1103/PhysRevD.83.074020](https://doi.org/10.1103/PhysRevD.83.074020). arXiv: [1101.5947 \[hep-ph\]](https://arxiv.org/abs/1101.5947).
- [30] P. Nason, S. Dawson, and R. Keith Ellis. “The Total Cross-Section for the Production of Heavy Quarks in Hadronic Collisions”. *Nucl. Phys.* B303 (1988), pp. 607–633. DOI: [10.1016/0550-3213\(88\)90422-1](https://doi.org/10.1016/0550-3213(88)90422-1).
- [31] John M. Campbell, R. Keith Ellis, and Francesco Tramontano. “Single top production and decay at next-to-leading order”. *Phys. Rev. D* 70 (2004), p. 094012. DOI: [10.1103/PhysRevD.70.094012](https://doi.org/10.1103/PhysRevD.70.094012). arXiv: [hep-ph/0408158](https://arxiv.org/abs/hep-ph/0408158).
- [32] John M. Campbell et al. “Next-to-Leading-Order Predictions for t-Channel Single-Top Production at Hadron Colliders”. *Phys. Rev. Lett.* 102 (2009), p. 182003. DOI: [10.1103/PhysRevLett.102.182003](https://doi.org/10.1103/PhysRevLett.102.182003). arXiv: [0903.0005 \[hep-ph\]](https://arxiv.org/abs/0903.0005).
- [33] Tobias Neumann and Zack Edward Sullivan. “Off-Shell Single-Top-Quark Production in the Standard Model Effective Field Theory”. *JHEP* 06 (2019), p. 022. DOI: [10.1007/JHEP06\(2019\)022](https://doi.org/10.1007/JHEP06(2019)022). arXiv: [1903.11023 \[hep-ph\]](https://arxiv.org/abs/1903.11023).
- [34] John M. Campbell and Francesco Tramontano. “Next-to-leading order corrections to Wt production and decay”. *Nucl. Phys. B* 726 (2005), pp. 109–130. DOI: [10.1016/j.nuclphysb.2005.08.015](https://doi.org/10.1016/j.nuclphysb.2005.08.015). arXiv: [hep-ph/0506289](https://arxiv.org/abs/hep-ph/0506289).
- [35] John M. Campbell, Doreen Wackeroth, and Jia Zhou. “Study of weak corrections to Drell-Yan, top-quark pair, and dijet production at high energies with MCFM”. *Phys. Rev. D* 94.9 (2016), p. 093009. DOI: [10.1103/PhysRevD.94.093009](https://doi.org/10.1103/PhysRevD.94.093009). arXiv: [1608.03356 \[hep-ph\]](https://arxiv.org/abs/1608.03356).
- [36] Edmond L. Berger and John M. Campbell. “Higgs boson production in weak boson fusion at next-to-leading order”. *Phys. Rev. D* 70 (2004), p. 073011. DOI: [10.1103/PhysRevD.70.073011](https://doi.org/10.1103/PhysRevD.70.073011). arXiv: [hep-ph/0403194](https://arxiv.org/abs/hep-ph/0403194).
- [37] John M. Campbell and R. Keith Ellis. “Higgs Constraints from Vector Boson Fusion and Scattering”. *JHEP* 04 (2015), p. 030. DOI: [10.1007/JHEP04\(2015\)030](https://doi.org/10.1007/JHEP04(2015)030). arXiv: [1502.02990 \[hep-ph\]](https://arxiv.org/abs/1502.02990).
- [38] John M. Campbell et al. “NLO predictions for t-channel production of single top and fourth generation quarks at hadron colliders”. *JHEP* 10 (2009), p. 042. DOI: [10.1088/1126-6708/2009/10/042](https://doi.org/10.1088/1126-6708/2009/10/042). arXiv: [0907.3933 \[hep-ph\]](https://arxiv.org/abs/0907.3933).
- [39] Tom Melia et al. “Next-to-leading order QCD predictions for W^+W^+jj production at the LHC”. *JHEP* 12 (2010), p. 053. DOI: [10.1007/JHEP12\(2010\)053](https://doi.org/10.1007/JHEP12(2010)053). arXiv: [1007.5313 \[hep-ph\]](https://arxiv.org/abs/1007.5313).

- [40] R. Keith Ellis and Satyajit Seth. “On Higgs boson plus gluon amplitudes at one loop”. *JHEP* 11 (2018), p. 006. DOI: [10.1007/JHEP11\(2018\)006](https://doi.org/10.1007/JHEP11(2018)006). arXiv: [1808.09292](https://arxiv.org/abs/1808.09292) [[hep-ph](#)].
- [41] Lucy Budge et al. “The one-loop amplitudes for Higgs + 4 partons with full mass effects”. *JHEP* 05 (2020), p. 079. DOI: [10.1007/JHEP05\(2020\)079](https://doi.org/10.1007/JHEP05(2020)079). arXiv: [2002.04018](https://arxiv.org/abs/2002.04018) [[hep-ph](#)].
- [42] John M. Campbell, R. Keith Ellis, and Giulia Zanderighi. “Next-to-Leading order Higgs + 2 jet production via gluon fusion”. *JHEP* 10 (2006), p. 028. DOI: [10.1088/1126-6708/2006/10/028](https://doi.org/10.1088/1126-6708/2006/10/028). arXiv: [hep-ph/0608194](https://arxiv.org/abs/hep-ph/0608194).
- [43] John M. Campbell et al. “Predictions for diphoton production at the LHC through NNLO in QCD”. *JHEP* 07 (2016), p. 148. DOI: [10.1007/JHEP07\(2016\)148](https://doi.org/10.1007/JHEP07(2016)148). arXiv: [1603.02663](https://arxiv.org/abs/1603.02663) [[hep-ph](#)].
- [44] John M. Campbell, David J. Miller, and Tania Robens. “Next-to-Leading Order Predictions for WW+Jet Production”. *Phys. Rev. D* 92.1 (2015), p. 014033. DOI: [10.1103/PhysRevD.92.014033](https://doi.org/10.1103/PhysRevD.92.014033). arXiv: [1506.04801](https://arxiv.org/abs/1506.04801) [[hep-ph](#)].
- [45] John Campbell, David Miller, and Tania Robens. “WW + jet at 14 and 100 TeV”. *PoS ICHEP2016* (2016), p. 686. DOI: [10.22323/1.282.0686](https://doi.org/10.22323/1.282.0686). arXiv: [1611.01700](https://arxiv.org/abs/1611.01700) [[hep-ph](#)].
- [46] John M. Campbell, Giuseppe De Laurentis, and R. Keith Ellis. “Vector boson pair production at one loop: analytic results for the process $q\bar{q}\ell\bar{\ell}'\ell'g$ ”. *JHEP* 07 (2022), p. 096. DOI: [10.1007/JHEP07\(2022\)096](https://doi.org/10.1007/JHEP07(2022)096). arXiv: [2203.17170](https://arxiv.org/abs/2203.17170) [[hep-ph](#)].
- [47] John M. Campbell and R. Keith Ellis. “ $t\bar{t}W^{+-}$ production and decay at NLO”. *JHEP* 07 (2012), p. 052. DOI: [10.1007/JHEP07\(2012\)052](https://doi.org/10.1007/JHEP07(2012)052). arXiv: [1204.5678](https://arxiv.org/abs/1204.5678) [[hep-ph](#)].
- [48] John Campbell, R. Keith Ellis, and Raoul Röntsch. “Single top production in association with a Z boson at the LHC”. *Phys. Rev. D* 87 (2013), p. 114006. DOI: [10.1103/PhysRevD.87.114006](https://doi.org/10.1103/PhysRevD.87.114006). arXiv: [1302.3856](https://arxiv.org/abs/1302.3856) [[hep-ph](#)].
- [49] E. W. Nigel Glover and J. J. van der Bij. “Higgs boson pair production via gluon fusion”. *Nucl. Phys.* B309 (1988), pp. 282–294. DOI: [10.1016/0550-3213\(88\)90083-1](https://doi.org/10.1016/0550-3213(88)90083-1).
- [50] Claude Amsler et al. “Review of Particle Physics”. *Phys. Lett.* B667 (2008), pp. 1–1340. DOI: [10.1016/j.physletb.2008.07.018](https://doi.org/10.1016/j.physletb.2008.07.018).
- [51] Howard Georgi. “Effective field theory and electroweak radiative corrections”. *Nucl. Phys.* B363 (1991), pp. 301–325. DOI: [10.1016/0550-3213\(91\)80022-E](https://doi.org/10.1016/0550-3213(91)80022-E).
- [52] Fabio Maltoni and Tim Stelzer. “MadEvent: Automatic event generation with MadGraph”. *JHEP* 02 (2003), p. 027. DOI: [10.1088/1126-6708/2003/02/027](https://doi.org/10.1088/1126-6708/2003/02/027). arXiv: [hep-ph/0208156](https://arxiv.org/abs/hep-ph/0208156) [[hep-ph](#)].
- [53] Michelangelo L. Mangano et al. “AlpGen” (). URL: <http://mlm.home.cern.ch/mlm/alpgen/>.
- [54] Stefan Dittmaier and Markus Roth. “Lusifer” (). URL: <http://wwwth.mppmu.mpg.de/members/roth/Lusifer/lusifer.html>.
- [55] Stefano Frixione. “Isolated photons in perturbative QCD”. *Phys. Lett.* B429 (1998), pp. 369–374. DOI: [10.1016/S0370-2693\(98\)00454-7](https://doi.org/10.1016/S0370-2693(98)00454-7). arXiv: [hep-ph/9801442](https://arxiv.org/abs/hep-ph/9801442) [[hep-ph](#)].

- [56] Thomas Gehrmann, Thomas Luebbert, and Li Lin Yang. “Calculation of the transverse parton distribution functions at next-to-next-to-leading order”. *JHEP* 06 (2014), p. 155. DOI: [10.1007/JHEP06\(2014\)155](https://doi.org/10.1007/JHEP06(2014)155). arXiv: [1403.6451](https://arxiv.org/abs/1403.6451) [hep-ph].
- [57] Georgios Billis et al. “A toolbox for q_T and 0-jettiness subtractions at N^3 LO”. *Eur. Phys. J. Plus* 136.2 (2021), p. 214. DOI: [10.1140/epjp/s13360-021-01155-y](https://doi.org/10.1140/epjp/s13360-021-01155-y). arXiv: [1909.00811](https://arxiv.org/abs/1909.00811) [hep-ph].
- [58] Thomas Becher, Matthias Neubert, and Lorena Rothen. “Factorization and N^3LL_p +NNLO predictions for the Higgs cross section with a jet veto”. *JHEP* 10 (2013), p. 125. DOI: [10.1007/JHEP10\(2013\)125](https://doi.org/10.1007/JHEP10(2013)125). arXiv: [1307.0025](https://arxiv.org/abs/1307.0025) [hep-ph].
- [59] Matteo Cacciari, Gavin P. Salam, and Gregory Soyez. “The anti- k_t jet clustering algorithm”. *JHEP* 04 (2008), p. 063. DOI: [10.1088/1126-6708/2008/04/063](https://doi.org/10.1088/1126-6708/2008/04/063). arXiv: [0802.1189](https://arxiv.org/abs/0802.1189) [hep-ph].
- [60] L. Bourhis, M. Fontannaz, and J. P. Guillet. “Quarks and gluon fragmentation functions into photons”. *Eur. Phys. J. C* 2 (1998), pp. 529–537. DOI: [10.1007/s100520050158](https://doi.org/10.1007/s100520050158). arXiv: [hep-ph/9704447](https://arxiv.org/abs/hep-ph/9704447) [hep-ph].
- [61] A. Gehrmann-De Ridder and E. W. Nigel Glover. “Final state photon production at LEP”. *Eur. Phys. J. C* 7 (1999), pp. 29–48. DOI: [10.1007/s100520050382](https://doi.org/10.1007/s100520050382), [10.1007/s100529800958](https://doi.org/10.1007/s100529800958). arXiv: [hep-ph/9806316](https://arxiv.org/abs/hep-ph/9806316) [hep-ph].
- [62] John Campbell and Tobias Neumann. “Precision Phenomenology with MCFM”. *JHEP* 12 (2019), p. 034. DOI: [10.1007/JHEP12\(2019\)034](https://doi.org/10.1007/JHEP12(2019)034). arXiv: [1909.09117](https://arxiv.org/abs/1909.09117) [hep-ph].
- [63] Zoltan Nagy. “Next-to-leading order calculation of three jet observables in hadron hadron collision”. *Phys. Rev. D* 68 (2003), p. 094002. DOI: [10.1103/PhysRevD.68.094002](https://doi.org/10.1103/PhysRevD.68.094002). arXiv: [hep-ph/0307268](https://arxiv.org/abs/hep-ph/0307268) [hep-ph].
- [64] Gavin P. Salam. “Towards Jetography”. *Eur. Phys. J. C* 67 (2010), pp. 637–686. DOI: [10.1140/epjc/s10052-010-1314-6](https://doi.org/10.1140/epjc/s10052-010-1314-6). arXiv: [0906.1833](https://arxiv.org/abs/0906.1833) [hep-ph].
- [65] Yuri L. Dokshitzer et al. “Better jet clustering algorithms”. *JHEP* 08 (1997), p. 001. DOI: [10.1088/1126-6708/1997/08/001](https://doi.org/10.1088/1126-6708/1997/08/001). arXiv: [hep-ph/9707323](https://arxiv.org/abs/hep-ph/9707323).
- [66] M. Wobisch and T. Wengler. “Hadronization corrections to jet cross-sections in deep inelastic scattering”. *Workshop on Monte Carlo Generators for HERA Physics (Plenary Starting Meeting)*. Apr. 1998, pp. 270–279. arXiv: [hep-ph/9907280](https://arxiv.org/abs/hep-ph/9907280).
- [67] S. Catani et al. “Longitudinally invariant K_t clustering algorithms for hadron hadron collisions”. *Nucl. Phys. B* 406 (1993), pp. 187–224. DOI: [10.1016/0550-3213\(93\)90166-M](https://doi.org/10.1016/0550-3213(93)90166-M).
- [68] Stephen D. Ellis and Davison E. Soper. “Successive combination jet algorithm for hadron collisions”. *Phys. Rev. D* 48 (1993), pp. 3160–3166. DOI: [10.1103/PhysRevD.48.3160](https://doi.org/10.1103/PhysRevD.48.3160). arXiv: [hep-ph/9305266](https://arxiv.org/abs/hep-ph/9305266).
- [69] John M. Campbell, Stefan Höche, and Christian T. Preuss. “Accelerating LHC phenomenology with analytic one-loop amplitudes: A C++ interface to MCFM”. *Eur. Phys. J. C* 81.12 (2021), p. 1117. DOI: [10.1140/epjc/s10052-021-09885-0](https://doi.org/10.1140/epjc/s10052-021-09885-0). arXiv: [2107.04472](https://arxiv.org/abs/2107.04472) [hep-ph].
- [70] Lance J. Dixon, Z. Kunszt, and A. Signer. “Helicity amplitudes for $O(\alpha_s)$ production of W^+W^- , $W^\pm Z$, ZZ , $W^\pm\gamma$, or $Z\gamma$ pairs at hadron colliders”. *Nucl. Phys. B* 531 (1998), pp. 3–23. DOI: [10.1016/S0550-3213\(98\)00421-0](https://doi.org/10.1016/S0550-3213(98)00421-0). arXiv: [hep-ph/9803250](https://arxiv.org/abs/hep-ph/9803250) [hep-ph].

- [71] Lance J. Dixon, Z. Kunszt, and A. Signer. “Vector boson pair production in hadronic collisions at order α_s : Lepton correlations and anomalous couplings”. *Phys. Rev. D* 60 (1999), p. 114037. DOI: [10.1103/PhysRevD.60.114037](https://doi.org/10.1103/PhysRevD.60.114037). arXiv: [hep-ph/9907305](https://arxiv.org/abs/hep-ph/9907305) [[hep-ph](#)].
- [72] R. Keith Ellis, W. James Stirling, and B. R. Webber. “QCD and collider physics”. *Camb. Monogr. Part. Phys. Nucl. Phys. Cosmol.* 8 (1996), pp. 1–435.
- [73] A. Djouadi et al. “The Higgs photon - Z boson coupling revisited”. *Eur. Phys. J. C* 1 (1998), pp. 163–175. DOI: [10.1007/BF01245806](https://doi.org/10.1007/BF01245806). arXiv: [hep-ph/9701342](https://arxiv.org/abs/hep-ph/9701342) [[hep-ph](#)].
- [74] Stefano Goria, Giampiero Passarino, and Dario Rosco. “The Higgs Boson Lineshape”. *Nucl. Phys. B* 864 (2012), pp. 530–579. DOI: [10.1016/j.nuclphysb.2012.07.006](https://doi.org/10.1016/j.nuclphysb.2012.07.006). arXiv: [1112.5517](https://arxiv.org/abs/1112.5517) [[hep-ph](#)].
- [75] Giampiero Passarino, Christian Sturm, and Sandro Uccirati. “Higgs Pseudo-Observables, Second Riemann Sheet and All That”. *Nucl. Phys. B* 834 (2010), pp. 77–115. DOI: [10.1016/j.nuclphysb.2010.03.013](https://doi.org/10.1016/j.nuclphysb.2010.03.013). arXiv: [1001.3360](https://arxiv.org/abs/1001.3360) [[hep-ph](#)].
- [76] J. G. Korner and Z. Merebashvili. “One loop corrections to four point functions with two external massive fermions and two external massless partons”. *Phys. Rev. D* 66 (2002), p. 054023. DOI: [10.1103/PhysRevD.66.054023](https://doi.org/10.1103/PhysRevD.66.054023). arXiv: [hep-ph/0207054](https://arxiv.org/abs/hep-ph/0207054) [[hep-ph](#)].
- [77] John Campbell, Tobias Neumann, and Zack Sullivan. “Single-top-quark production in the t -channel at NNLO”. *JHEP* 02 (2021), p. 040. DOI: [10.1007/JHEP02\(2021\)040](https://doi.org/10.1007/JHEP02(2021)040). arXiv: [2012.01574](https://arxiv.org/abs/2012.01574) [[hep-ph](#)].
- [78] John Campbell, Tobias Neumann, and Zack Sullivan. “Testing parton distribution functions with t -channel single-top-quark production”. *Phys. Rev. D* 104.9 (2021), p. 094042. DOI: [10.1103/PhysRevD.104.094042](https://doi.org/10.1103/PhysRevD.104.094042). arXiv: [2109.10448](https://arxiv.org/abs/2109.10448) [[hep-ph](#)].
- [79] Ian Richard Blokland et al. “Next-to-next-to-leading order calculations for heavy-to-light decays”. *Phys. Rev. D* 71 (2005). [Erratum: *Phys.Rev.D* 79, 019901 (2009)], p. 054004. DOI: [10.1103/PhysRevD.71.054004](https://doi.org/10.1103/PhysRevD.71.054004). arXiv: [hep-ph/0503039](https://arxiv.org/abs/hep-ph/0503039).
- [80] Andrzej Czarnecki. “QCD corrections to the decay $t \rightarrow W b$ in dimensional regularization”. *Phys. Lett. B* 252 (1990), pp. 467–470. DOI: [10.1016/0370-2693\(90\)90571-M](https://doi.org/10.1016/0370-2693(90)90571-M).
- [81] Tobias Neumann and Ciaran Williams. “The Higgs boson at high p_T ”. *Phys. Rev. D* 95.1 (2017), p. 014004. DOI: [10.1103/PhysRevD.95.014004](https://doi.org/10.1103/PhysRevD.95.014004). arXiv: [1609.00367](https://arxiv.org/abs/1609.00367) [[hep-ph](#)].
- [82] Tobias Neumann. “NLO Higgs+jet production at large transverse momenta including top quark mass effects”. *J. Phys. Comm.* 2.9 (2018), p. 095017. DOI: [10.1088/2399-6528/aadfbf](https://doi.org/10.1088/2399-6528/aadfbf). arXiv: [1802.02981](https://arxiv.org/abs/1802.02981) [[hep-ph](#)].
- [83] R. Keith Ellis et al. “Higgs Decay to $\tau^+ \tau^-$: A Possible Signature of Intermediate Mass Higgs Bosons at the SSC”. *Nucl. Phys. B* 297 (1988), pp. 221–243. DOI: [10.1016/0550-3213\(88\)90019-3](https://doi.org/10.1016/0550-3213(88)90019-3).
- [84] U. Baur and E. W. Nigel Glover. “Higgs Boson Production at Large Transverse Momentum in Hadronic Collisions”. *Nucl. Phys. B* 339 (1990), pp. 38–66. DOI: [10.1016/0550-3213\(90\)90532-I](https://doi.org/10.1016/0550-3213(90)90532-I).

- [85] S. P. Jones, M. Kerner, and G. Luisoni. “Next-to-Leading-Order QCD Corrections to Higgs Boson Plus Jet Production with Full Top-Quark Mass Dependence”. *Phys. Rev. Lett.* 120.16 (2018). [Erratum: *Phys.Rev.Lett.* 128, 059901 (2022)], p. 162001. DOI: [10.1103/PhysRevLett.120.162001](#). arXiv: [1802.00349 \[hep-ph\]](#).
- [86] X. Chen et al. “Top-quark mass effects in H+jet and H+2 jets production”. *JHEP* 03 (2022), p. 096. DOI: [10.1007/JHEP03\(2022\)096](#). arXiv: [2110.06953 \[hep-ph\]](#).
- [87] R. Bonciani et al. “Next-to-leading-order QCD Corrections to Higgs Production in association with a Jet” (June 2022). arXiv: [2206.10490 \[hep-ph\]](#).
- [88] V. Ravindran, J. Smith, and W. L. Van Neerven. “Next-to-leading order QCD corrections to differential distributions of Higgs boson production in hadron hadron collisions”. *Nucl. Phys.* B634 (2002), pp. 247–290. DOI: [10.1016/S0550-3213\(02\)00333-4](#). arXiv: [hep-ph/0201114 \[hep-ph\]](#).
- [89] Carl R. Schmidt. “ $H \rightarrow ggg(gqq)$ at two loops in the large- M_t limit”. *Phys. Lett.* B413 (1997), pp. 391–395. DOI: [10.1016/S0370-2693\(97\)01102-7](#). arXiv: [hep-ph/9707448 \[hep-ph\]](#).
- [90] D. de Florian, M. Grazzini, and Z. Kunszt. “Higgs production with large transverse momentum in hadronic collisions at next-to-leading order”. *Phys. Rev. Lett.* 82 (1999), pp. 5209–5212. DOI: [10.1103/PhysRevLett.82.5209](#). arXiv: [hep-ph/9902483 \[hep-ph\]](#).
- [91] Christopher J. Glosser and Carl R. Schmidt. “Next-to-leading corrections to the Higgs boson transverse momentum spectrum in gluon fusion”. *JHEP* 12 (2002), p. 016. DOI: [10.1088/1126-6708/2002/12/016](#). arXiv: [hep-ph/0209248 \[hep-ph\]](#).
- [92] John M. Campbell, R. Keith Ellis, and Satyajit Seth. “H + 1 jet production revisited”. *JHEP* 10 (2019), p. 136. DOI: [10.1007/JHEP10\(2019\)136](#). arXiv: [1906.01020 \[hep-ph\]](#).
- [93] R. Kleiss and W. James Stirling. “Top quark production at hadron colliders: Some useful formulae”. *Z. Phys.* C40 (1988), pp. 419–423. DOI: [10.1007/BF01548856](#).
- [94] John M. Campbell et al. “Associated production of a Z Boson and a single heavy quark jet”. *Phys. Rev. D* 69 (2004), p. 074021. DOI: [10.1103/PhysRevD.69.074021](#). arXiv: [hep-ph/0312024](#).
- [95] John M. Campbell, R. Keith Ellis, and Ciaran Williams. “Direct Photon Production at Next-to-Next-to-Leading Order”. *Phys. Rev. Lett.* 118.22 (2017). [Erratum: *Phys.Rev.Lett.* 124, 259901 (2020)], p. 222001. DOI: [10.1103/PhysRevLett.118.222001](#). arXiv: [1612.04333 \[hep-ph\]](#).
- [96] John M. Campbell, R. Keith Ellis, and Ciaran Williams. “Driving missing data at the LHC: NNLO predictions for the ratio of $\gamma + j$ and $Z + j$ ”. *Phys. Rev. D* 96.1 (2017), p. 014037. DOI: [10.1103/PhysRevD.96.014037](#). arXiv: [1703.10109 \[hep-ph\]](#).
- [97] John M. Campbell et al. “Direct photon production and PDF fits reloaded”. *Eur. Phys. J. C* 78.6 (2018), p. 470. DOI: [10.1140/epjc/s10052-018-5944-4](#). arXiv: [1802.03021 \[hep-ph\]](#).
- [98] Zvi Bern, Lance J. Dixon, and Carl Schmidt. “Isolating a light Higgs boson from the diphoton background at the CERN LHC”. *Phys. Rev. D* 66 (2002), p. 074018. DOI: [10.1103/PhysRevD.66.074018](#). arXiv: [hep-ph/0206194 \[hep-ph\]](#).

- [99] Tobias Neumann. “The diphoton q_T spectrum at $N^3LL' + NNLO$ ”. *Eur. Phys. J. C* 81.10 (2021), p. 905. DOI: [10.1140/epjc/s10052-021-09687-4](https://doi.org/10.1140/epjc/s10052-021-09687-4). arXiv: [2107.12478](https://arxiv.org/abs/2107.12478) [[hep-ph](#)].
- [100] Thomas Becher and Tobias Neumann. “Fiducial q_T resummation of color-singlet processes at $N^3LL+NNLO$ ”. *JHEP* 03 (2021), p. 199. DOI: [10.1007/JHEP03\(2021\)199](https://doi.org/10.1007/JHEP03(2021)199). arXiv: [2009.11437](https://arxiv.org/abs/2009.11437) [[hep-ph](#)].
- [101] Fabrizio Caola, Andreas Von Manteuffel, and Lorenzo Tancredi. “Diphoton Amplitudes in Three-Loop Quantum Chromodynamics”. *Phys. Rev. Lett.* 126.11 (2021), p. 112004. DOI: [10.1103/PhysRevLett.126.112004](https://doi.org/10.1103/PhysRevLett.126.112004). arXiv: [2011.13946](https://arxiv.org/abs/2011.13946) [[hep-ph](#)].
- [102] Ming-xing Luo et al. “Unpolarized quark and gluon TMD PDFs and FFs at N^3LO ”. *JHEP* 06 (2021), p. 115. DOI: [10.1007/JHEP06\(2021\)115](https://doi.org/10.1007/JHEP06(2021)115). arXiv: [2012.03256](https://arxiv.org/abs/2012.03256) [[hep-ph](#)].
- [103] Markus A. Ebert, Bernhard Mistlberger, and Gherardo Vita. “Transverse momentum dependent PDFs at N^3LO ”. *JHEP* 09 (2020), p. 146. DOI: [10.1007/JHEP09\(2020\)146](https://doi.org/10.1007/JHEP09(2020)146). arXiv: [2006.05329](https://arxiv.org/abs/2006.05329) [[hep-ph](#)].
- [104] Ming-xing Luo et al. “Quark Transverse Parton Distribution at the Next-to-Next-to-Next-to-Leading Order”. *Phys. Rev. Lett.* 124.9 (2020), p. 092001. DOI: [10.1103/PhysRevLett.124.092001](https://doi.org/10.1103/PhysRevLett.124.092001). arXiv: [1912.05778](https://arxiv.org/abs/1912.05778) [[hep-ph](#)].
- [105] John M. Campbell and Ciaran Williams. “Triphoton production at hadron colliders”. *Phys. Rev. D* 89.11 (2014), p. 113001. DOI: [10.1103/PhysRevD.89.113001](https://doi.org/10.1103/PhysRevD.89.113001). arXiv: [1403.2641](https://arxiv.org/abs/1403.2641) [[hep-ph](#)].
- [106] Thomas Gehrmann and Lorenzo Tancredi. “Two-loop QCD helicity amplitudes for $q\bar{q} \rightarrow W^\pm \gamma$ and $q\bar{q} \rightarrow Z^0 \gamma$ ”. *JHEP* 02 (2012), p. 004. DOI: [10.1007/JHEP02\(2012\)004](https://doi.org/10.1007/JHEP02(2012)004). arXiv: [1112.1531](https://arxiv.org/abs/1112.1531) [[hep-ph](#)].
- [107] D. De Florian and A. Signer. “W gamma and Z gamma production at hadron colliders”. *Eur. Phys. J. C* 16 (2000), pp. 105–114. DOI: [10.1007/s100520050007](https://doi.org/10.1007/s100520050007). arXiv: [hep-ph/0002138](https://arxiv.org/abs/hep-ph/0002138) [[hep-ph](#)].
- [108] John M. Campbell, Tobias Neumann, and Ciaran Williams. “ $Z\gamma$ Production at NNLO Including Anomalous Couplings”. *JHEP* 11 (2017), p. 150. DOI: [10.1007/JHEP11\(2017\)150](https://doi.org/10.1007/JHEP11(2017)150). arXiv: [1708.02925](https://arxiv.org/abs/1708.02925) [[hep-ph](#)].
- [109] John M. Campbell et al. “Production of a Z boson and two jets with one heavy-quark tag”. *Phys. Rev. D* 73 (2006). [Erratum: *Phys.Rev.D* 77, 019903 (2008)], p. 054007. DOI: [10.1103/PhysRevD.77.019903](https://doi.org/10.1103/PhysRevD.77.019903). arXiv: [hep-ph/0510362](https://arxiv.org/abs/hep-ph/0510362).
- [110] John M. Campbell et al. “Associated Production of a W Boson and One b Jet”. *Phys. Rev. D* 79 (2009), p. 034023. DOI: [10.1103/PhysRevD.79.034023](https://doi.org/10.1103/PhysRevD.79.034023). arXiv: [0809.3003](https://arxiv.org/abs/0809.3003) [[hep-ph](#)].
- [111] J. M. Campbell et al. “NLO QCD predictions for $W + 1$ jet and $W + 2$ jet production with at least one b jet at the 7 TeV LHC”. *Phys. Rev. D* 86 (2012), p. 034021. DOI: [10.1103/PhysRevD.86.034021](https://doi.org/10.1103/PhysRevD.86.034021). arXiv: [1107.3714](https://arxiv.org/abs/1107.3714) [[hep-ph](#)].
- [112] Jannis Teunissen. *config_fortran - A configuration file parser for Fortran*. 2019. URL: https://github.com/jannisteunissen/config_fortran.
- [113] Daan van Vugt and Koen Beljaars. *Modern fortran implementation of a Sobol sequence*. 2016. URL: <https://github.com/Exteris/sobseq>.

- [114] S. Joe and F. Y. Kuo. *Sobol sequence direction numbers*. 2010. URL: <https://web.maths.unsw.edu.au/~fkuo/sobol/>.